

**On the Development of
a Cooled Metallic
Thermal Protection System
for Spacecraft**

On the Development of a Cooled Metallic Thermal Protection System for Spacecraft

Proefschrift

ter verkrijging van de graad van doctor
aan de Technische Universiteit Delft,
op gezag van de Rector Magnificus prof.dr.ir. J.T.Fokkema,
voorzitter van het College voor Promoties,
in het openbaar te verdedigen op woensdag 21 december 2005 om 13.00 uur
door Jeroen BUURSINK
ingenieur in de luchtvaart en ruimtevaart
geboren te Borculo

Dit proefschrift is goedgekeurd door de promotor:

Prof.dr.Z.Gürdal

Samenstelling promotiecommissie:

Rector Magnificus

voorzitter

Prof. dr. Z. Gürdal

Technische Universiteit Delft, promotor

Prof. dr. ir. R. Benedictus

Technische Universiteit Delft

Prof. dr. ir. A.de Boer

Universiteit Twente

Prof. Dr. -Ing. M.Auweter-Kurz

Universität Stuttgart

Prof. dr. C.Bruno

Università degli Studi di Rome 'La Sapienza'

Ir. T.J.van Baten

Technische Universiteit Delft

Prof. dr. A.Rothwell

Technische Universiteit Delft, reservelid

Publisher: TU Delft, Faculteit Luchtvaart- en Ruimtevaarttechniek

Printed by: Wöhrmann Print Service

ISBN-10 9056230808

ISBN-13 9789056230807

Keywords: Thermal Protection System, Water Cooling, Re-entry

Copyright ©2005 by Jeroen Buursink

All rights reserved. No part of the material protected by this copyright notice may be reproduced or utilized in any form or by any means, electronic or mechanical, including photocopying, recording or by any information storage and retrieval system, without written permission from the publisher: TU Delft, Faculteit Luchtvaart- en Ruimtevaarttechniek.

Printed in the Netherlands

[this page was intentionally left blank]

[this page was intentionally left blank]

Acknowledgements

I owe thanks to the people who helped in the course of this research. First and foremost, Tom van Baten, who gave me the opportunity in the first place to work on this subject and covered me on the management and bureaucracy side. Together we hold the patent on the Enhanced Radiation Cooling System, which shows how closely he was involved in this work. Kees Sudmeijer has played an essential role in this research, and without his input and the many discussions we had on all areas of this work and everything else that came to mind the result would not have been the same. Many trips together to various meetings and conferences hold fine memories of our cooperation. Undoubtedly, in twenty years time he will still be here working on ten subjects at the same time.

A number of students have done parts of this work as their thesis or internship assignments. Claudio Lopes did the first laboratory tests and finite element modelling. Later lab work was done by or together with Onne Sypkens, Jarne Verpoorten and Ab El Abbadi. Modelling was performed by Vasco Pimenta, Daniel Garcia Yarnoz, Gianni Campoli and Diana Sciullu.

For all the experiments, the staff of the labs has been very helpful. Fons Klompé was instrumental in setting up the thermal test facility and the initial thermal tests, Maarten Bakker played an essential role in the later tests. Hans, Niels, Bertil and Frans helped in preparation and execution of various tests; Bertus, Herman and Ed in the workshop made our larger test models.

The people of the aerospace materials and aerospace structures groups provided the working atmosphere that made it a pleasure to spend this time working at the Faculty of Aerospace Engineering.

Outside of the Faculty, thanks goes to Jean Muylaert at ESA-ESTEC for his support of our work from that side, for the people at DutchSpace; Erwin, Jack, Sjaam, Gerard, Javad, Martin and others for their support and cooperation.

Last but certainly not least, I have to thank my parents for their unconditional support, and Elaine for the same as well as for checking my English.

On the Development of a Cooled Metallic Thermal Protection System for Spacecraft

<i>Symbols</i>	<i>xiii</i>
----------------	-------	-------------

<i>Summary</i>	<i>xvii</i>
----------------	-------	-------------

<i>Samenvatting</i>	<i>xxi</i>
---------------------	-------	------------

CHAPTER 1 *Scope and introduction to Thermal Protection Systems* **1**

1.1	Scope and setup of the study	1
1.2	Use of TPS: historical perspective	2
1.2.1	Requirements to TPS	2
1.2.2	Types of TPS, their strong points and weaknesses	7
1.2.3	The ultimate goal: a cheap launch vehicle	13
1.2.4	Types of vehicle shapes and related TPS types; classes of re-entry vehicles	15
1.2.5	Hot structures	18
1.2.6	Current developments, non-metallic TPS	19
1.3	Motivation for using metallic TPS	20
1.4	Advantages of high L/D vehicles and TPS aspects thereof	22
1.4.1	Advantages of high L/D	22
1.4.2	Disadvantages and problems of sharp nose and leading edges	25
1.4.3	Past studies of high L/D vehicles	25
1.5	Objectives of this research	27

CHAPTER 2 *Metallic TPS* **31**

2.1	Aerodynamic heating & re-entry	31
2.1.1	Aerodynamic heating	31
2.1.2	Metallic TPS under aerodynamic heating	33
2.1.3	Advantages & disadvantages of metallic TPS	34
2.2	Materials	35
2.2.1	Requirements to metallic TPS materials	35
2.2.2	List of materials	35
2.2.3	Desired characteristics of materials of choice	39
2.3	Use of metallic TPS to date	40
2.3.1	Flight experience	41
2.3.2	Vehicle and TPS concepts	41
2.4	Cooled metallic TPS	48

2.4.1	Patents	48
2.4.2	Proposed vehicle and structure concepts using cooled TPS	54
2.4.3	Hot structures and TPS developments in the Netherlands	59
2.4.4	Cooled TPS concepts at TU Delft	60
2.4.5	The potential of cooled metallic TPS: reasons for its application	61

CHAPTER 3 *Theoretical background of cooled metallic TPS* **63**

3.1	Enhanced Radiation Cooling	63
3.1.1	Basic principle of enhanced radiation cooling	63
3.1.2	Basic operating principle	64
3.1.3	Exposure to vacuum	69
3.1.4	Behaviour of the porous material	69
3.1.5	PM1000 characterization	78
3.1.6	Other possible material combinations	79
3.2	Engineering Model	84
3.2.1	Model description	84
3.2.2	sensitivity analysis	85
3.3	Analytical Model of Vapour Flow	90
3.4	Finite Element Models of Tests	96
3.4.1	Issues with Finite Element Modelling	97
3.4.2	Convection modelling	97
3.5	Other aspects of interest	100
3.5.1	Extended solar heating in space	100
3.5.2	Re-filling with water	105

CHAPTER 4 *Experiments with cooled metallic TPS* **109**

4.1	Material testing	109
4.1.1	Strength and physical properties	110
4.1.2	Environmental and oxidation tests	115
4.2	Basic Operation Tests	117
4.2.1	Test setup & model description	117
4.2.2	Proof of concept tests	118
4.2.3	Drying out of ZAL-15	121
4.2.4	Determination of the turnover point and critical saturation	132
4.2.5	Changing the surface tension of water	137
4.2.6	Conclusions of basic operation tests	138
4.3	Large lab model tests	139
4.3.1	Model design and test setup	139

4.3.2	Objectives and expected results	142
4.3.3	Test results	143
4.3.4	Finite element model	145
4.4	Other tests	146
4.4.1	Vacuum chamber tests	146
4.4.2	Water filling tests	150
4.5	Conclusions of the tests	153

CHAPTER 5 *Designing with cooled metallic TPS* . 155

5.1	DART: the Delft Aerospace Re-entry Test Vehicle	155
5.1.1	Goals of the DART mission	155
5.1.2	Design of the vehicle shape & TPS	156
5.1.3	TPS layout: nose and cone	157
5.1.4	Predictions of performance	160
5.1.5	DART project conclusions	164
5.2	Flight experiment for cooled TPS	164
5.2.1	The Expert mission	165
5.2.2	Design evolution	166
5.2.3	Sensors and measurements	167
5.2.4	Predictions of flight measurements	168
5.2.5	FE analysis of the test sample	170
5.2.6	Lab tests on the flight experiment	173
5.2.7	Qualification tests	173
5.3	Cooled leading edge	174
5.3.1	Basic analysis of a cooled leading edge	174
5.3.2	Design issues	174
5.4	TPS tiles with enhanced radiation cooling	175
5.4.1	Potential for use	175
5.4.2	Design issues	175
5.5	Design issues - conclusions	176

CHAPTER 6	<i>Conclusions</i>	179
	<i>References</i>	183
	<i>Appendix A: Materials properties</i>	193
	<i>Appendix B: Colour plates</i>	201

Symbols

a_g	[m/s ²]	(Effective) acceleration of gravity
A	[m ²]	Surface area
C_p	[J/kg·K]	Specific heat
d_p	[m]	Mean pore size
g	[m/s ²]	Effective acceleration (NB: not simply acc.of gravity)
h	[m]	Height
h	[W/m ² ·K]	Convective heat transfer coefficient
h_v	[J/kg]	Heat of evaporation (of water)
H	[m ⁻¹]	Mean curvature of gas-liquid interface
K	[m ²]	Permeability
k	[W/m·K]	Thermal conductivity
k_{rl}	[-]	Relative permeability for the liquid
L	[m]	Length
m	[kg]	Mass
\dot{m}	[kg/s]	Rate of mass change (evaporation)
p	[N/m ²]	Pressure
p_c	[N/m ²]	Capillary pressure
\dot{Q}	[W/m ²]	Heat flux

On the Development of a Cooled Metallic Thermal Protection System for Spacecraft

r	[m]	Radius of curvature
R	[m]	Radius
S	[-]	Saturation level
S_{ir}	[-]	Irreducible saturation
t	[m]	Gap width
t	[m]	Thickness (of skin)
T	[K]	Temperature
v	[m/s]	Velocity
V	[m/s]	Velocity of vapour outflow from porous medium
β	[K ⁻¹]	Volumetric coefficient of thermal expansion
δ	[m]	Thickness of a layer
ε	[-]	Emissivity
ε	[-]	Porosity
θ	[rad]	Contact angle between liquid and solid phase
μ	[kg/m·s]	Viscosity
ρ	[kg/m ³]	Density
σ	[W/m ² ·K ⁴]	Stefan-Boltzmann's constant ($5.67 \cdot 10^{-8}$ W/m ² K ⁴)
σ	[N/m]	Surface tension
φ	[rad]	Angle from stagnation point along a spherical nose
∂	[m ² /s]	Temperature conductivity

subscripts

allowable	Allowable (heat flux) for given temperature limit
applied	Applied aerodynamic (heat flux)
boil	Boiling (temperature)
conv	Convective
g	Of the gas (phase)
gl	Of the gas-liquid interface
in	Inward (heat flux)
l	Of the liquid (phase)
m	Averaged (flow velocity)
max	Maximum

Symbols

out	Outward (heat flux)
porous	Of the porous material
stag	At the stagnation point
v, vapour	Of the water vapour
wall	At the wall or of the wall
ZAL	Of the ZAL-15
0	Of the flow

On the Development of a Cooled Metallic Thermal Protection System for Spacecraft

Summary

On the Development of a Cooled Metallic Thermal Protection System for Spacecraft

For significant cost reduction for space launch, in the order of a factor of 10 to 100, reuse of the launch vehicle, or at least large parts thereof, is necessary, because of the high cost of production of even fairly simple launch vehicles. This automatically means that launcher stages have to be returned to Earth after their mission and part of that return involves an atmospheric deceleration phase exposing the vehicle to high temperature flow around it. A thermal protection system is required for the vehicle to survive exposure to this flowfield.

Since maintenance and inspection cost are an important part of the total cost of a reusable launcher, this should be minimised for a low cost launch system. Experience from the Space Shuttle system shows how high maintenance cost can lead to an extremely costly vehicle rather than a cheap one. Metallic Thermal Protection Systems (TPS) hold the promise of offering lower maintenance and inspection cost when compared to Ceramic reusable TPS. Current metallic TPS however is limited to lower temperatures than Ceramic TPS because of material limitations. Cooling the metallic TPS with water can extend its applicability to higher thermally loaded parts of a vehicle. Also, cooled TPS might open possibilities for designing re-entry vehicles with sharper nose and leading edges, which will improve the flying characteristics and allow the vehicle to decelerate at high altitude, reducing the heat load.

Enhanced Radiation Cooling was invented at TU Delft as a means to allow metallic TPS to be used on a small re-entry capsule under development here. It reduces the temperature of a heated metallic skin by allowing it to radiate thermal energy not just out to space as in a classic insulated TPS, but also inward to an underlying layer of material that is kept at a low temperature by saturating it with water. The evaporation of water accommodates the heat radiated inward and the high heat of evaporation of water ensures that a relatively small mass of water is required. The internal layer containing the water is a porous Alumina

material that can contain about 70% water by volume. It is low in mass and the internal structure ensures that water is transported to the evaporation surface by capillary action. Capillarity also ensures that water is contained under g-loads to a sufficient extent. The performance of the system depends heavily on the optical properties of the materials used, specifically the emissivity, which should be as high as possible. The metallic skin material, the Nickel-Chromium alloy PM1000, has an emissivity of 0.85 and the porous water-containing material one of 0.91. A one-dimensional heat balance analysis predicts a gain in allowable heat load for the metallic skin for a given temperature of about 92%.

Laboratory tests of small samples of the TPS were performed where a cooled sample was compared directly with an uncooled one under the same heat load. A cooling effect close to the predicted maximum was reached from the earliest tests, showing that the system worked as expected. Similar tests were used to determine one of the critical parameters of the system that can not be predicted on the basis of theory alone: the level of saturation below which the capillary transport breaks down and the cooling effect stops. This so-called critical saturation level depends on the required water transport rate, and thus on the applied heat load, and varies between 15-20% saturation for skin temperatures of 1000 to 1200°C, with a bandwidth of up to 10%.

In operational use the system has to be shielded from vacuum exposure. Laboratory tests have shown that exposure to pressures below about 25mbar will lead to water boiling at room temperature and then freezing. The boiling expels part of the water from the porous material and in vacuum sublimation leads to further water loss, amounting to a significant percentage already in as little as half an hour of exposure (about 20% water loss in 30 minutes). A minimum pressure in the system of 30mbar is therefore prescribed.

Prolonged exposure of the cooled TPS to solar radiation in orbit would heat up the materials to such an extent that water would start to evaporate after about 14 orbits (assuming half the orbit in direct sunlight perpendicular to the skin and half the orbit in darkness). The perpendicular striking sunlight is a worst case assumption but even if evaporation would start after two or three times as long an exposure (14 orbits equals about 1 day), use of this system on a Space Shuttle like vehicle will require it to be able to reside in orbit for many days without a problem. (Re)filling just before re-entry can be a way to cope with this problem.

Room for improvement of the system could be found in changing materials to ones with better material properties, but the current choice of materials already performs close to theoretical optimum. Replacing the skin material by one with higher allowable temperature will increase the allowable heat load, but the capillary transport will be unable to cope with the required flow rate at higher remaining saturation, so a larger percentage of water remains unused. This could be countered by adding a continuous refilling system that resupplies the

Summary

water from the back side of the porous layer. The high emissivity of the materials leaves little room for improvement in that area; the performance of the porous material might be tailored to somewhat higher performance (better capillary characteristics or lower mass).

The Enhanced Radiation Cooling system was developed for application on a small re-entry vehicle that was to use metallic TPS. Low cost requirements resulted in a small vehicle and a specific launcher selection leading to rather high heat loads, that necessitated cooling of the metallic skin. A short ballistic re-entry required less than 5.6kg of water to cool a 1.86m² surface. The nose was to be cooled by direct water cooling, where water is in direct contact with the metallic skin. 4.6kg of water was required to cool a 25cm radius nose exposed to more than 2MW/m² at the stagnation point.

On the Development of a Cooled Metallic Thermal Protection System for Spacecraft

Samenvatting

On the Development of a Cooled Metallic Thermal Protection System for Spacecraft

Om een belangrijke kostenreductie van het lanceren van ruimtevoertuigen te kunnen bewerkstelligen, tot een factor 10 to 100, is het onvermijdelijk dat delen van of de gehele lanceerder meerdere malen gebruikt kan worden. Dit omdat zelfs vrij eenvoudige lanceerders bijzonder kostbaar zijn. Dit hergebruik impliceert dat de trappen van de lanceerder moeten terugkeren naar de grond aan het eind van hun missie en een deel van deze terugkeer behelst een afremming in de atmosfeer die het voertuig blootstelt aan gassen van hoge temperatuur. Een hitteschild is nodig om het voertuig deze terugkeer door de atmosfeer te laten overleven.

Omdat onderhoud en controle een belangrijk deel uitmaken van de operationele kosten van een herbruikbare lanceerder, is het belangrijk deze kosten te minimaliseren. De ervaring met de Space Shuttle laat zien dat hoge kosten voor onderhoud en controle leiden tot een extreem kostbaar lanceersysteem in plaats van het beoogde goedkope. Metalen hitteschilden houden de belofte in deze kosten te reduceren in vergelijking met keramische herbruikbare hitteschilden. De huidige metalen hitteschilden hebben echter een lagere maximale gebruikstemperatuur dan de keramische vanwege de beperkingen van de gebruikte materialen. Het koelen van het metalen hitteschild met water kan het gebruik ervan bij hogere warmtebelastingen mogelijk maken. Ook kan het koelen van een hitteschild het mogelijk maken een voertuig te ontwerpen met scherpere neus en vleugelvoorranden, wat tot verbeterde vliegeigenschappen leidt en wat ook het voertuig op grotere hoogte laat afremmen, wat de warmtebelasting weer reduceert.

‘Verbeterde Stalingskoeling’ is uitgevonden aan de TU Delft om een metalen hitteschild te kunnen gebruiken op een kleine experimentele terugkeercapsule die aan de universiteit werd ontwikkeld. Het reduceert de temperatuur van een metalen huid door deze te laten uitstralen naar binnen zowel als naar buiten, waar de straling naar binnen wordt opgenomen door een

met water verzadigde poreuze laag. Het water houdt de poreuze laag koel, en het verdampen van het water neemt een grote hoeveelheid thermische energie op, zodat relatief weinig water volstaat voor de koeling. De poreuze laag bestaat uit aluminium-oxide isolatiemateriaal met hoge porositeit, dat tot 70 volume-% water kan bevatten. De interne structuur zorgt ervoor dat het water wordt vastgehouden in het poreuze materiaal en naar het verdampingsoppervlak stroomt door capillaire werking. De werking van het systeem hangt sterk af van de optische eigenschappen van de materialen die worden gebruikt, met name van de emissiviteit, die zo hoog mogelijk moet zijn. De metalen huid, van het materiaal PM1000, heeft een emissiviteit van 0.85 en het verzadigde poreuze materiaal van 0.91. Een eendimensionale analyse voorspelt een toename van de toelaatbare warmtebelasting voor een gegeven temperatuur van de huid van ongeveer 92%.

Tests op dit gekoelde hitteschild in het laboratorium hebben een gekoeld proefstuk direct vergeleken met een ongekoeld proefstuk onder dezelfde warmtebelasting. Een koelingseffect dicht bij het voorspelde maximaal haalbare werd al in de eerste testen waargenomen. Verdere tests hebben een van de bepalende eigenschappen van het systeem vastgelegd: de verzadigingsgraad van het met water gevulde poreuze materiaal waarbij het capillaire transport ophoudt en dus het koelings-effect ook stopt. Deze kritische verzadigingsgraad hangt af van de vereiste watertransportsnelheid, en dus van de verdampingssnelheid. Ze varieert van 15-20% verzadiging bij temperaturen van de huid van 1000-1200°C met een variatie tot 10%.

In operationeel gebruik moet worden voorkomen dat het water wordt blootgesteld aan vacuum. Een luchtdruk onder ongeveer 25mbar leidt tot koken van het water bij kamertemperatuur gevolgd door bevriezing en sublimatie van het ijs waarbij een significante hoeveelheid water verloren gaat. Een minimale interne luchtdruk van 30 mbar wordt dus voorgeschreven voor het systeem.

Het voor langere tijd blootstellen van het systeem aan verwarming door direct zonlicht in de ruimte leidt tot verdamping van water na ongeveer 14 omlopen (waarbij wordt aangenomen dat de helft van elke omloop in de schaduw plaatsvindt). Hoewel dit een 'worst-case' aanname is, is dit niet acceptabel voor een herbruikbare lanceerder die misschien weken in een baan om de aarde moet kunnen blijven. Het vullen van de poreuze laag met water kort voor de terugkeer in de dampkring kan dit probleem voorkomen.

Er kan gezocht worden naar verbeteringen van dit systeem door de gebruikte materialen te vervangen door materialen met betere eigenschappen. Echter, de huidige combinatie van materialen voldoet al zo goed dat het theoretisch optimum bijna bereikt is. Het vervangen van de metalen huid door een materiaal met een hogere toelaatbare temperatuur zal de toelaatbare warmtebelasting vergroten, maar het capillaire transport van water in de poreuze laag moet wel in staat zijn om voldoende water aan te voeren naar het verdampingsvlak. Een

Samenvatting

groter deel van het water zal overblijven nadat de kritische verzadigingsgraad bereikt is. Dit kan worden opgelost door continu water aan te voeren door buisjes achter het poreuze materiaal. De hoge emissiviteit van de gebruikte materialen laat weinig ruimte voor verbetering, maar het poreuze materiaal kan wellicht nog verder geoptimaliseerd worden voor deze toepassing.

Het gekoelde hittschild is ontwikkeld voor gebruik op een klein terugkeervoertuig dat als doel had om een metalen hittschild te vliegen. Eisen aan lage kosten leidden tot een klein voertuig en een goedkope lanceerder die tot vrij hoge warmtebelastingen bij terugkeer in de atmosfeer leidde. Hierdoor werd het noodzakelijk het hittschild te koelen. Een korte ballistische vlucht door de dampkring zou voor de koeling minder dan 5.6kg water gebruiken voor het koelen van het 1.86m² grote oppervlak van het voertuig. De neus werd gekoeld door een andere methode van waterkoeling waar water in direct contact met de buitenhuid werd gebruikt. Hier was 4.6kg water nodig voor het koelen van een ronde neus met een straal van 25cm en blootgesteld aan een warmtebelasting tot 2 MW/m² in het stagnatiepunt.

On the Development of a Cooled Metallic Thermal Protection System for Spacecraft

Scope and introduction to Thermal Protection Systems

This chapter provides an introduction to the subject of this thesis. It gives the scope of the thesis research, as well as provides general background information on thermal protection systems (TPS), the types that are used and the kind of vehicles that use the different types.

Also, the reasons for researching metallic TPS are given, as well as the benefits that are to be had by using it. The advantages of high lift re-entry vehicles are given, to support the case for research into cooled TPS.

1.1 Scope and setup of the study

This thesis describes the work done over a number of years in the development of a cooled metallic thermal protection system. This system was invented and developed at the Faculty of Aerospace Engineering of Delft University of Technology from 1999 onwards. The so called Enhanced Radiation Cooled TPS was patented by TU Delft. Initially the program was aimed specifically at designing, building and flying a small re-entry vehicle for scientific research, to be built and operated by the university. Cost and technology considerations led to the selection of metallic TPS, and vehicle characteristics forced the need for cooling of this TPS (see [16],[17],[18]).

The history of a direct application of the cooled TPS in a re-entry vehicle made for a development and research program with a highly practical approach. Therefore, throughout this thesis, practical considerations are always there in the background when a choice has to be made on what to study and which direction to take for the research and development.

Since the ultimate goal is the development of a thermal protection system that can be applied to future reusable launchers, the very complex, and as of yet not fully defined, set of requirements of such vehicles is used throughout this study to make certain decisions.

Following this introductory chapter, the second chapter treats metallic TPS in more depth, with some information on the materials, including the non-metallic ones which are in competition with the metallics. Also an overview of the developments in the field of metallic TPS from the 1950's to today is given, with special regard to developments of vehicles, though none made it to actual flight. Prior concepts for cooled (metallic) TPS are shown as well.

Chapter 3 covers the theory of the Enhanced Radiation Cooling system for metallic TPS, treating the physics involved in the system, as well as modelling both on engineering level and more detailed Finite Element modelling. Some operational considerations are treated as well. Chapter 4 describes the experiments that have been performed to underpin the theoretical description of the cooled TPS, as well as some experimental studies to determine operational aspects or material properties needed in the larger scope of bringing the TPS to operational readiness. Chapter 5 treats some design cases; most notably the design of a flight experiment of the cooled TPS for a small experimental re-entry capsule. Also some preliminary examples of future operational applications are given.

1.2 Use of TPS: historical perspective

This section gives an overview of thermal protection systems and their use. First, the general requirements which apply to TPS are given, followed by a brief overview of the broad classes of TPS that are in use or under development. Then, the different basic types of re-entry vehicles are introduced, with some remarks on which TPS best suits which vehicle or mission. This is followed by some remarks on the ongoing effort to reduce launch cost by creating a cheap reusable launcher, and the benefits of metallic TPS for this mission. Finally, the advantages of high-lift vehicles are mentioned to substantiate the effort of developing cooled TPS for such applications.

1.2.1 Requirements to TPS

The TPS of a re-entry vehicle is one of the critical systems, with the main objective to protect the underlying structure and/or payload from the high temperatures on the outside. While doing this, it should retain adequate mechanical properties and, in order to be reusable, resist any form of degradation, e.g. by oxidation [21]. In practice this means as well that the reusable TPS should have a high resistance against oxidation and maintain a sufficiently smooth surface in order to prevent premature boundary layer transition to turbulence.

Major technical issues for reusable TPS are [91]:

- reusability and maintainability

Chapter 1: Scope and introduction to Thermal Protection Systems

- weather proofing
- oxidation protection
- refurbishment of oxidation protection
- interfaces with primary (cold) structures
- repair / replace procedures (find out when to repair and when (and how) to replace)
- non-destructive inspection methodologies.
- Sealing where necessary

Added to this list can be:

- behaviour with respect to low-, high and hypervelocity impact

The expected operational environment for TPS for a two-stage reusable launcher are given in [41]:

	Location	Typ.temperature (°C)	Typical area (m ²)
Second stage	Fuselage	450	110
	Payload bay	950	70
	Wing windward	1000	90
	Wing leading edge	1300	30
First stage	Fuselage / bottom	600	1200
	Wing windward	700	1300
	Wing leading edge	1000	40

Table 1.1 : typical temperatures and surface area for sections of TPS for a 2-stage RLV [41]

Here the environment is given in terms of temperatures. For comparison of different TPS types, especially with cooled TPS, the actual thermal load given in Watts per square meter, is more useful. Many references giving the temperature values do not give the corresponding heat flux rates, but these can be estimated with a thermal balance equation in which incoming heat flux is balanced by radiated energy from the high temperature wall. When the emissivity of the material is known, the temperature and heat flux can be directly related to each other. In practice, high emissivity is desired, and for most TPS materials an emissivity

in the order of 0.85 can be used in first approximations. Furthermore also the catalicity is an important factor and low catalicity is desired in a TPS material. For completeness it must be noted that the simple heat balance approach works when the thermal mass of the TPS is not too high and when the heating profile is not too short (i.e. the re-entry is not a short ballistic one with a high but short heating peak, but a more extended re-entry with more moderate heat loads).

The X-38 / CRV programme used to following design reference heat loads or the stagnation point: 1065kW/m^2 , with a 500sec rise up to that level, 500sec constant maximum level and 500sec fall-off. The real worst case was one of the abort scenarios which led to loads some 15% higher, though the duration was not given [66].

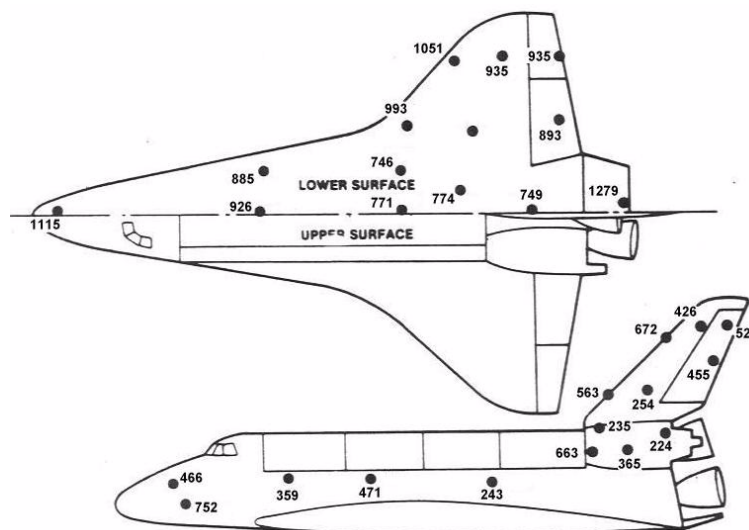


Figure 1-1: Space Shuttle temperatures measured during the second flight STS-2 in 1981, in °C (from [63], converted to °C)

The Space Shuttle encounters a stagnation heat load of up to 200 kW/m^2 (1510°C) [33]. Temperatures as measured in an actual flight are shown in Figure 1-1.

As a final example; the Dutch space industry is developing technology for a rudder of an RLV built as a metallic hot structure [29]. The baseline vehicle is a concept from the ESA

future launcher study, based on the German Sub-orbital Hopper concept. Figure 1-2 shows the heating history for this vehicle during launch and re-entry, both for the stagnation point and the rudder that is under design. It shows a brief heating pulse reaching just over 600 kW/m² at the stagnation point.

It should be noted that this short heating pulse is not characteristic for lifting re-entry vehicles, which tend to have a longer period of more or less constant heating rate. For this rudder design however, the temperature gradient was design-driving rather than the duration of the heating pulse.

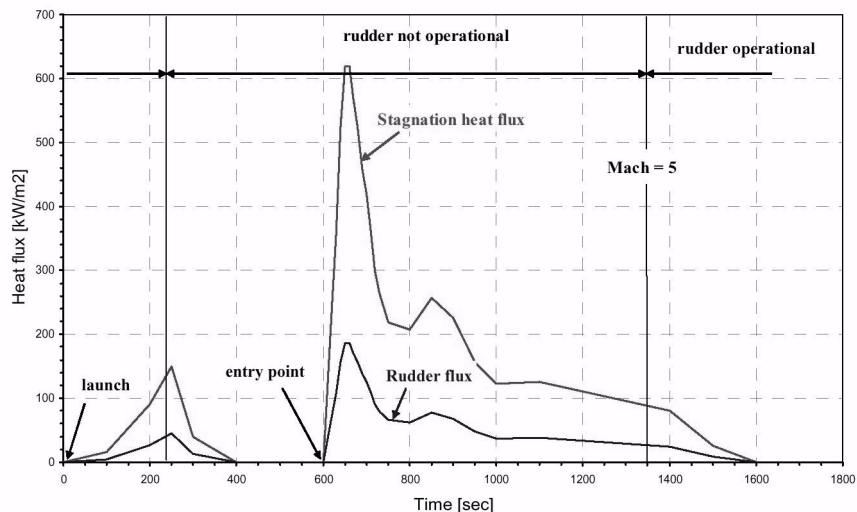


Figure 1-2: heat flux history for the Hopper RLV for the stagnation point and the rudder [29]

With regard to temperatures and heat loads it is important to note that the maximum temperature is mainly important to determine which materials can be used in a specific location, while the actual thickness of the TPS or the amount of insulation (or coolant) required is determined by the entire heating history during re-entry, so by the integrated heat load given in J/m².

Sealing is very important in regions with high pressure; if there is a connection from the high pressure to a low pressure location, through the TPS, even a small hole can lead to flow of the extremely hot boundary layer gases through the interior of the TPS, where the thermal energy is transferred to the structure. Since internally, there is nowhere for this thermal energy to go, except into heating up the structure, and materials used there are usually less tolerant to high temperatures to begin with (e.g. Aluminium in the Space Shuttle), this will lead to catastrophic failure (as seen in the accident with the Space Shuttle Columbia).

Typically, it can be said that large re-entry vehicles like X-33 with large empty propellant tanks (resulting in low density) will have much more benign entry loads than smaller, more dense vehicles like X-38, which has no propellant tanks of significant size. The smaller vehicle will require higher performing TPS, but of course over a much smaller surface area.

At the end of the day, cost will also play a very important role of course. In the quest for a reusable launcher that is 10 to 1000 times cheaper in cost-per-kilogram to orbit the cost of the components, especially the operations cost in the case of a reusable launcher, are of paramount importance. So much so, in fact, that it is likely that the actual building of a reusable launcher will not be undertaken until the technologies are mature enough to produce the needed cost reduction, rather than being in principle applicable but at higher cost.

Low operations cost will require robustness, reasonable to large performance margins, ease of inspection and replacement and also low acquisition cost. This is where metallic materials are expected to be superior to ceramics.

Hypervelocity impact

Resistance to hypervelocity impact can be a requirement for TPS materials. The impact penetration of a small object on a semi-infinite metal plate is given by [46]:

$$P_{\infty} = k \cdot \rho_p^{\frac{1}{6}} \cdot m^{0.352} \cdot V_n^{\frac{2}{3}} \quad (1.1)$$

where P_{∞} is the penetration depth (mm)

k is a constant; 0.25 for steel

ρ_p is the penetrator density (g/cm^3)

m is the penetrator mass (g)

V_n is the penetrator velocity perpendicular to the surface (km/s)

To prevent perforation, the plate thickness should be 1.8 times P_{∞} , to prevent spalling on the inside it should be 2.2 times P_{∞} and to prevent spalling on the outside 3 times P_{∞} .

Since no value of k for PM1000, the material used in the TPS described in this thesis, is known, the one for steel is used as an approximation; assuming that it depends on material density this seems a reasonable first assumption. This allows an example calculation for a 5 gram steel object impacting at 7 km/s giving a penetration of 2.27mm. This means that a thickness of over 4mm is required to prevent perforation. Clearly this is excessive, and no metallic outer skin can reasonably be expected to prevent perforation. In reality, a small puncture of the outermost layer of TPS would be acceptable if it does not endanger the vehicle during re-entry. The total of all TPS layers together would have to withstand the impact sufficiently to allow a safe landing after which the damaged panel can be replaced or repaired.

It seems more reasonable to accept the risk of impact for a reusable launcher, since adding extra protection against this would quickly erode the payload carrying capacity. Since the risk of impact is directly proportional to the time spent in orbit, an RLV which spends little time there is not exposed to large risk. The Space Shuttle Columbia accident in February of 2003 does show that resistance against low and high velocity impact is important for a TPS.

1.2.2 Types of TPS, their strong points and weaknesses

There are different ways of classifying TPS; here a classification based on material type will be used.

Ablative TPS is non-reusable and of little concern in the remainder of this study. As for reusable TPS, these can be divided in metallic and non-metallic. Non-metallic TPS can be insulative, like the Silica tiles of Space Shuttle, stand-off or hot structure ceramic, mainly Carbon-Carbon (C-C) or Carbon Silicon Carbide (C-SiC), both classed as Ceramic Matrix Composites (CMC's) or the new Ultra-High Temperature Ceramics (UHTC).

Metallic TPS can be applied as a hot structure or a stand-off TPS depending on the application. Here, stand-off TPS is a TPS where a rigid outer shell is mounted on spacers (stand-offs) over an underlying (cool) structure with low-density insulation material in between. This type of TPS carries the thermal and pressure loads, with the insulation protecting the underlying structure against high temperatures and the stand-offs transferring the pressure load to the internal structure.

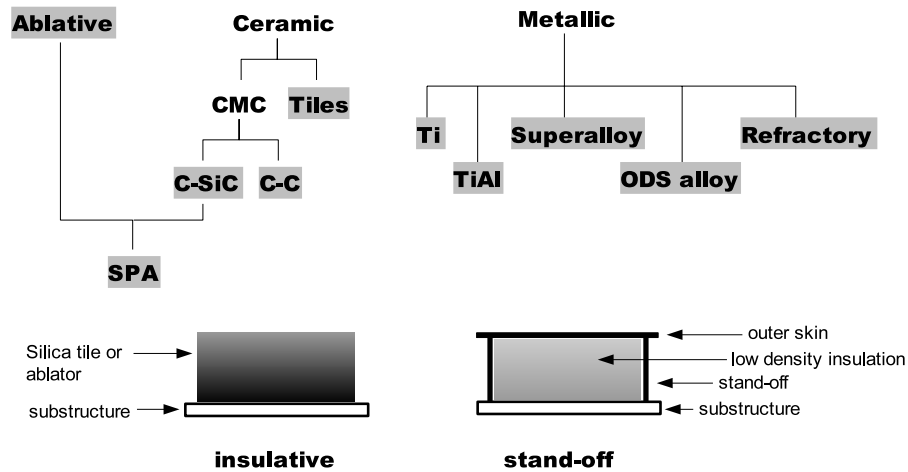


Figure 1-3: Classification of TPS by material type and principle of insulative and stand-off TPS

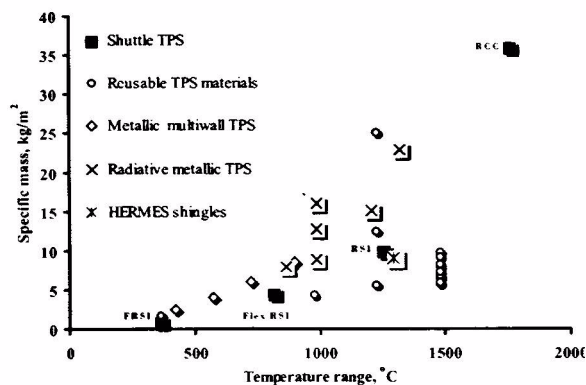
The different TPS material classes and materials that are in use today are shown in Figure 1-3. UHTC is not in this figure; it would be another class of Ceramic TPS next to CMC and Tiles. SPA stands for Surface-Protected Ablator.

The figure also shows the difference between insulative and stand-off TPS. The insulative TPS carries the thermal load, and to a limited extent the aerodynamic load, in addition to providing insulation for protection of the substructure from the high temperature at the outer surface. In stand-off TPS, the outer skin carries the thermal and structural loads, but the insulation of the substructure against the high temperature is done by dedicated low-density insulation material. This allows for optimising the outer skin material for strength and stiffness, and the insulation for maximum efficiency per unit of mass.

Modern low-density insulation that is used in this concept is very effective, and the stand-off supports become major heat leaks to the interior. Careful design to minimise this heat leak is essential (see e.g. [13]).

Figure 1-4 shows mass versus operational temperature limit for some TPS types. It is somewhat dated; it does show that the metallic TPS options, while being more or less in line with the general trend, are on the heavier side of the scale. Blosser [13] presents an

optimised metallic TPS reaching 5.2 kg/m^2 for a peak temperature of 1000°C , showing a large reduction in specific mass compared with the earlier metallic TPS concepts.



Ceramic tiles

Ceramic tiles were developed initially at Lockheed in the 1960s. They consist of mainly fibrous Silica formed into low-density bricks which have a very low thermal conductivity, but are also very fragile and brittle. Available in several densities they have, over the years, been improved by adding a tougher outer coating (resulting in the so-called TUFIT tile, Toughened Uni-Piece Fibrous Insulation) that significantly reduces occurrence of damage from minor impacts [22]. The tiles exhibit minimal thermal expansion, so they are limited in size and mounted on pads that eliminate stress from the underlying structure which does exhibit more expansion.

Tiles and blankets need to be re-waterproofed between flights [23]. Based on Space Shuttle experience, tiles are considerably less costly than C-C hot structure [40]. On the Space Shuttle, all tiles have their individual shape, so all are different, which is one of the factors that make maintenance of the TPS extremely costly.

Flexible blankets

These are a flexible version of the ceramic tiles, using Silica fibers encased in woven cloth of the same [22]. The advantage over the tiles is that the blanket can be made and applied in larger sizes, reducing the part count. Also, the brittleness problem is much reduced. Blankets are used on the leeward sides of the Space Shuttle, and were planned for the X-33 and X-38 as well (also on leeward sides).

Blankets have been produced in various types for temperatures up to 1100°C [8]; they are damage-prone, require water-proofing and are too rough to use on areas with thin boundary layer (i.e. the windward side), where they would trigger transition to turbulent flow [79]. Currently, development of blankets covered with CMC materials is underway. This also increases the maximum application temperature to 1000-1100°C, and allows the application on the windward side with much reduced problems regarding boundary layer transition.

Ceramic Matrix Composites (CMC's)

Ceramic Matrix Composites consist of a fiber, Carbon or Silicon Carbide, in a ceramic matrix of e.g. Carbon or Silicon Carbide. This gives the combinations currently in use and/or development: C-C, C-SiC and SiC-SiC. Production of these materials is rather complex, and great care must be taken to prevent oxidation of the Carbon fibres. The high brittleness causes cracks to appear, which can lead to oxygen reaching the carbon fibres inside the material.

C-C has higher density and lower strength than C-SiC [96]. It can in some way be seen as a predecessor of this newer material, though C-C has higher temperature capabilities.

C-SiC needs a coating to prevent oxidation at temperatures above 500°C. Coatings are available to protect the material. It is not clear how long these coatings last; tests up to 6 hours at high temperature have been successfully performed [24]. Nevertheless, oxidation protection is a difficult and laborious process. For example, any holes drilled in the finished product for e.g. connectors need to be re-coated with a special slurry coating to prevent oxidation.

The best solution by 1998 was a multilayer coating of first thermoviscose, then $\text{SiO}_2\text{-ZrO}_2$ deposited by physical vapour deposition. This coating was tested to 1600°C and showed little degradation after 20 cycles [6].

High cost and long duration of fabrication (factors which are of course related) is another disadvantage [53]. More recent developments like Liquid Polymer Infiltration replacing the Chemical Vapour Deposition used before are reducing the cost of production [90].

A very attractive characteristic of C-SiC is the low thermal expansion. [70] quotes thermal expansion of 0.065% at 500°C, 0.19% at 1000°C and 0.36% at 1500°C for Sepcarb-Inox C-SiC material. Emissivity is 0.8 at all temperatures and density about 2 kg/dm².

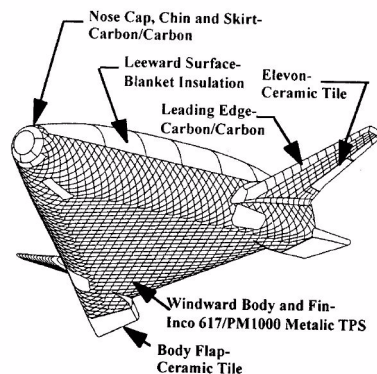


Figure 1-5: X-33 TPS types and distribution (from [68])

C-C is used on the Space Shuttle for the nose cap and leading edges and was to be used for the same areas on the X-33. C-SiC has been flown on the Express capsule in the form of a tile at the stagnation point, and as part of the surface-protected ablator of MIRKA. On the X-33 the elevons and body flaps were to be made of C-SiC (see Figure 1-5), and on the X-38 the nose cap, leading edges and body flaps. These components have been produced and successfully ground-tested.

Metals (non-refractory)

Metallic materials for thermal protection systems are limited to a lower temperature range than ceramic TPS materials.

A major disadvantage of metals is their relatively large thermal expansion coefficient which leads to thermal stresses and to mismatching of parts. Gaps between parts of the TPS exposed to the flowfield need to be minimised, in order to avoid tripping the boundary layer to turbulent flow. For the X-38 vehicle, requirements to gaps in the nose TPS structure are that gaps are to be less than 1mm wide and no forward facing step of more than 1mm or backward facing step of more than 2mm shall be allowed [89].

Metallic TPS materials are Titanium (limit temperature about 450°C), intermetallic γ -TiAl (Titanium Aluminide, limit temperature about 850°C), Nickel-Chromium superalloys (limit temperature about 1000°C) and Oxide Dispersion Strengthened superalloys (limit temperature up to about 1250°C). Future developments are intermetallics [98] like Molybdenum and Titanium Silicide and Nickel and Iron Aluminides which could lead to high temperature resistant alloys with lower density than the rather heavy superalloys and ODS alloys. Molybdenum Silicide appears to be useful to 1600°C [65].

Refractory metals

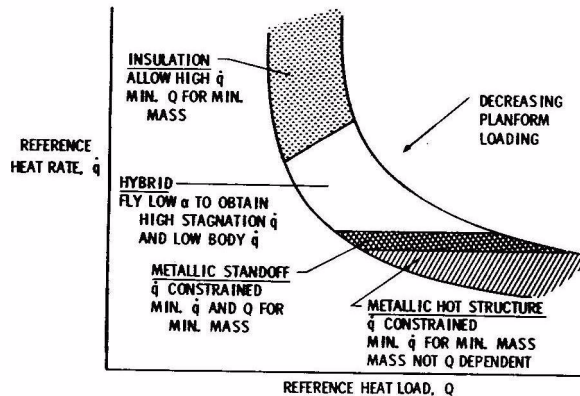
These are metals like Tungsten, Molybdenum, Niobium (a.k.a. Columbium) and Tantalum. They have very high melting temperatures, but are also very heavy and need oxidation protection coating. The X-20 was to use a coated Molybdenum heat shield for the windward side of the vehicle. These days, refractory alloys are no longer considered for TPS applications, except for specialty applications for small parts.

Insulation

CMC and metallic TPS need insulation to protect underlying structure from the high temperatures reached by those materials.

The most common option is low-density fibrous insulation based on Silica (temperature limit some 815°C [33]) and Alumina (limit 1425-1600°C). A more recent development is Internal Multilayer Insulation (IMI) based on layers of highly reflective foil operating in a similar way to the external multilayer insulation on satellites, by blocking radiation heat transfer. This can be used to over 1700°C [33]. It is also much lighter than fibrous insulation, at 1.4 kg/m² vs 4.4 kg/m² for the fibrous insulation in the X-33 case.

Figure 1-6 shows how different types of TPS are suited for different combinations of peak heat load and integrated heat load.



Typical SSTO entry trajectory heating characteristics for four classes of TPS.

Figure 1-6: figure from [97]

1.2.3 The ultimate goal: a cheap launch vehicle

Much effort has gone into the development of a launch vehicle that is significantly cheaper in price per kilogram delivered to orbit than the past and current expendable launchers.

The only (partially) reusable launch systems that made it to flight to date are the American Space Shuttle and the Soviet Buran system, of which only the Space Shuttle is used regularly. Even though it is technologically successful (to what level will not be discussed here), it did not achieve the cost reduction that was the objective, partially because of a much reduced launch rate compared to original plans, partially because of the very high

maintenance effort required. A maintenance burden of nearly 32,000 man-hours per flight was quoted for the Space Shuttle [60], or even 40,000 hours per flight [12].

Since then, many studies have been performed or are under way with the goal of eventually developing a low-cost reusable launch system. Examples are the X-30 / National AeroSpace Plane and the X-33 / VentureStar in the USA, the European Future Launcher Technology programmes (RRL, FLTP, FESTIP), the German Sänger and the Japanese HOPE-X. Not going into the different opinions on what the cost level of a future vehicle should be, whether there would be sufficient demand and what such a vehicle should look like, some general remarks can be made.

It is generally recognised that for a radical reduction in launch cost, the launch vehicle should be reusable, either fully or to a large extent, in order to recover the expenses of building the vehicle(s). Typically, a goal of 50 or 100 flights is set, during which the components should nominally not need replacement [41],[74]. Secondly, the cost of operating such a launcher should be minimised. With respect to the TPS, this means using a system that requires minimal maintenance and check-out in between flights. To quote Russo: “the cost of transportation to space by shuttle-type vehicles depends to a great extent on the effectiveness of the TPS. To minimize cost, the TPS must be fully reusable and have a long service life” [76]. Using a single-stage ‘transatmospheric vehicle’ like the X-30/ NASP proposed in the 1980s was also expected to reduce the operating cost, to 1/100 of that of the Space Shuttle [57]. Since then, it became clear that the technology level is not yet there for such a single stage airbreathing launcher.

A second trend is that of a smaller vehicle just for ferrying astronauts to and from orbit, specifically the International Space Station (ISS). Such a vehicle can be made reusable, making use of the same TPS technologies that can be used for a reusable launcher. Examples of these vehicles are the X-38/CRV and the Orbital Space Plane (OSP).

Both the large reusable launcher and the smaller astronaut ferry vehicles will be used here as operational examples for the use of metallic TPS. With regard to TPS, an important difference between these two classes of vehicles is the level of thermal loads. The large vehicles have a low specific mass upon re-entry because of the large empty propellant tanks, leading to a low ballistic coefficient and thus lower heat load. The smaller X-38 like vehicles have no propellant tanks, and therefore a much higher density and ballistic parameter, resulting in higher thermal loads.

1.2.4 Types of vehicle shapes and related TPS types; classes of re-entry vehicles

Ballistic capsules

A ballistic re-entry is by definition one without lift. The heating depends mainly on entry velocity and angle, furthermore on the ballistic parameter, which determines how deep the capsule will penetrate the atmosphere before the major deceleration takes place, and finally on the nose radius. The time of heating is quite short, so heat sink solutions can be applicable, and have been used. For single-use vehicles, ablators are often used, since they provide good protection also against high thermal loads, at relatively low cost.

The DART and Expert missions are ballistic, and there the demand for clean boundary layer flow drives the choice for non-ablating TPS, in case of DART fully metallic. Other examples of ballistic re-entry capsules are military warheads, planetary landers (Viking, Pioneer-Venus, Mars Pathfinder, Galileo Jupiter probe etc), MIRKA and EXPRESS.

For ballistic capsule applications, metallic TPS is not a logical option except in special circumstances like the DART/Expert non-polluted boundary layer requirement, or where testing of metallic material or TPS is a mission goal.

Low L/D re-entry vehicles

These are re-entry vehicles with a hypersonic L/D lower than 1 that have some limited cross-range capability and can reduce the g-load and thermal load by applying some lift. The most used vehicles of this class were designed for manned missions where low g-loads are desirable; examples are the Apollo capsule, the ARD (Ariane Re-entry Demonstrator, a copy of the Apollo shape) and the Soviet-Russian Soyuz and its Chinese derivative Shenzhou.

Like ballistic capsules, these vehicles are not a logical candidate for metallic TPS, since they are not reusable (up to now). Also, the windward heating rates are too high for metals. For leeward applications on a reusable capsule, metallic TPS could be an option.

Moderate L/D re-entry vehicles

Moderate L/D is here defined as having a hypersonic L/D of 1-2. This class contains lifting bodies (ASSET, X-23, X-33, X-38) and blunt-nosed gliders such as the Space Shuttle and Buran.



ASSET [101]

ASSET on Thor launcher [102]

X-23 PRIME [104]

Figure 1-7: US lifting body re-entry vehicles of the 1960's

ASSET (see Figure 1-7) was a test vehicle in the US Air Force lifting body research programme in the 1960's and 6 flights were made from 1963 to 1965 [94][101]. One was recovered. There were two types for Aerothermodynamic structural studies (ASV) and aerothermoelastic studies (AEV). 4 ASV and 2 AEV were built and flown.

Three X-23 PRIME (see Figure 1-7) lifting bodies were flown in 1966-67 [94]. One was recovered successfully. It was protected by a spray-on ablative heat shield. It is a small scale version of the X-24A vehicle, of which the much later X-38 was a scaled-up version.

Russia flew the BOR-4 test vehicle in the development programme of the Buran shuttle to test heat shield materials in four flights from 1982 to 1984. Earlier, the BOR-1, 2 and 3 were flown suborbitally in the Spiral space plane research programme [101]. The timeline of the Russian and American hypersonic flight programmes are given in Figure 1-8. Japan flew the Hyflex test bed in 1996 in the development effort for the HOPE-X shuttle.

These flights are the full flight experience of lifting body re-entry vehicles to date. A large number of vehicles have been proposed or are still under study, but to date none have made it to an actual flight.

The small lifting bodies from Asset and X-23 up to the size of X-38 have a fairly high ballistic coefficient and therefore high thermal loads. The large lifting bodies of the X-33 class and larger have much lower ballistic coefficient but a much larger surface area.

Metallic TPS is certainly applicable to the large vehicles, and NASA's choice for metallic TPS for the X-33 indicates that it is a favourable choice for this class of re-entry vehicles. The smaller vehicles are often one-off research missions, mostly with the goal of testing some sort of TPS material. Since reusability is not a major requirement, the choice for metallic TPS is less obvious here.

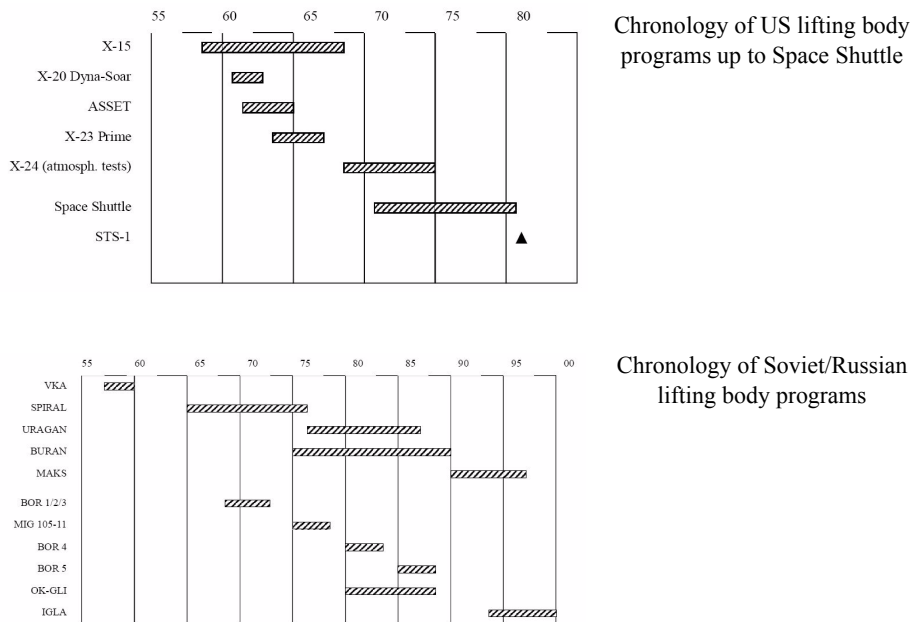


Figure 1-8: Timelines of US (top) and Russian (bottom) lifting body programs

High L/D re-entry vehicles

High L/D vehicles are defined as those in which extraordinary effort has been taken to increase the L/D parameter for improved flying characteristics or reduced thermal load. The high L/D requires reduced drag, so small radius nose and leading edges compared to more 'classical' shapes like the Space Shuttle and X-33 and X-38-like lifting bodies. Airbreathing

hypersonic transports and transatmospheric vehicles like the X-30 typically have sharp leading edges and nose to allow extended flight through the atmosphere.

No high L/D re-entry vehicles have flown to date. The X-43 scramjet test vehicle can be considered to be in this class; it was tested to Mach 10, but only for a very short period. Thermal protection was a large refractory alloy nose with a heat sink for the body combined with CMC leading edges.

The sharp nose and leading edges lead to very high local heating rates, which require either very high temperature materials, like the Ultra-High Temperature Ceramics (UHTC) currently under development e.g. in the USA and Italy, refractory metals, or actively cooled structures.

Some examples of high L/D vehicles studied in the past are the Ames Mach-10 demonstrator configuration B which achieved high L/D by putting the fuselage under the wing [42]. This also led to severe heating problems due to flow interactions. Cooled TPS was considered, as were advanced Niobium and Molybdenum-based alloys.

The X-20 Dyna-Soar (~1960-63) was to be a one-man spaceplane with metallic and refractory alloys TPS, superalloy hot inner structure and water-cooling for crew and equipment compartments. Development was stopped before a prototype was completed but many subsystems were built and tested [35].

In the 1980's, the US attempted the development of a large airbreathing single-stage to orbit spaceplane; the National AeroSpace Plane (NASP) with its experimental predecessor the X-30. A large effort went into developing systems, among which TPS, for this vehicle. CMC materials and Titanium Aluminide intermetallic alloys were among the TPS options. The hottest parts would be regeneratively cooled by the Hydrogen fuel. In more recent years, USAF studies in such vehicles are being conducted, but little is disclosed in open literature.

More recently, NASA-Ames proposed a high-L/D version of the X-38 Crew Return Vehicle, using the UHTC materials under development there. This Sharp-CRV would have significantly improved flying characteristics compared to the X-38 CRV [43]. A similar approach to reach improved flying characteristic and also reduced thermal loads by decelerating at high altitude is proposed by Monti et al in [59].

1.2.5 Hot structures

A hot structure can be defined as a structure that carries both (high) thermal and mechanical loads. These are the most challenging structural parts of a reusable launch vehicle to develop

[91]. Insulating material is added inside when an inside structure or component needs to be protected from high temperatures. Note that this might not always be necessary; e.g. a control surface can be envisioned which does not contain internal parts that are not high-temperature resistant, thus consisting entirely of one large hot structure.

Typical hot structures in an RLV are the nose cap, leading edges and control surfaces. The design of hot structures also includes fasteners, fittings, stand-offs, seals, bearings (on control surfaces), insulation and the interface to the cold structure. Hot structures can oftentimes provide the minimum weight design possible, and even the only feasible solution if the available thickness is small [23].

The Dutch space industry has concentrated on developing metallic hot structures for control surfaces applications, resulting in a rudder for the X-38 vehicle and several ‘building blocks’ of a large rudder for a generic RLV, using the German Hopper RLV concept as a design example.

Technological challenges are the thermal stresses and resulting deformations, coupled with ‘normal’ loads. Issues to be taken into account in design of a hot structure are [96]:

- surface temperature (function of heat load, emissivity, catalicity, thermal mass)
- thermal stresses
- mechanical loads
- shape distortion by thermal and mechanical stresses
- mounting on primary structure that can cope with thermal expansion
- thermal insulation to primary structure
- allowing thermal expansion in panel-to-panel joints (need for gaps or sliding connections)
- sealing of gaps against inflow of hot boundary layer gasses
- assembly, inspection, disassembly aspects
- chemical effects (oxidation).

1.2.6 Current developments, non-metallic TPS

Ceramic Matrix Composites

First generation CMC material Carbon-Carbon is supplanted by C-SiC. Oxidation protection is still a major problem, especially in combination with small damage. Cracks expose the Carbon fibers which are prone to oxidation. Self-healing coatings are under development but success is limited.

SiC undergoes ‘active oxidation’ above a certain combination of temperature and Oxygen partial pressure, where gaseous oxides are produced, thereby removing material from the substrate. Obviously, this is to be avoided in operational use.

Oxide-oxide CMC consists of Nextel fibers in an Oxide matrix (Alumina or Silica) and can be produced at much lower cost than C-C or C-SiC because no pyrolyzation is required, but rather a simple lay-up process as with fibre-reinforced plastics [24].

Ultra-High Temperature Ceramics (UHTC)

A new class of ceramic TPS materials is under development at NASA and other places [74], so-called Ultra-High Temperature Ceramics (UHTC). These materials have a very high melting point, up to 2760°C, high thermal conductivity, thermal shock and fatigue resistance and low thermal expansion. A typical application for these materials is sharp nose caps and leading edges, where the very high heating rate is sustained through the rapid conduction of heat away from the stagnation point combined with re-radiation some distance behind.

The material appears to be quite fragile and brittle, as well as very heavy. Applications will be limited to very small areas in the stagnation regions. There, it is a competitor to directly cooled TPS solutions.

Blanket TPS

Conformal Reusable Insulation (CRI) is a new development based on flexible blankets, now covered with a CMC layer to increase operational temperature limits and increase smoothness. Various levels of smoothness and temperature limit (1000-1200°C) are available, and are baselined for the X-37 experimental re-entry vehicle [79].

The blanket that is used as an insulator below the CMC here is of higher density than would be used in CMC or metallic tile TPS; the would be supposedly offset by an increase in robustness and ease of handling. Also the blanket could provide some support to the CMC shell which could then be lighter since it does not have to support all the loads imposed on it.

1.3 Motivation for using metallic TPS

It is time to investigate why metallic TPS is an attractive option for re-entry vehicles. A number of characteristics of metallic TPS can be given:

Robustness

The inherent ductility of metals when compared to ceramic materials give metals an advantage in robustness. Small impacts or strikes are dealt with through the elasticity and deformation of the material rather than by cracking or breaking.

Oxidation resistance

In the highly oxidizing environment of re-entry most materials can not stand exposure to the flow without some sort of protective coating, be it the oxide of the material itself or a separately applied coating. When the coating is breached it exposes the base materials to oxidation, and unless there is a component that can form a new barrier, this degradation will continue and can lead to failure.

Metallic alloys that are candidate TPS materials like Nickel-Chromium superalloys or Titanium Aluminide form a protective oxide layer which seals the base material from further oxidation, or at least reduces the oxidation rate to a very low level which can be sustained for a large number of mission cycles. This oxide layer is self-healing, meaning that any scratch that occurs is sealed by oxidation of the exposed material, thereby restoring the protective coating.

For temperatures up to some 900°C, intermetallic γ -TiAl seems to be very attractive, due to its good oxidation protection and low density (3.9 g/cm³); for higher temperatures Oxide-Dispersion Strengthened iron and nickel base alloys are most attractive, though their density is much higher (around 8 g/cm³).

Carbon based ceramics are sensitive to oxidation and need protection by a coating which is subject to damage. Development of self-healing coatings is pursued, but it remains to be seen how successful this will be.

Maintenance / inspection

In direct relation to the robustness and oxidation resistance, the inspection and maintenance effort for metallic TPS promises to be much less than for Ceramics. This is where a large cost benefit is to be had; the Space Shuttle TPS requires thousands of man-hours of maintenance every mission and if this can be reduced to a minimum, large savings are to be gained.

The self-healing properties mean that the TPS does not require careful inspection for minor scratches or cracks, since they would not lead to critical material degradation and failure. This drastically cuts down required inspection time.

Design / production

While design of metallic hot structures is a difficult process, with all the problems of thermal expansion and thermal stress, a large body of knowledge exists in constructing flight vehicles from metallic materials. Existing forming and joining methods can be applied. Production of Ceramic materials on the contrary is very expensive at the moment.

Cost

Metals hold the promise of drastically reducing maintenance cost, as well as being attractive from a mass standpoint [91]. For design and production metals might be cheaper than ceramics, but this picture is a complicated one. Metals are probably more costly in base material (base material for CMC being considered before actual production of the CMC part), cheaper in production and possibly more expensive in design and analysis, though this is difficult to quantify, because little or no cost data is available, and in any case, most current work is at prototype level, not representative for a production phase.

1.4 Advantages of high L/D vehicles and TPS aspects thereof

1.4.1 Advantages of high L/D

Cooling of the TPS allows for using it at increased thermal loads. This capability can be used to reduce the radius of the nose and/or leading edges, since the heat load is inversely proportional to the square root of this radius.

Sharper nose and leading edges lead to lower drag, which in turn gives a higher lift-to-drag ratio. For comparison, the Space Shuttle has a hypersonic L/D of about 2 [88]. This ratio is a defining parameter in a number of vehicle characteristics, and increasing it gives the following advantages.

Less drag during ascent

The drag is reduced also during ascent, “thus providing consistent saving in the cost per mass expended to put payloads into orbit” [59],[74],[91]. Especially for launch vehicles

which use lift during ascent; i.e. which do not lift off vertically until they leave the dense atmosphere, drag losses are substantial, and reducing them reduces the amount of propellant needed to achieve orbit, which in turn reduces vehicle size for the same payload. In fact, low drag is essential for this kind of vehicle to be able to reach orbit at all.

Cross-range

High L/D gives high range and cross-range during re-entry; global range can be reached with a hypersonic L/D of 3.23. Making turns does increase the heating rate, so manoeuvres need to be planned away from the point of maximum heating. A 90° turn leads to 30% increase in heating; 180° to 40% increase [88]. The manoeuvrability is increased [74],[91] and better low-speed flying characteristics are achievable [82].

More re-entry options / fewer landing sites

Since high L/D gives high longitudinal and cross-range, from a given re-entry point more landing sites are reachable, or inversely, a given landing site can be reached from more orbits. So, manoeuvrability enhances mission flexibility and increases the choice of landing sites [88]. Especially for manned spacecraft, this flexibility is of great importance, because it has a large positive impact on mission risk.

Cross-range improvements also affect launch aborts, increasing safety [91]. It reduces or eliminates so called ‘dead zones’; periods during the ascent where no recovery of the vehicle is possible in case of an engine, or other in itself non-catastrophic, failure.

Lower g-forces and heating

Lift can also be used to alleviate the deceleration loads and aerodynamic heating accompanying atmospheric entries [88]. Because lift enables the vehicle to delay sinking into the denser parts of the atmosphere and decelerate at higher altitude, heating rates are lower, being proportional to the square root of air density times the third power of velocity.

The lower drag does mean that deceleration is spread over more time, so the deceleration is lower, but the integrated heat load over time will be larger. At the end of the day, the same amount of kinetic energy has to be dissipated for a given vehicle mass.

A sharp nose and leading edge also reduce thermal loads because of boundary layer thickening. The very tip of the nose and leading edge experience high thermal loads, but these quickly drop off to relatively low values at some distance behind them [58].

Figure 1-9 shows that metallic hot structure re-entry vehicles decelerate at high altitude, to minimise the heating rate. Higher lift enables this sort of trajectory.

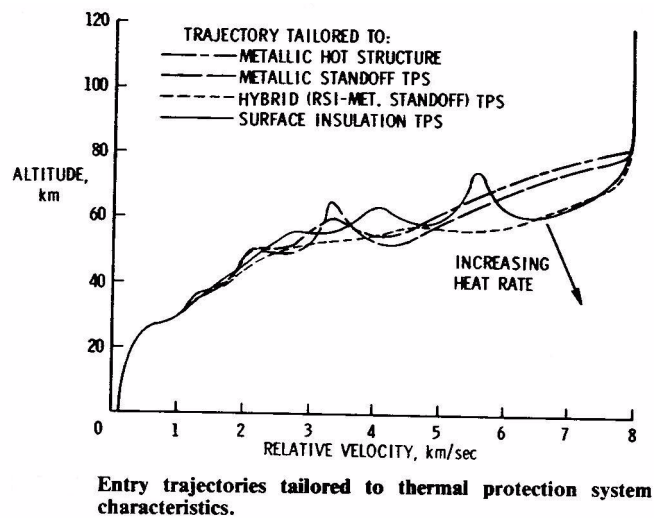


Figure 1-9: figure from [97]

Black-out

Sharp leading edges minimize the interference with radio frequency transmissions during re-entry thus minimizing black-out [74],[91], during which communication between ground control and the re-entering spacecraft are impossible.

Conclusion

The sharp leading edge and nose technology would enable several vehicles [69]:

- airbreathing ascent concepts such as rocket based combined cycle (RBCC),
- catapult and maglev launch assist,
- global cross-range reentry bodies.

1.4.2 Disadvantages and problems of sharp nose and leading edges

The relation between nose or leading edge radius and heating level

The thermal loads on the nose and leading edges are proportional to the nose radius:

$$\dot{Q} = \frac{C}{\sqrt{R_N}} \sqrt{\frac{\rho_\infty}{\rho_0}} \left(\frac{V}{V_C} \right)^3 \quad (1.2)$$

where C is a constant, R_N is the nose or leading edge radius, ρ_0 and ρ_∞ are the air density at sea level and in the undisturbed flow at the actual altitude, V is velocity and V_C is the circular (orbital) velocity for the actual altitude.

Clearly, reducing this radius will lead to increased thermal load if all else is equal. Reduced nose and leading edge radius will lead to lower drag, and thus higher L/D, allowing the vehicle to fly a higher-altitude re-entry, which reduces the air density part in the equation, giving an effect of reducing the thermal load. This can partly balance the increase due to the reduced radius.

Packaging

A more ‘pointy’ vehicle has less internal volume with respect to its length or width/span. To accommodate the same amount of equipment and payload, the sharp-nosed vehicle will be larger than a more blunt vehicle (a sphere being the other extreme of course). A high L/D vehicle will have a larger surface area than a blunt one, so more square meters of TPS.

In general, it can be stated that a sharp-nosed vehicle will in general be more expensive than an equivalent blunt-nosed one, with respect to design and production. This should be offset by superior performance and/or lower operational cost.

1.4.3 Past studies of high L/D vehicles

X-15

The X-15 was an experimental rocket aircraft designed to investigate hypersonic flight to Mach 6-7. X-15 reached the following temperature limits: leading edge 1588K, body 810-1150K, nose 1270K. Materials used were mainly Titanium, with ablative coatings for higher speed flights [42]. Maximum speed that was reached was about Mach 6.7. The construction was a hot structure.

X-20

X-20 was a project for a small single-seat spaceplane launched by an expendable rocket. Operational vehicles were envisioned for reconnaissance and strike missions. 13000hrs of wind tunnel tests were performed (1800 subsonic, 2700 supersonic, 8500 hypersonic). Hypersonic L/D was 1.5, hypersonic C_L 0.6, cross range was expected to be 2800 km.

While the X-20 does not have an L/D of more than 2, it is considered to be a high L/D vehicle, especially considering the time of its development

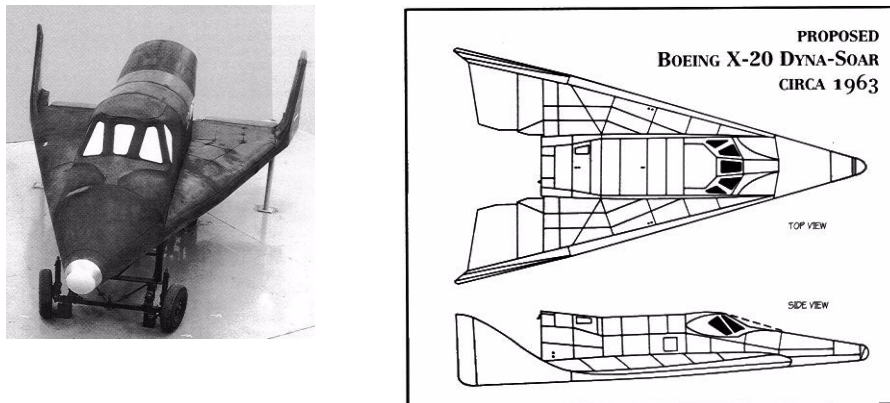


Figure 1-10: Boeing X-20 [42]

SHARP-CRV

SHARP-CRV is a conceptual study for a Crew Return Vehicle making use of Ultra-High Temperature Ceramics to enable sharp nose and leading edges in order to increase the L/D and thereby the flying characteristics. Much enhanced performance was shown in a series of papers published on the study [43],[44],[71],[75].

SHEFEX

The Sharp Edge Flight Experiment (SHEFEX) is a German DLR-led project for a re-entry test vehicle to show the advantage of a sharp-edged faceted shape. Based on the idea that an

economical reusable TPS requires advances in maintenance, inspection, repair and production, which encourage using flat panels of standard sizes, the vehicle TPS is faceted [95]. This is in fact not a high L/D vehicle but it does show a sharp nose / leading edges.

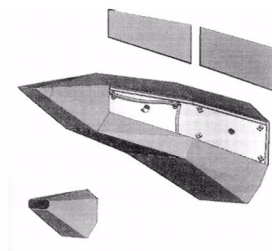


Figure 1-11: the SHEFEX vehicle showing the faceted TPS panels and the single-piece nose cone.

A faceted version of the Hopper RLV concept was also looked at in a superficial way. It was expected that the performance of this version would not be much different than the original rounded version, while cost for the TPS of the studied section (the front one-third of the vehicle) was expected to be 45% lower by using 70 flat panels instead of 20 curved ones [95].

1.5 Objectives of this research

This thesis describes the results of the development effort for the cooled metallic thermal protection system that was invented at TU Delft by the author and Tom van Baten in 2000. The objectives of the research that is described in this thesis are the following:

- Advance the technology readiness level of the cooled metallic TPS to a higher level.
NASA uses a definition with a scale of 1 to 9 for this. Since level 6 involves flight testing in a relevant environment, that can not be reasonable expected within the time and cost constraints of this work; level 4 or 5 are more realistic goals involving component/bread board validation in laboratory and relevant environments respectively. See below for a complete overview.
- Give an as complete as possible theoretical basis to the behaviour of the TPS.
- Provide engineering models and finite element models that can be used in designing with this TPS.
- Perform tests to validate critical aspects of the behaviour of the system and determine critical parameters.

On the Development of a Cooled Metallic Thermal Protection System for Spacecraft

- Perform supporting research and tests on e.g. materials used in order to be able to model and design with reasonable margins for material properties, and to answer specific questions regarding the viability of aspects of the cooling system (e.g. behaviour in vacuum).
- Provide a clear case for the usefulness of the system in future operational applications.

Technology Readiness Level

NASA defines Technology Readiness Levels as follows [62]:

TRL 1	Basic principles observed and reported. Basic properties of algorithms, representations & concepts. Mathematical formulations. Mix of basic and applied research.
TRL 2	Technology concept and/or application formulated. Basic principles coded. Experiments with synthetic data. Mostly applied research.
TRL 3	Analytical and experimental critical function and/or characteristic proof-of-concept. Limited functionality implementations. Experiments with small representative data sets. Scientific feasibility fully demonstrated.
TRL 4	Component and/or breadboard validation in laboratory environment. Standalone prototype implementations. Experiments with full scale problems or data sets.
TRL 5	Component and/or breadboard validation in relevant environment. Prototype implementations. Experiments with realistic problems. Simulated interfaces to existing systems.
TRL 6	System/subsystem model or prototype demonstration in a relevant environment (Simulated or Operational). Prototype implementations on full scale realistic problems. Partially integrated with existing hardware/software systems. Limited documentation available. Engineering feasibility fully demonstrated.
TRL 7	System prototype demonstration in an operational environment. Most functionality available for demonstration and test. Well integrated with operational hardware/software systems. Most software bugs removed. Limited documentation available.

Chapter 1: Scope and introduction to Thermal Protection Systems

TRL 8	Actual system completed and “operationally qualified” through test and demonstration (Simulated or Operational). Thoroughly debugged software. Fully integrated with operational hardware and software systems. Most user documentation, training documentation, and maintenance documentation completed. All functionality tested in simulated and operational scenarios. V&V completed.
TRL 9	Actual system “operationally proven” through successful mission operations. Thoroughly debugged software. Fully integrated with operational hardware/ software systems. All documentation completed. Successful operational experience. Sustaining software engineering support in place. Actual system fully demonstrated.

This chapter will provide an overview of metallic TPS, starting with the basic operating principles. An overview of metallic TPS candidate materials is given with some properties, advantages and disadvantages. The material PM1000 which was used in the research for this thesis will be treated in more depth.

A historical overview of the use of metallic TPS is given, necessarily mainly limited to studies, since flight experience is very limited to date. An overview of earlier cooled TPS concepts is given as well, to show what kind of ideas were proposed in the past. Finally, the cooled TPS concepts that have been studied at the Faculty of Aerospace Engineering of Delft University of Technology will be introduced.

2.1 Aerodynamic heating & re-entry

2.1.1 Aerodynamic heating

The level of aerodynamic heating that is encountered by a re-entry vehicle depends on a large number of variables. For Earth re-entry missions from Low Earth Orbit, the major part of the heat flux is the convective heating from the hot boundary layer flow. The level of heating depends on the temperature gradient in the boundary layer close to the wall. This gradient depends on the temperature difference between the wall and the hot outer flow, and on the local thickness of the boundary layer (also on the catalicity of the material, more on which later). This is the basis of film cooling, where a fluid is introduced into the boundary layer, thereby thickening it, and thus reducing the temperature gradient. The water vapour from the water-cooled TPS could be used for this.

At high velocities, for Earth entry more than about 10 km/s, radiative heating by the ionised gas around the vehicle starts to become important. Because the TPS under consideration in

this thesis is meant for reusable launchers, which do not reach such high velocities, this aspect is disregarded.

The chemistry of the flow plays a role as well. In the shock, air is dissociated to some extent, and the atomic constituents of this plasma can recombine to molecules, releasing the energy that went into the dissociation in the first place. If the wall material is catalytic, it encourages this recombination to take place at the wall, and the energy to be released to the wall, leading to an increase in incident heat flux. Catalicity is a material characteristic, which is typically low for ceramic materials and high to very high for metals. Fully catalytic means that recombination is instantaneous; Copper is a material that is very close to being fully catalytic. PM1000 (in its oxidised state) has fairly low catalicity for a metal; this is because of the Chromium Oxide on the outside of the material.

A simplified relation for the convective heating in the stagnation point of a re-entry vehicle is given by:

$$\dot{Q} = \frac{C}{\sqrt{R_N}} \cdot \left(\frac{V}{V_c}\right)^3 \cdot \sqrt{\frac{\rho}{\rho_{sl}}} \quad (2.1)$$

where \dot{Q} is the applied heat load,

C is a constant,

R_N is the nose radius of the re-entry vehicle

V is the velocity and V_C the circular velocity (the velocity needed to maintain a circular orbit for a given altitude)

ρ and ρ_{sl} are the local and sea-level air density, respectively.

From this equation it can be seen that heating reduces with larger nose radius, and increases when high velocity and high air density are combined. So, it can be concluded that a small nose radius will increase heating problems, and that decelerating must be done at the highest possible altitude, to minimise the product of the velocity and air density terms.

The altitude at which deceleration takes place depends on the ballistic parameter $\frac{W}{C_D A}$

(weight divided by the drag area), with high ballistic parameter leading to high thermal loads because a more massive (dense) vehicle will penetrate deeper into the atmosphere before decelerating. Introducing a lift force can keep the vehicle at altitude longer, and will reduce heating. This is more effective with higher lift-over-drag (L/D) which in turn requires a low drag, and that requires a small nose (and leading edge) radius.

First and foremost, the re-entry conditions determine the level of heating. In general, higher entry velocity and steeper entry (higher entry angle) lead to higher heat loads. Returning from low Earth orbit, the entry velocity is basically the orbital velocity, or some 7.6 km/s. Returning from higher orbits, or from beyond Earth orbit, will give higher entry velocities.

The entry angle is usually kept to a minimum to reduce heating problems, certainly for reusable vehicles which are the scope of this study. Too low an entry angle can lead to 'skipping' where the vehicle bounces out of the atmosphere, so the entry angle can not be reduced too much. A typical value is about 1.5° for the Space Shuttle.

2.1.2 Metallic TPS under aerodynamic heating

The reaction of a metallic TPS under the influence of heating is best described through an energy balance.

The incident heat flux, a combination of convective heating, radiative heating and the effect of recombination, is balanced by several components of this balance:

- heating up of material,
- conduction through the material to the interior and, possibly, sideways,
- re-radiation of thermal energy following Stefan-Boltzmann's law,
- phase change of material:

$$\begin{aligned} \dot{Q} = & c_p \cdot m_{TPS} \cdot \Delta T + k \cdot \delta_{insul} \cdot (T_{wall} - T_{interior}) + & (2.2) \\ & k \cdot x \cdot (T_{wall} - T_{(wall,2)}) + \\ & \sigma \cdot \varepsilon \cdot ((T_{wall})^4 - (T_{\infty})^4) + h_p \cdot m_p \end{aligned}$$

where the first term after the equal sign is the heating up, the second the conduction inwards, the third the conduction sideways, the fourth the re-radiation and the fifth the phase change.

Here c_p is the specific heat of the TPS (equivalent value summed for all parts),

m_{TPS} is the mass of the TPS,

ΔT is the rise in temperature of the TPS,

k is the thermal conductivity of the material,

T_{wall} is the wall (TPS skin) temperature,

$T_{interior}$ is the interior temperature,

$T_{wall,2}$ is the wall temperature off to the side of the point under consideration,

T_{∞} is the temperature of the outside environment ('space'),

x is the distance to that point off to the side,
 σ is Stefan-Boltzmann's constant,
 ε is the emissivity of the material,
 h_p is the heat of phase change,
 m_p is the mass of the phase change material.

When we consider that the level of applied heating does not change much along the surface, the sideways conduction can be neglected. Since light weight is essential for launchers, the minimum amount of material is used, also limiting the heat capacity to a minimum, and therefore the energy needed for heating the material can be neglected in a first approximation (unless a structure is evaluated where the heat sink effect was deliberately included). The skin material will be insulated on the inside, to prevent the heating up of the internal structure and components, so the heat transfer to the inside is also minimized. A first approximation then allows us to neglect this part as well. It must be noted that for short flights (ballistic flights) the heat sink effect can have a quite large influence.

For uncooled TPS, no phase change material is included, so to a first approximation, the energy balance reduces to a balance between incident heat load and re-radiated thermal energy, where the temperature of the background ('space') can be neglected with respect to the high skin temperature. This will allow us to immediately determine the wall temperature:

$$\dot{Q} = \sigma \cdot \varepsilon \cdot T^4 \Rightarrow T = \sqrt[4]{\frac{\dot{Q}}{\sigma \cdot \varepsilon}} \quad (2.3)$$

Obviously, with all the simplifications and assumptions made, this gives a upper limit estimation of the temperature.

2.1.3 Advantages & disadvantages of metallic TPS

To quote Wurster [97]: "Fairly large mass penalties are associated with the material changes required for increased temperature capability". Metallic TPS is different from Space Shuttle type ceramic tile and blanket TPS in that it decouples the structural function of maintaining the outer vehicle shape and carrying aerodynamics loads from that of insulating the underlying structure and components. This allows using materials that are optimised for each task, structurally efficient materials in combination with thermally efficient insulation [12]. Note that in some cases hot structures can do without insulation altogether. This can be done where there is no 'interior' which needs to be kept at lower temperature, e.g. in thin wing or control surface structures. It must also be noted that Ceramic-Matrix Composite

materials can use the same decoupled concept as the metallic TPS. The strong points of metallic TPS are robustness, low maintenance cost, no need for waterproofing and self healing oxidation protection (for suitable alloys).

2.2 Materials

2.2.1 Requirements to metallic TPS materials

The general requirements to TPS materials are given in section 1.2.1.

In the X-30 era (1980s), major issues that were identified were creep resistance, durability and damage tolerance, reusability, oxidation resistance, hydrogen compatibility, thermal stability, fabricability, joining and scale-up [28].

Since metallic TPS will compete with ceramics on the basis of its superior characteristics with respect to damage and robustness, TPS for a reusable launch vehicle that is expected to 'launch on demand' should be resistant to damage from ground handling impact, ice falling during launch, launch acoustics, weather, micro-meteoroid and space debris and oxidation and surface erosion during reentry [23]. All this will lead to reduced maintenance and inspection costs.

It should be durable, operable, cost effective and of low mass. Durable means resistant to damage and able to operate with some level of damage; operability includes ease of replacement, removal, repair and minimal maintenance (e.g. waterproofing) [12].

2.2.2 List of materials

An overview of TPS materials has been given in section 1.2.2. Here some metallic TPS materials will be presented in more detail. It is impossible to give a definitive overview of metallic TPS materials. Many materials have been developed for different applications, like use in gas turbines, and have been or can be applied for TPS applications, since many requirements to the materials are similar for different applications (namely high temperature capability and oxidation resistance).

The material used in the research presented in this thesis is PM1000, which will be treated in this section as well. This section will allow this material to be compared with some of the others that are available.

Superalloys

The website *stainless steel world* [103] gives the following definition for superalloys: 'Lightweight metal alloys designed specifically to withstand extreme conditions. Conventional alloys are iron-based, cobalt-based, nickel-based, and titanium-based.' Plansee defines them as alloys which exhibit high heat resistance even at temperatures up to 85% of their absolute melting point [56]. For TPS applications, extreme conditions can be read to mean high temperatures and oxidizing atmosphere.

For the temperature range from 800 to 1250°C, a large number of alloys with main constituents Nickel, Chromium, Iron and Cobalt have been developed. Well known brand names like Inconel and Hastelloy cover a range of materials that have been developed since the 1950s and are still being improved.

There is a wide range of strengths at intermediate temperatures; yield stresses range from 200 to 1000 MPa at 600°C, but all superalloys exhibit a dramatic drop in strength between 700°C and 1000°C, where yield stress ranges from about 30 to 150 MPa [19].

It must be noted that all of the Nickel-Chromium, Iron-Chromium and Cobalt based alloys are rather heavy at 8000 to over 9000 kg/m³ [38] so the 'lightweight' in the above definition is a rather dubious description.

Oxide Dispersion Strengthened (ODS) alloys

ODS stands for Oxide Dispersion Strengthened. These are alloys that are largely comparable to some superalloy, but with the addition of small particles of an oxide with high melting temperature; in the alloys used here, Yttrium Oxide. A small amount of 0.5-0.6% by mass is added to the alloy, and in order to get a homogeneous structure, the material is made by mechanical alloying (also known as powder metallurgy) where the base superalloys is ground down to a powder, mixed with the oxide additive, and then mechanically alloyed in a ball mill, followed by hot pressing. Melting the material would cause the oxide additive to concentrate at the grain boundaries where it does not give a positive contribution to the material properties.

The oxide particles block the movement of dislocations in the material, giving it high creep strength at high temperatures. Comparison with non-ODS superalloys shows that the ODS materials have higher strength at temperatures above about 1050°C .

ODS alloys used in the research program of the Dutch space industry are PM1000 and PM2000 made by Metallwerk Plansee in Austria/Germany. PM1000 is a Nickel-Chromium alloy, PM2000 an Iron-based alloy.

constituent (mass %)	Ni	Cr	Fe	Al	Ti	Y ₂ O ₃
PM1000	75.6	20.0	3.0	0.3	0.5	0.6
PM2000	-	19.0	74.5	5.5	0.5	0.5

Table 2.1 : chemical composition of PM1000 and PM2000

Intermetallics: TiAl

Gamma Titanium Aluminide (γ -TiAl) is a new material that is applicable at temperatures up to some 850-900°C [30]. Much development work on the material was done in the US NASP (National AeroSpace Plane, a.k.a. X-30) program in the 1980s. To quote Ellis: “titanium aluminides (..) are new generation materials that make the X-30 feasible” [28].

Since then, work has been done on improving the material, and now it is very competitive at temperatures from some 250°C to 800-900°C, with significantly higher specific yield strength than Nickel-based alloys. Indirect indications from the tests reported in [30] indicated very low catalicity and the tests show an emissivity of about 0.8. Its good characteristics and low density / high specific strength make γ -TiAl the most attractive material in its applicable temperature range of some 250 to 800-950°C. This will allow it to cover a large part of the surface of many concept RLVs.

Silicides and Nitrides

For temperatures above 1000°C to 1200°C, superalloys can no longer be used. For this range, Silicate materials could be applied [65].

MoSi₂ has a melting point of 2030°C, density of 6.24 g/cm³ and good oxidation resistance. Problems are low ductility below 1000°C, low fracture toughness and spalling of the oxide scale under thermal cycling. Some of these can be countered by adding Aluminium, to get an alloy with roughly equal proportions of Molybdenum, Silicon and Aluminium. These alloys

showed yield stress of 300-450 MPa at 1200°C, 100-150 MPa at 1400°C and about 50 MPa at 1600°C [36]. This compares very well with PM1000 which has a yield strength of about 110 MPa at 1200°C.

For aerospace applications (turbine engines) MoSi₂-Si₃N₄ composites are under development, and MoSi₂-SiC and MoSi₂-Al₂O₃ are also under study. MoSi₂-SiC has been measured to have a strength of 600 MPa at 1250°C (5-6 times higher than PM1000). All these materials need quite some additional development before they can be used in the same way as PM1000 is now used for TPS, so their potential for use is still very uncertain. The very high temperature capability makes them very interesting for possible future use.

Refractory alloys and metals

Refractory metals are Molybdenum, Tungsten, Niobium (called Columbium in America) and Tantalum. According to definition, these are alloys that, due to hardness or abrasiveness present difficulty in maintaining close tolerances. These elements have very high melting points, but also rather high density []:

Material	Melting temp. (°C)	Density (g/cm ³)
Niobium	2477	8.57
Molybdenum	2623	10.2
Tantalum	3017	16.4
Tungsten	3422	19.3

Table 2.2 : Refractory alloys

These materials need to be coated to protect them against oxidation. “Surface protection is the most significant obstacle to the widespread use of refractory metals in high-temperature oxidizing environments” [2]. Coatings are limited to some 1650°C and, up to those temperatures, the use of Tantalum and Tungsten are not justified, because lighter alternatives are available.

Refractory alloys are too heavy, too oxidation prone and too difficult to process into appropriate product forms to be prime candidates for TPS covering large areas of the vehicle

[41]. All in all it can be said that refractory alloys are currently not a serious contender for TPS applications, certainly not for applications covering a substantial area.

In conclusion, Figure 2-1 gives an overview of high temperature materials with their operational temperature ranges and strength. It shows that PM1000 has a higher operational use temperature than normal superalloys, but a lower strength than ceramics. Because ceramics also have a lower density, it is clear that there should be additional benefits apart from simply strength to justify the use of the ODS alloys. The justification of their use can be found in their resistance to oxidation and damage (the self healing properties of the protective oxide layer). More details on PM1000 are given in the next section.

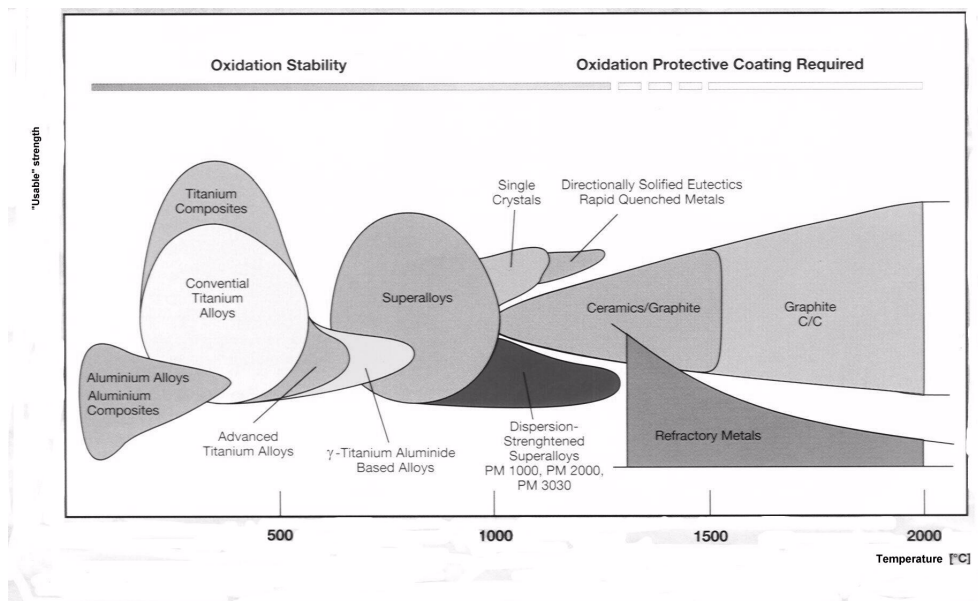


Figure 2-1: Operational use ranges of high temperature materials (from: [56])

2.2.3 Desired characteristics of materials of choice

The Dutch space community has been working for a number of years on hot structure technology for reusable launcher applications using the PM1000 and PM2000 alloys. The community consists of (in no particular order) DutchSpace, TNO-PML applied physics lab,

NLR (Dutch aerospace labs), TU Delft Faculty of Aerospace Engineering and until recently also Stork SPE. More on this in section 2.4.3.

For TPS applications, the following material properties are especially of interest:

- density
- yield strength and ultimate strength (as function of temperature)
- Young's modulus
- thermal conductivity (as function of temperature)
- thermal expansion coefficient (as function of temperature)
- ductility
- specific heat (as function of temperature)
- emissivity (as function of temperature)
- catalicity (as function of temperature)
- oxidation resistance
- creep and stress rupture properties
- resistance to impact

At the outset, a set of data from the material brochures of the manufacturer are available ([55],[56]). This is mainly in the form of small graphs with limited accuracy, and no indication on how the data was acquired, how many measurements were made, what the spread in the measurements was, et cetera. Not all of the properties mentioned above are available from manufacturer's data. In addition, there is some literature data, most notably a paper on catalicity measurements by NASA Ames Research Center [83]. More recently, some measurements have been made at the von Karman Institute in Belgium and in France.

To improve on the data available, the Dutch space industry has performed studies of some of the materials properties mentioned above. In the scope of the TPS and hot structures research of which this thesis is a part at Delft University, also some material properties were studied, which will be reported in chapter 4. The available material data on PM1000 will be presented in Appendix A.

2.3 Use of metallic TPS to date

The overview of the use of metallic TPS is limited mainly to the higher temperature range, above the operational use temperature of Titanium and Titanium Aluminide; i.e. above 800-900°C., because this is the temperature range we are targeting with the ODS alloys based

TPS concepts. This is not to say that low temperature behaviour is not important; especially launch loads can be very substantial and driving to the design. Sufficient stiffness under launch vibration and acoustic loads, shock loads, decompression loads can all be important factors in the design just as much as thermal and thermostructural loads during re-entry.

2.3.1 Flight experience

Flight experience of metallic TPS materials is limited. The X-15 used a metallic hot structure, but the temperatures that were reached were not extreme by current standards; about 730°C was reached by the Titanium structure [94]. The ASSET flights to test TPS materials used Zirconium, Niobium and Molybdenum refractory alloys. No data was found on results.

2.3.2 Vehicle and TPS concepts

X-20 Dyna-Soar

The TPS for the X-20 Dyna-Soar was the first complete design of a metallic TPS. The vehicle was built around a truss structure of René-41 superalloy (a Nickel-Chromium-Cobalt-Molybdenum alloy [38]). This truss ensures that thermal stresses are contained. The pilot's and equipment compartments are mounted inside this truss and are made of Aluminium with passive water cooling to ensure a sufficiently low internal temperature in these compartments. Outside the truss is the heat shield made of corrugated René-41 panels covered with thin-gauge René-41 and backed by insulation or, on the hotter parts, by coated refractory alloy panels (Molybdenum or Niobium). The nose cap is monolithic Carbon with Zirconia rod reinforcement at the stagnation point [35].

The Molybdenum alloy heat shield on the windward side protects to 1755K. Coated TZM Molybdenum at the leading edges is exposed to 1920K; the reinforced C-ZiO nose cap to 2644 K. The heat shield was expected to be reusable for 4 flights. The Niobium and Molybdenum had to be coated with silicide after every flight for oxidation protection. The black colour seen on X-20 photographs is this coating. The X-20 program was discontinued in budget cuts in the late 1960's.

Space Shuttle development

In the 1970s some metallic TPS was developed for possible use in the Space Shuttle programme. A cobalt-based metallic heat shield was built and tested in 1976-7. The

On the Development of a Cooled Metallic Thermal Protection System for Spacecraft

operational use temperature was about 1260K (1000°C). Unit mass was 13.23kg/m² for a panel size of 154x108 cm made from 50x108 cm sections (see Figure 2-2). It had a corrugated skin design with corrugations in the flow direction [76]. It is unclear what this would do when the airflow is not aligned with the panels, whether it is possible to fly a trajectory that would prevent cross-flow during the high-heating phase of re-entry.

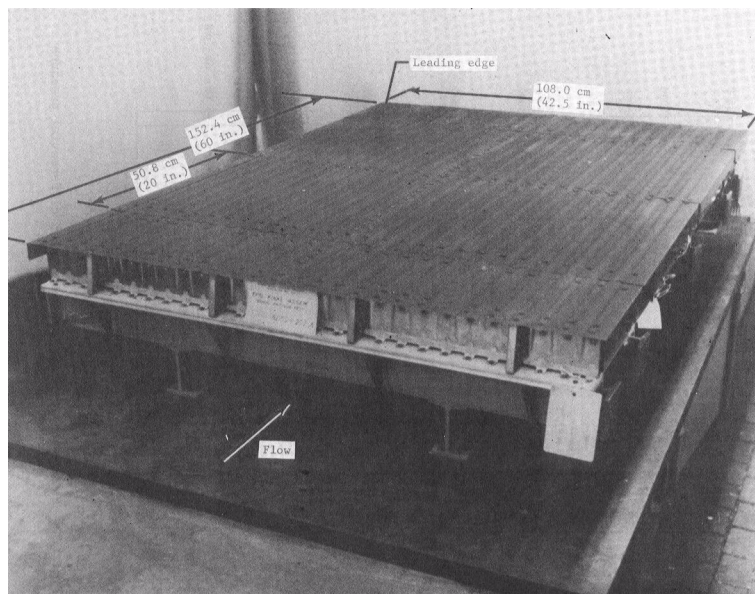


Figure 2-2: Cobalt-base TPS panel built and tested by NASA in 1977 with longitudinal corrugations (from: [76])

In the same period, a René-41 panel was developed (Figure 2-3) which had a mass of 10.6 kg/m². This also used a corrugated skin panel made up of two 148x50 cm sections. The operational temperature limit of this panel was 1090K (820°C) [25].

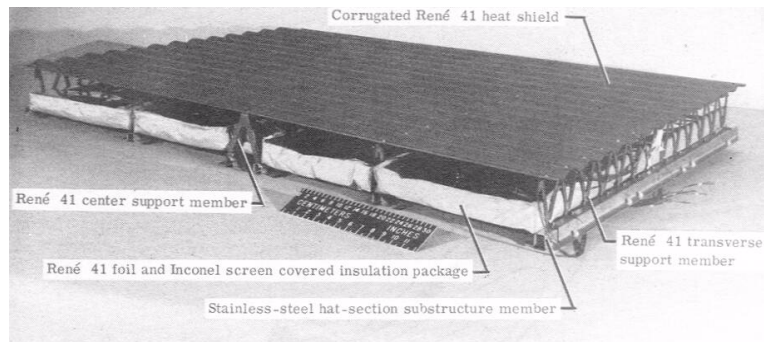


Figure 2-3: René-41 TPS panel showing corrugated skin and flexible supports, as well as fibrous insulation packages underneath (from:[25])

It can be noted that both these panels are quite large in size, much more so than later developments. Large panels give greater thermal expansion problems at interpanel edges, because there is more expansion per panel to cope with. Also, the insulation material underneath is fairly exposed, though this could be solved by packing it in superalloy foil. Insulation exposed in this way would lead to problems with water absorption.

X-30 NASP (National AeroSpace Plane)

The X-30 program was an attempt to develop an airbreathing single-stage-to-orbit vehicle in the 1980's. After several years of effort and several billions of dollars invested, the program was stopped.

The requirements of the X-30 drove an extensive research and development program aimed at materials combining high specific strength with high temperature capability, and focused on Titanium-Aluminide intermetallics, Titanium based metal matrix composites, Carbon-Carbon and ceramic matrix composites, Beryllium alloys and coatings. The most intensely heated parts were to be cooled by the Hydrogen fuel [57] (see Figure 2-4 and Figure 2-5).

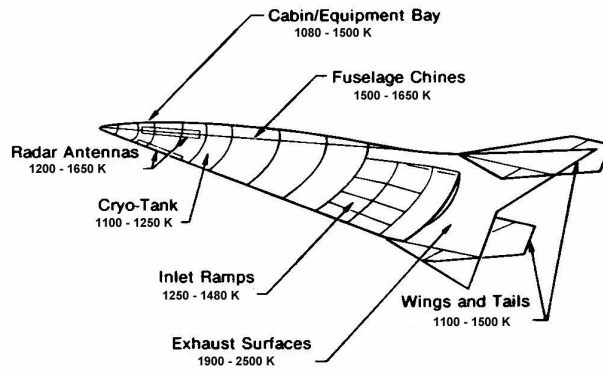


Figure 2-4: X-30 temperatures [28]

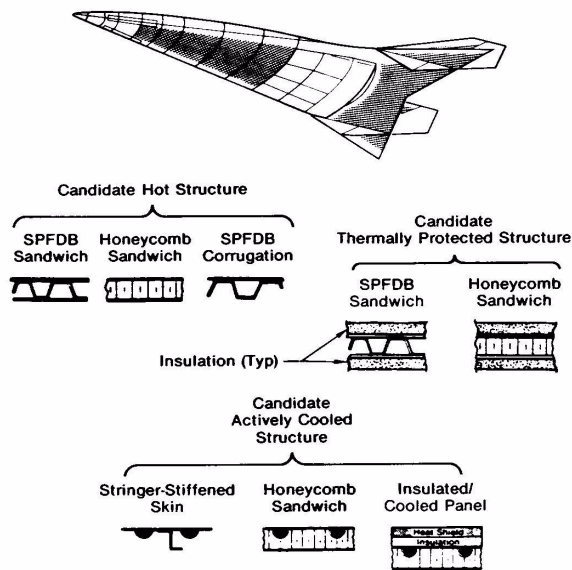


Figure 2-5: X-30 TPS concepts, including cooled ones [28] (SPFDB: SuperPlastic Forming, Diffusion Bonded)

X-33 / VentureStar

X-33 was a test vehicle designed to fly up to Mach 15 to test systems and operations for a proposed single-stage to orbit rocket vehicle, called VentureStar. The programme was cancelled after the vehicle had been built for about 75% due to technical problems, most notably with the composite cryogenic tanks. The TPS was partly metallic: Up to 480°C RSI blankets were to be used, up to 700°C; Ti-1100, up to 925°C; Inconel 617 and up to 1090°C; MA754 (an equivalent material to PM1000) or PM1000 and above that; C-C and C-SiC. Stagnation heat load was about 193 kW/m² (giving a temperature of 1165°C); windward it was just 35-45 kW/m² (650-700°C) [33]. The distribution of the different types of TPS is shown in Figure 2-6.

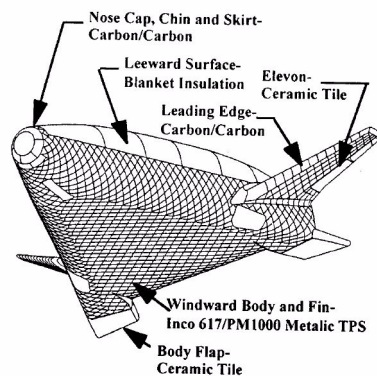


Figure 2-6: proposed TPS on the X-33 (as of 1998) [77]

The high temperature metallic TPS were superalloy shingles; a sandwich outer skin with fibrous insulation beneath. There is no radius of curvature on the X-33 smaller than 12” (305mm) because of thermal reasons. The lower surface, which is covered with metallic tiles, is flat, thus facilitating the design of the tiles at least for that region [57]. Gaps between insulation packages allow radiation to reach the substructure, which could overheat in a heating environment with a longer heat pulse than on the X-33. The panels need to be sealed along their boundary to prevent hot gas intrusion; this might be problematical [12]. The concept is illustrated in Figure 2-7.

Phase I development of the metallic shingles was done by McDonnell Douglas Aerospace; detailed design and production at BF Goodrich Aerospace (formerly Rohr, Inc) with conception, test and evaluation at NASA Langley. During tests the shingles were coated with Pyromark 2500 black paint which is able to withstand (at least) 1090°C and gives high emissivity [77].

This TPS was not able to be used in longer missions, because of the open structure which allows thermal radiation to the inside between the insulation packages. The insulation is fibrous Alumina sealed in Inconel foil, and is located under the individual shingles, leaving gaps in between.

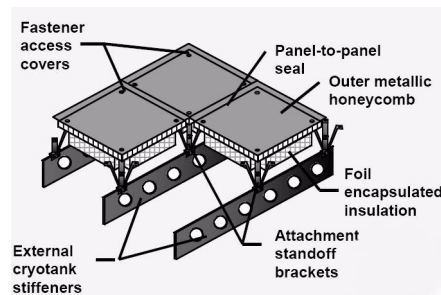


Figure 2-7: close-up of layout of the X-33 TPS [77]

Superalloy honeycomb TPS

NASA Langley further developed metallic TPS after the X-33 solution. Their next generation was a superalloy honeycomb carried on beaded Inconel side walls, with low-density insulation inside. The advantage is that the sealing is on the cool side of the panels; they are vented so aerodynamic pressure is not carried by the hot outer wall. The disadvantage is the complexity of the design and the structural coupling between outer and inner honeycomb through the sidewalls [12]. Since there has to be some distance between individual tiles (covered on the outside by overlapping strips) there is still radiation heat transfer to the substructure through these gaps. Blosser [13] has shown that this significantly increases total TPS mass. The ARMOR TPS was developed to improve on this design.

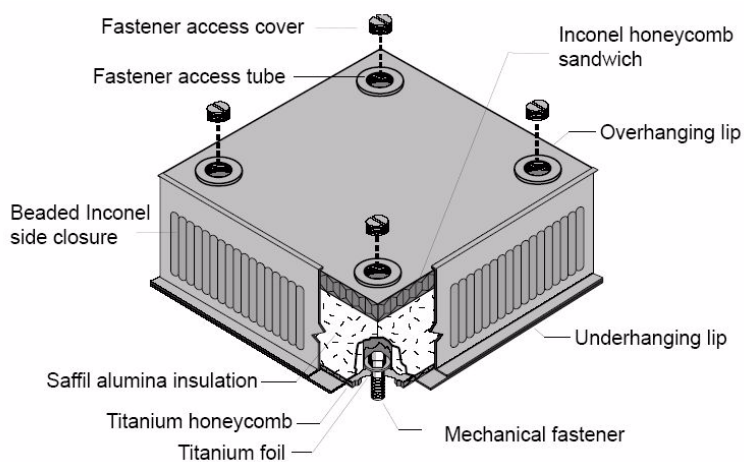


Figure 2-8: schematic of superalloy honeycomb TPS [12]

ARMOR TPS

Developed at NASA-Langley, this is a further development of the superalloy honeycomb TPS.

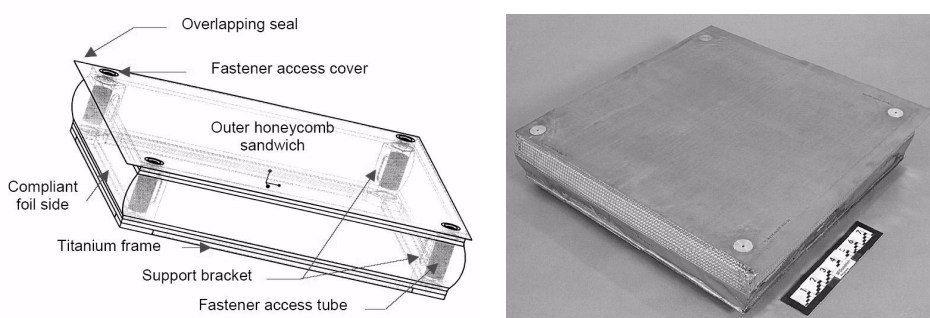


Figure 2-9: ARMOR TPS panel [14].

The sidewalls are curved, so as to close off the intertile gap. These walls are foil-gauge, and they do not have a structural role, but are only there to enclose the internal fibrous insulation and to close off the intertile gaps. The corners of these curved side walls are a problem from a thermal stress point of view; no solution was developed for that before the programme was stopped [15].

METAShield

Metashield is a NASA developed concept of an RLV with a few large structural shells that carry the thermal load and aerodynamic pressure loads, with a load-carrying integral tank inside. It is presented as an intermediate between integral hot structure airframe and an airframe with discrete TPS tiles. The low number of TPS panels gives advantages in safety, maintenance and cost; connections that accommodate the thermal expansion and sealing are difficult [80].

2.4 Cooled metallic TPS

A literature study was performed to try and find existing concepts and designs of cooled (metallic) TPS. No actively cooled TPS has flown on real re-entry vehicles as far as is known. A number of proposals and patents of different cooled TPS concepts have been found.

2.4.1 Patents

- 1) *United Aircraft Corp (East Hartford, Conn.), H.H.Hoadley, US patent 2,908,455; Oct.13, 1959 [39].*

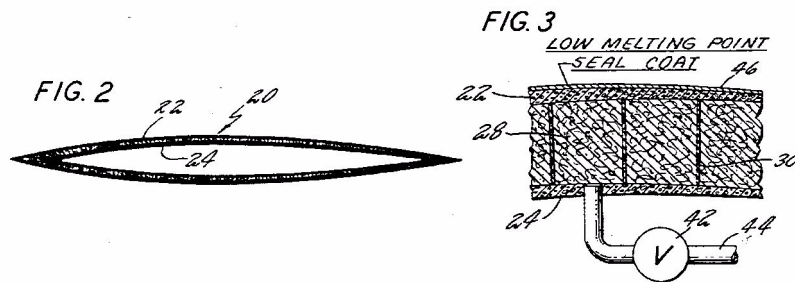


Figure 2-10: sketch of evaporating cooling system (from [39]; see text for explanation)

Chapter 2: Metallic TPS

This patent describes an evaporating cooling system where an outer skin (22) is made from a sandwich (22-24-30) which contains a porous insulation (28) saturated with coolant. The outer sandwich skin is perforated and then covered with a low-melting coating to close the holes. When heated, the coating melts and the evaporating coolant is vented through the holes into the boundary layer, leading to a blocking effect. The coolant can be resupplied continuously through a duct (44) and valve (42) if needed.

2) US Navy, D.W.Fox and R.M.Nivello, US Patent 2,922,291; Jan.26, 1960 [31].

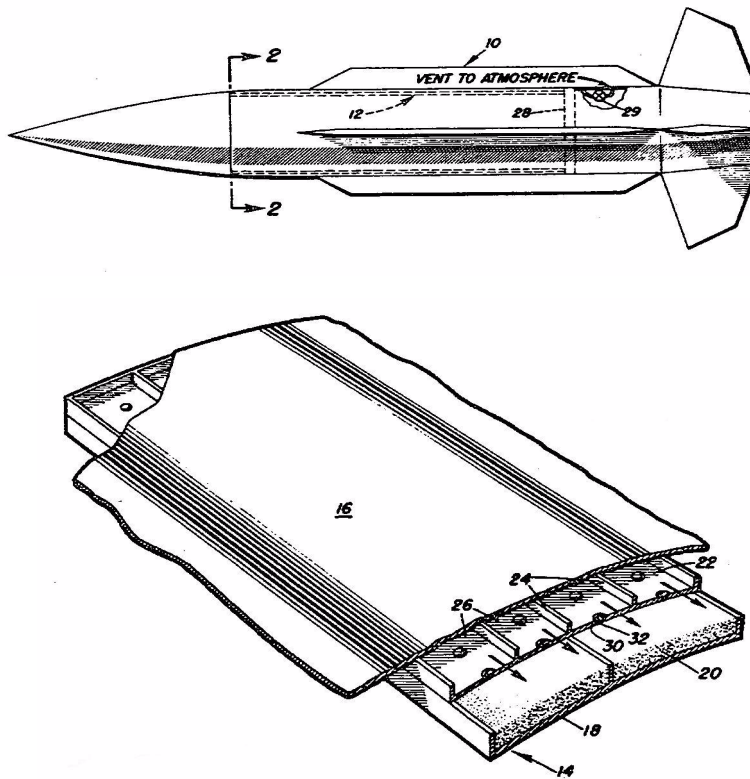


Figure 2-11: sketch of evaporative cooling system (from [31], explanation in text)

This patent describes a cooling system very close to the enhanced radiation cooling system described in this thesis. Actually, the patent was found only long after the enhanced radiation cooling system was developed. It consists of (see Figure 2-11) an outer skin (16) underneath which a ribbed perforated plate (22-24-32) is mounted, forming channels (26) underneath the skin. Underneath that, a tray (14) with a coolant-saturated insulation material (20) is placed. When heated, the coolant evaporates, escapes through the holes (32) into the channels and is vented at some downstream location. A pressure regulating valve (29) can be used to maintain a minimum pressure.

The patent does not specify how the insulation with coolant is heated (radiation of conduction or a combination), nor does it specify a requirement for a high emissivity of the perforated plate to enhance radiation heat transfer. It is illustrated with a missile resembling the Mach-4/5 Phoenix air-to-air missile, and was probably aimed at vehicles in sustained low-hypersonic flight (Mach 4-6). Then, skin temperature would be significantly less than that aimed at in the enhanced radiation cooling system.

3) *North American Aviation, C.N.Scully and J.Castelfranco, US Patent 3,014,353, Dec 1961 [81].*

This is a cooling system where the vehicle skin is a sandwich with a mesh outer surfaced, and a suitable substance which evaporates or decomposes at a certain temperature in the sandwich. Materials like copper sulfate, ammonium carbonate or simply gelled water are proposed. The coolant is not contained in a porous medium, and cools the outer skin by film cooling.

4) *The Catacycle company, R.B.Bland, F.J.Ewing, Cooling with endothermic chemical reactions, US Patent 3,067,594, Dec.1962 [11].*

This patent proposes the use of an endothermic reaction with a fluid that is pumped into a double-walled skin with a catalyst inside (see Figure 2-12). It is shown that the dehydrogenation of cyclohexane at 600K uses more heat than the evaporation of water. The reaction products are benzene and hydrogen, so just venting them in the boundary layer will not be an option. They can be used as propellants though.

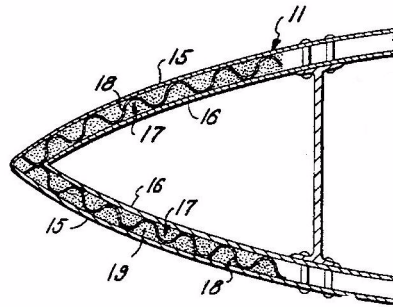


Figure 2-12: sketch of cooling system with endothermic decomposition

5) *NASA Langley, US Patent 3,090,212 of May 1963 [7].*

This cooled sandwich skin (see Figure 2-13) is a rather complex structure of a sandwich with corrugated core (16), in which wicking material (28) is fixed (29) to the inside of the hot side wall, and with pipes (25) in every other corrugation channel with spray holes (27) to spray coolant onto the wicking material. The other corrugation channels carry vapour vent pipes (32) to remove the evaporated coolant. The actual outer wall (11) is fixed to the outside of the sandwich.

Since the wick is in direct contact with the hot wall, the outer wall will be cooled to close to the coolant evaporation temperature. It is said to be able to cope with 57 kW/m^2 over larger areas and up to some 230 kW/m^2 at small spots (in the order of 5 cm^2). This would cool the inside of the structure to some 65°C .

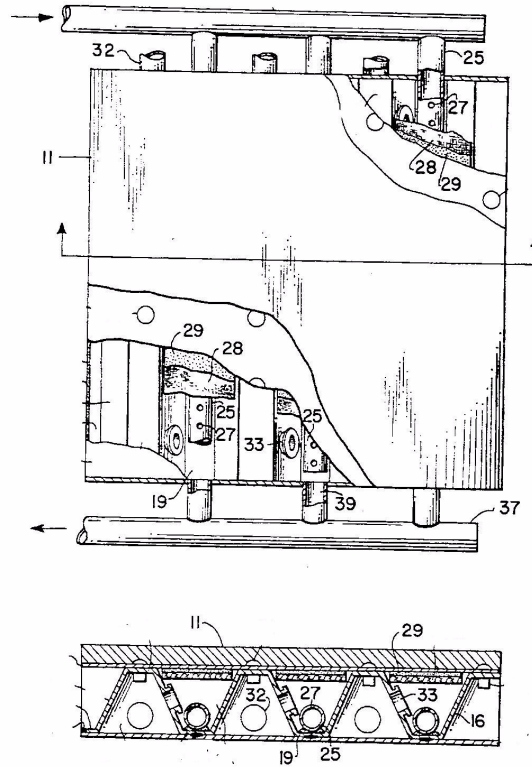


Figure 2-13: sketch of cooled sandwich skin (adapted from [7])

6) *Ling-Temco-Vought Inc, US Patent 3,082,611 of Mar.1963 [5].*

This patent proposes a colloidal mixture (gel) of water with some gelling agent to be placed at a distance behind the heated wall, thereby protecting the underlying structure. The colloidal mixture is contained in a foam, but it is not clear how the foam would withstand the high temperature once the (topmost layer of the) gel has evaporated, since no capillary

transport is provided. The idea of using the thermal energy to evaporate water and vent this overboard, thereby removing the thermal energy from the system is mentioned specifically. The reusability of this system is doubtful.

7) *Aerospatiale; US Patent 4,482,111 of Nov. 1984, 4,592,950 of June 1986 and 5,330,124 of July 1994 [47],[48],[49].*

These patents describe a thermal protection system where a vaporizing or decomposing material is contained in a porous medium (e.g. fibre mat). The second patent describes a 'two-stage' version with two vaporizing media in different layers. The porous medium is in direct contact with the hot outer wall, generally leading to much reduced temperatures compared with enhanced radiation cooling, and also the system does not appear to be reusable, since irreversible material degradation occurs.

The third patent describes a system with a liquid contained in a porous layer (fibre mat) between two sheets, with the outer sheet in contact with the hot environment. A fluid resupply is foreseen, but the fluid is prevented from entering the porous medium by a membrane which is permeable to the vapour. This should prevent uneven distribution of liquid under varying g-forces during flight.

8) *Boeing; US Patent 5,322,725 of June 1994 [4].*

This patent describes a TPS with an outer wall (which can be metallic), on top of a thick layer of ceramic fibrous insulation (e.g. ZAL-15). The rearmost layer of this ceramic insulation is composed of a sandwich of perforated electrode plates and layers of insulation. This sandwich is filled with gelled water which can be solidified by applying a low DC current of the electrodes. So, only the innermost layer of the ceramic insulation is filled with water.

This system does not rely on radiation heat transfer as does the enhanced radiation cooling system. It was developed as an improvement on the X-20 water wall (see below).

2.4.2 Proposed vehicle and structure concepts using cooled TPS

Ames Mach 10 demonstrator [42]

This is a vehicle that was proposed by NASA Ames as a hypersonic flight test vehicle. Some of the TPS concepts proposed for this vehicle were actively cooled; options for the leading edges included monolithic material and cooled leading edges see Figure 2-14).

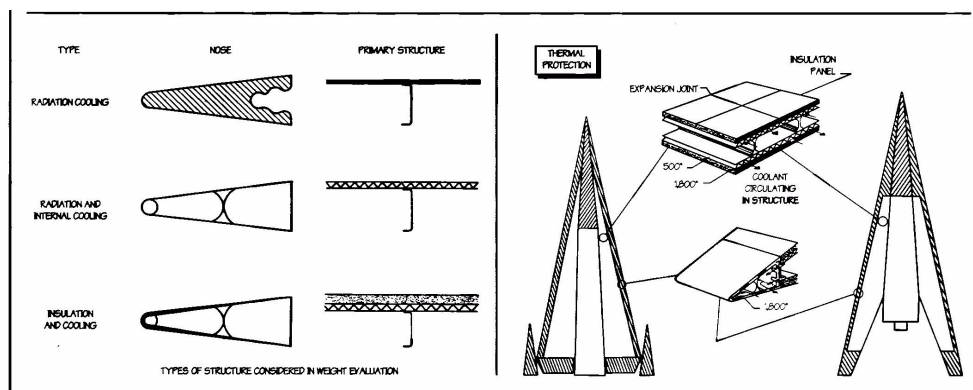


Figure 2-14: TPS concepts of the Ames Mach 10 Demonstrator [42]

Bell BoMi (bomber-missile) [42]

The Bell Bomber-Missile (see Figure 2-16) was a proposal for a hypersonic weapons system like the Sänger concept from World War II. Leading edges were cooled with liquid Lithium or Sodium.

The main structure was water-cooled Aluminium under a hot superalloy outer skin. Vapour was dumped overboard. Coolant requirements were calculated to be mass-competitive and the systems were lab-tested.

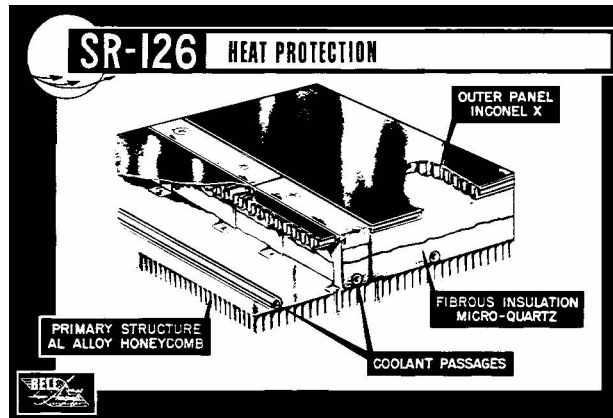


Figure 2-15: Cooled TPS concept for the Bell Bomber-Missile (BoMi)

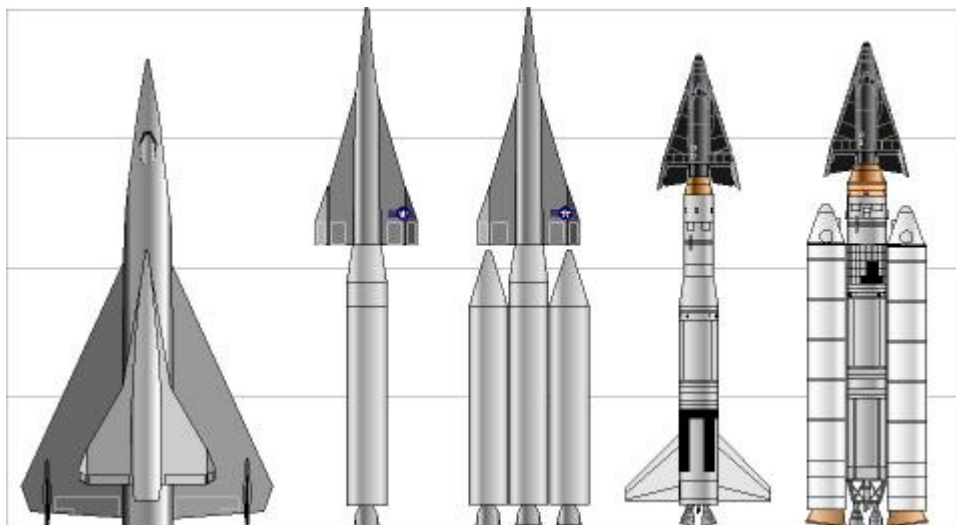


Figure 2-16: US boost-glide vehicles in the 1950s, from left to right: Bomi, two views of Robo and X-20 on Titan-I and Titan-II [101].

X-20 [42]

The X-20 (Figure 2-16) was to use a 'water-wall' to cool the inner structure using the latent heat of evaporation of water [57]. This consisted of a water-saturated open cell polyurethane foam between the inner wall and outer hot skin, using the latent heat of evaporation of water to cool the inner wall [4]. Problems with this system were the possibility of drying out, leading to degradation of the polyurethane material. The even distribution of water during acceleration was also a problem, which was countered by adding a gelling agent to the water. This used cyanides to be compatible with the foam, giving rise to toxicity problems. Maintenance, inspection, repair, refilling and check-out were extremely complicated and labour intensive.

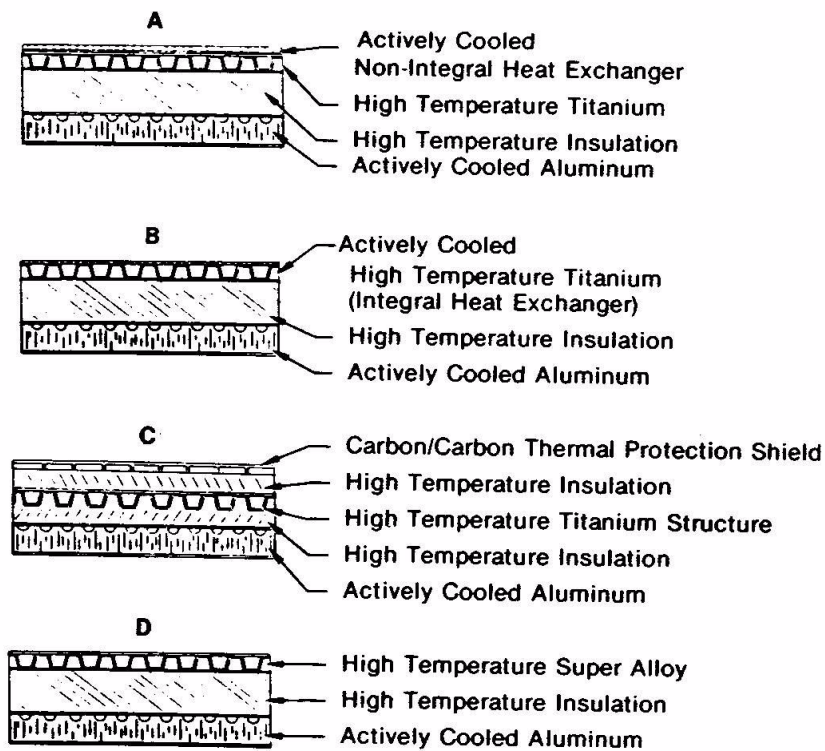
From X-20 documentation [35], the TPS and water wall concept consists of (from the outside inward) the outer skin (refractory alloy or Rene-41 superalloy, depending on location), a gap in which a truss, the main load-carrying structure, is located; fibrous insulation (Q-felt in Inconel foil), and the water wall consisting of aluminium sheets with a 'wick-held water heat sink' in between.

X-23A PRIME

The X-23 was a small lifting body re-entry vehicle for tests of the lifting body shape, manoeuvring during re-entry and of its ablative heat shield. Inside the vehicle, some of the electronic components were cooled with 'cold plate wicking' where a piece of wicking material with water was put into contact with the hot parts of the electronics, and the compartment was vented to the low atmospheric pressure. This allowed the water to boil at low temperature and the steam was vented. The system removed 1 MJ of energy from the vehicle, suggesting the use of about 0.5 kg of water [57].

X-30 [28]

Figure 2-17 shows some actively cooled structures for the X-30. Mass estimates are: A: 20.3 kg/m²; B: 22.4 kg/m²; C: 20.8 kg/m²; D: 36.6 kg/m² [28]. Leading edges and other hot parts were to be cooled with the Hydrogen fuel. This way, the thermal energy extracted from the outer skin would be put into the propulsion system, increasing the vehicle efficiency.



**X-30 Forward Fuselage Candidate
Structural/Material Concepts**

Figure 2-17: Actively cooled structures of the X-30 [28]

BOR-4

The Russian BOR-4 vehicle, used to test TPS for the Buran shuttle, used a water-cooled structure on part of the wings [51]. A wetted wicking material was mounted inside the wing cooling the metallic structure by evaporating fluid. This method was necessary because the thin wing section required did not give room for sufficient thickness of the TPS tiles.

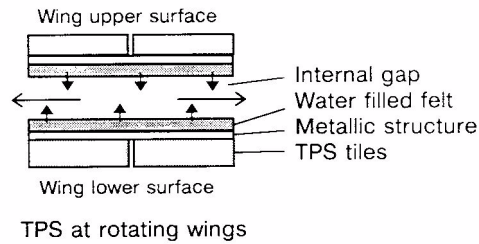


Figure 2-18: water-cooled TPS of BOR-4 [51]

Roton

The Roton reusable SSTO launcher that was under development in the late 1990s was to be water-cooled during re-entry [101]. A base heat shield was exposed to the flow and this was to use water cooling, though in which way is not known.

Cooled leading edge

CIRA and AleniaSpazio are proposing cooled sharp leading edges made with heat pipes. The main goal is to spread the heat load over the entire leading edge, so reducing the thermal gradient and thermal stress. Both CMC and superalloy leading edges are considered, with Caesium, Rubidium, Potassium, Sodium or Lithium as working fluids. The interaction between working fluid and leading edge material needs to be determined [52].

NASA Langley has proposed a similar solution and has actually built and tested a Molybdenum-Rhenium heat pipe for such a leading edge [34].

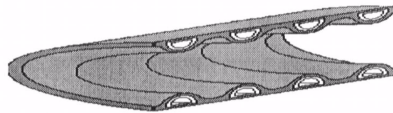


Figure 2-19: heat-pipe cooled leading edge as proposed by CIRA and AleniaSpazio

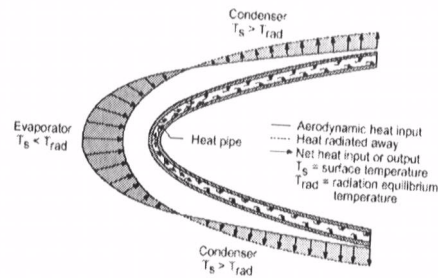


Figure 2-20: schematic of operation of heat-pipe cooled leading edge

It can be noted that the principle of absorbing the highest heat load at the stagnation point, transporting it some distance downstream and re-radiating there is the same that is used in UHTC leading edges, where the high thermal conductivity of the solid material takes care of the heat transport.

Conclusions

From these examples of prior designs for actively cooled structures it can be concluded that most are designed to cool the inner structure, and not so much to reduce the temperature of the outer structure. The exception is the cooled leading edge of NASA Langley and CIRA.

The fact that the enhanced radiation cooling is meant to extend the applicability of metallic TPS materials to higher heat loads than can normally be withstood is a unique feature of that concept. It is different from the other concepts in having the primary purpose of cooling the outer skin material and not as much of cooling the interior structure.

2.4.3 Hot structures and TPS developments in the Netherlands

For a number of years, the Dutch space industry and institutes have been working on the development of metallic hot structures for TPS applications. The materials PM1000 and PM2000 have been selected, and a number of 'building blocks' for use in a hot structure rudder have been developed [29], as well as several technologies to be used for forming and joining these materials.

Significant success was obtained in developing PM1000-PM2000 sandwich panels, which proved to be insensitive to thermal stress because of the way they are produced. A complete rudder for the X-38 vehicle was designed, built and tested successfully, only to become non-applicable when the specified heat loads were increased, before the programme was cancelled altogether [10]. More recently, DutchSpace was given the responsibility to develop the metallic TPS for ESA's Expert re-entry test capsule.

2.4.4 Cooled TPS concepts at TU Delft

Two cooled TPS concepts were studied at the Faculty of Aerospace Engineering of Delft University of Technology: direct water cooling and enhanced radiation cooling.

Both were developed for a small re-entry capsule with metallic TPS named DART. Because of the small size (and therefore small nose radius) combined with the harsh re-entry conditions dictated by the low-cost launcher, the thermal loads were actually too high for the metallic materials. To still allow the use of these materials, cooling had to be considered, in two ways: direct water cooling to cope with the extreme heat loads in the nose region and enhanced radiation cooling to deal with the lower but still somewhat too high loads behind the nose.

Direct water cooling

Direct water cooling is a cooling method that can cope with extremely high heat loads. The thermal energy incident to the outer skin is transferred by conduction through the thickness of the wall material and on the inside transferred to the coolant liquid.

This is the same method that keeps an aluminium pan or kettle on a stove from melting as long as it is filled with water. The maximum heat flux that can be transferred to the water is limited by the 'critical heat flux for pool boiling', above which a vapour film forms between the hot wall and the coolant liquid, which results in much reduced heat transfer, and therefore a much increased wall temperature. The level of this critical heat flux depends on many parameters, but it can safely be stated that this cooling method can cope with heat fluxes of several MW/m². The thickness of the wall needs to be such that no excessive thermal stress occurs because of the temperature gradient over the thickness; calculations show that a wall thickness of 0.5 to 1 mm can be used for heat loads of about 2 MW/m² [50]. More will be said about this in chapter 5.

Enhanced radiation cooling

Enhanced radiation cooling is a cooling method that allows the heat load that a metallic TPS material can withstand to be almost doubled. This is achieved by allowing the outer skin to radiate inwards into the vehicle, where the thermal radiation is absorbed by a water-saturated porous material. Water evaporates and is vented overboard. This system is the main focus of the work described in this thesis and will be described in detail in chapter 3.

2.4.5 The potential of cooled metallic TPS: reasons for its application

What would be a reason to apply cooled metallic TPS rather than uncooled ceramic TPS? The reason why (uncooled) metallic TPS is attractive is because of its improvements over ceramic TPS in terms of robustness and maintainability, while being mass-competitive. This should also apply to cooled metallic TPS. The mass competitiveness is likely to be less for cooled TPS, because the coolant mass has to be added. This can be offset to some extent by the removal of internal insulation.

Cooling metallic TPS allows it to be used over a larger part of the surface area of an RLV. Looking at current designs, it can be seen that the leeward surfaces are usually covered with flexible blanket TPS, while about 70-80% of the windward TPS is covered with uncooled metallic TPS, with CMC materials at the stagnation point and leading edges and the regions directly behind that (see Figure 2-21). The area of a vehicle that could be covered with enhanced radiation cooled metallic TPS is characterized by a thermal load of about 200 to 500 kW/m².

Comparing the cost of metallic and CMC TPS is difficult, both due to the fact that not much cost data is available, and because the development of components is not fully mature, so it is not fully clear what cost reductions are still possible.

Trabandt [90] comes out at a cost for CMC panels of 758 Euro/m²/flight and 1477 Euro/m²/flight for metallic shingles. Development cost is given as 3.8 million Euros for CMC and 56 million Euros for metallic. These figures seem to be somewhat biased in favour of the CMC option.

In any case, difference in development and production cost can be offset by differences in operations cost.

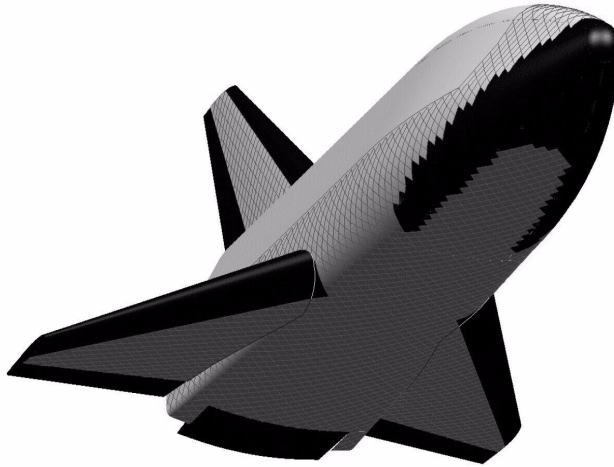


Figure 2-21: TPS of Hopper RLV concept (black: CMC, hatched: metallic, grey: flexible blanket) [90]

Theoretical background of cooled metallic TPS

Chapter 3 will give an overview of the theoretical background of Enhanced Radiation Cooling, which will be supported with experimental results in chapter 4. First the basic physical principles of the cooling system will be presented, with a phenomenological description of what happens during operation of the system. The influence of the properties of the materials that are used will be presented, with some operational consequences of the choice of materials. Models of the system, from simple 1-dimensional engineering models to full 3-dimensional finite element models will be presented, as well as a model of convection and vapour flow in a model of the cooling system. Finally some derived operational considerations are discussed.

3.1 Enhanced Radiation Cooling

Enhanced Radiation Cooling is a new method to improve the capabilities of a thermal protection system. In classic non-cooled TPS the outside of the TPS will heat up to radiate as much energy as possible back out to space while providing insulation underneath to minimise the amount of energy conducted inwards. Enhanced Radiation Cooling on the other hand allows radiation inward as well where the radiated energy is absorbed by an evaporating substance. This increases the amount of energy that is lost by the outer layer and thereby increases the allowable heat load for a given temperature, or reduces the temperature for a given heat load. This concept is new, and as such, it was patented in 2001.

3.1.1 Basic principle of enhanced radiation cooling

The enhanced radiation cooling system can be classified as a semi-passive or active cooling system, depending on whether water is actively supplied to the system or not. The

aerodynamic thermal load is accommodated by heating the outer wall which will radiate thermal energy proportional to the 4th power of the (absolute) temperature.

Another part of the thermal energy is used in heating the wall material, and is proportional to the thermal mass of the wall, the product of the mass and the specific heat coefficient of the material. In a heat sink TPS, this part of the equation is maximised by using a material with high specific heat like Beryllium. Finally, part of the thermal energy is passed to the interior. In a non-cooled reusable TPS this would be blocked as much as possible by an insulating material. In the cooled TPS this energy is transferred to a coolant which is heated and then removed (and resupplied).

The enhanced radiation cooling system is a means to allow a high temperature outer wall to withstand higher thermal loads without increase in temperature, i.e. increasing the maximum thermal load that can be carried by the TPS material for a given maximum temperature. This is accomplished by using the thermal energy flow to the interior for the evaporation of water and then removing the vapour, and thus the energy, from the system.

3.1.2 Basic operating principle

Most reusable thermal protection systems operate on the principle of allowing a high-temperature resistant material to heat up to almost equilibrium temperature, while being insulated at the rear to protect the underlying structure. The amount of insulation determines the temperature level that is reached by the underlying structure, or, reasoning from the other side, the allowable temperature for the underlying structure determines the required thickness of insulation for a given heating history.

Note that this description does not apply to TPS with a heat-sink function, where storing the thermal energy in the outer material leads to a lower temperature than thermal equilibrium. This requires a significant thermal mass (the product of mass and specific heat), so a significant thickness of the skin material. Of course, every structure has at least some thermal mass, and thus some heat sink effect, but in the majority of TPS designs, this is not an important contribution to the overall energy balance (though it will play a role in the detailed design of a TPS system). Blosser [13] has shown that increasing the thermal mass or allowable temperature of underlying structure can have a large positive (i.e. mass-reduction) effect on total (structure + TPS) mass, by reducing the required amount of insulation. Calculations performed at TU Delft for ESA's Expert program also show a great effect of thermal mass (i.e. skin thickness) on the temperature for a short ballistic flight. Thick skins however are not desirable for operational spacecraft because of their high mass.

Here we consider an insulated outer skin that is as thin as possible for being able to withstand the structural loads, to minimize mass. Such a thin skin heats up very rapidly

because of its low thermal mass and can, in good approximation, be considered to be in thermal equilibrium with the applied heat flux. The equilibrium temperature for a given applied heat flux can then be derived from:

$$\dot{Q}_{applied} = \sigma \cdot \epsilon_{wall} \cdot T_{wall}^4 \quad (3.1)$$

For a specific material, the maximum allowable temperature allows for calculating the maximum allowable heat flux for this material. For PM1000, assuming a maximum allowable temperature of 1500K and emissivity of 0.85, the allowable heat flux becomes:

$$Q_{allowable} = 5.668 \cdot 10^{-8} \cdot 0.85 \cdot 1500^4 = 243.9 \frac{kW}{m^2} \quad (3.2)$$

This is the upper limit for using this material under the conditions assumed here, i.e. no thermal conduction to the underlying insulation and structure, no transverse conduction to other parts of the skin to the sides and no energy storage in the skin material itself. All these assumptions give a ‘worst-case’ situation. The thinner the skin and the better the internal insulation, the closer to this worst case the reality will be, and since thin skin and high-performance insulation are desirable for a minimum-mass solution, real-life systems will in general strive to be fairly close to this situation.

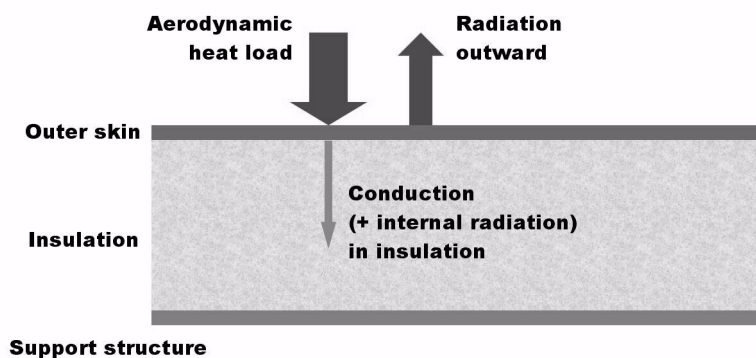


Figure 3-1: sketch of classical reusable TPS

Figure 3-1 shows the simplified heat balance of insulative reusable TPS including the energy transfer to the interior which is neglected in equations 3.1 and 3.2. Note that the formula contains the assumption of radiating to a cold background at 0K, which obviously is overly optimistic, but an actual background temperature in the range of 300K (a typical temperature for the Earth as a whole as a background to which energy is radiated) will lead to just 0.2% difference in thermal radiation, so it is neglected here ($1500^4 = 50625 \cdot 10^8$; $1500^4 - 300^4 = 50544 \cdot 10^8$, a difference of 1 part in 625).

If we want to apply this same material at heat loads higher than the one calculated in equation 3.2, some method has to be found to lose energy other than by radiation outward. If the wall were allowed to radiate not only outward, but also inward, this would effectively double the amount of energy that is lost under optimal conditions, and thus double the allowable heat flux. For this to work, there has to be a cool background to the inside which is able to absorb the heat radiated to it by the outer skin (see Figure 3-2). It is in providing this ability to radiate both outward and inward that the new and unique characteristics of the Enhanced Radiation Cooling lie.

The cool inner background is found in a porous material saturated with water. The evaporation of water absorbs a large amount of energy, and the temperature of the porous layer is limited to the temperature of the evaporating water. Capillary action in the porous layer will resupply the water to the surface where it evaporates.

The simplified energy balance of the outer skin in this case becomes:

$$\dot{Q}_{applied} = \sigma \cdot \epsilon_{wall} \cdot T_{wall}^4 + \sigma \cdot \frac{1}{\frac{1}{\epsilon_{wall}} + \frac{1}{\epsilon_{porous}} - 1} (T_{wall}^4 - T_{porous}^4) \quad (3.3)$$

where ϵ_{porous} is the emissivity of the saturated porous material and T_{porous} is its temperature. The second emissivity term is for two closely spaced large flat plates. The temperature of the outside background is still neglected, as is the heat capacity of the materials and the sideways conduction. It is assumed that the net energy radiated to the porous layer is absorbed by the heat capacity, and after reaching the boiling temperature, by the heat of evaporation of the water. It can easily be seen from the above formula that this concept will give a significant gain in allowable heat flux when the emissivity of the saturated porous layer is as high as possible and its temperature is low compared to the wall temperature.

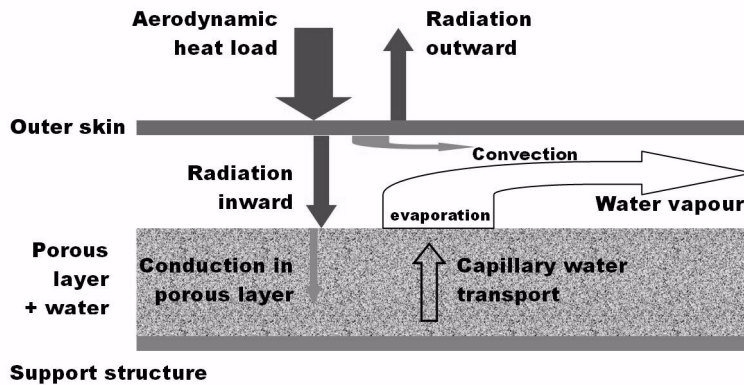


Figure 3-2: sketch of energy flows in Enhanced Radiation Cooled TPS

While the heat balance in equation 3.3 is simplified, Figure 3-2 shows the energy flows between the different elements of the TPS by radiation, conduction and convection. Using only the radiation terms gives a conservative upper boundary for the resulting skin temperature. In the worst case situation in operation, the convection and internal conduction terms will become very small, so this is a prudent approach, but more detailed (Finite Element) analysis will show that convection and heat sink effects can play a significant role under the right conditions.

The porous material of choice is an Alumina insulation material, with the trade name ZAL-15, which is 85% Al_2O_3 and 15% SiO_2 , with a porosity of 93% and a density of 0.24 g/cm^3 . The coolant contained in the porous material is water. It will keep the porous layer at a low temperature dictated by its evaporation temperature at the pressure at which the system operates, so ranging from 373K at 1atm pressure to lower temperatures at lower pressures. The temperature of up to 373K is sufficiently low for efficient heat transfer; compared to the theoretical maximum heat transfer to a 0K background, it still reaches 99.6% of that value. The emissivity of wetted ZAL-15 was measured at DutchSpace. Normal emissivity was measured of dry and wet ZAL-15 at room temperature with the following results:

Dry ZAL-15 $\varepsilon = 0.81$

Wet ZAL-15 $\varepsilon = 0.91$

It is expected that the emissivity remains almost constant up to relatively high temperatures. Since the operational temperature range is limited by the boiling temperature of water to a temperature range from about 0 to 100°C for the pressures expected, it is assumed that these values for emissivity can be used. When the material is dry, it will heat up very fast (at more than 10°/s) and the thermal radiation heat transfer will drop to very low levels. At that point, the cooling system is no longer working and only the insulating characteristics of ZAL-15 might be useful.

In operation, with a constant applied thermal load, the following will take place. The outer wall will be heated by the aerodynamic heat load. It will radiate thermal energy out to space, and also inward. The porous material with water will start heating up under this heat load from the outer wall. When the boiling temperature of water is reached at the surface, the water will start to evaporate. The temperature at the surface will remain at this temperature, while the underlying layers will rise in temperature until the porous layer and water are uniformly at the boiling temperature.

Evaporated water at the surface is vented to the atmosphere and inside the porous material water is supplied to the surface by capillary transport. This will continue until the water saturation level inside the porous material reaches a critical level, at which point the capillary action can no longer supply enough water to the surface to keep up with the evaporation rate. From then on, the surface dries out and will start to heat up. The evaporation plane will descend into the porous material, and a temperature rise will be seen to move into the material over some amount of time (drying out was observed to take several minutes for 1 inch thick ZAL-15). The heat transfer between the outer skin and the porous material will decrease while the temperature of the porous material rises to a similar level as the skin temperature, and the skin temperature will also rise because less heat is radiated inward, so a higher temperature is required to balance the incoming heat load with a higher radiation outward. This could of course cause the material to exceed its maximum temperature and melt.

The amount of water transported to the surface depends on the evaporation rate, which is linked directly to the temperature difference between the cooled outer wall and the ZAL-15. So for higher outer wall temperatures, the evaporation rate is higher, and therefore also the required capillary transport rate. The point at which the water saturation level drops below its critical value, the critical saturation, is where the useful period of operation of the cooled TPS is over. Therefore, a sufficient amount of water needs to be carried to ensure this does not happen in the duration of the re-entry. A low critical saturation level is advantageous,

since the water that is left at this point can be considered to be parasitic mass that can not be put to good use.

3.1.3 Exposure to vacuum

Since the system depends on the capillary transport of water, it is self-evident that water is required in the liquid phase. Freezing of the water can cause a problem if the water does not melt fast enough to allow the capillary transport of sufficient water. In addition to this, at low pressures no liquid phase can exist.

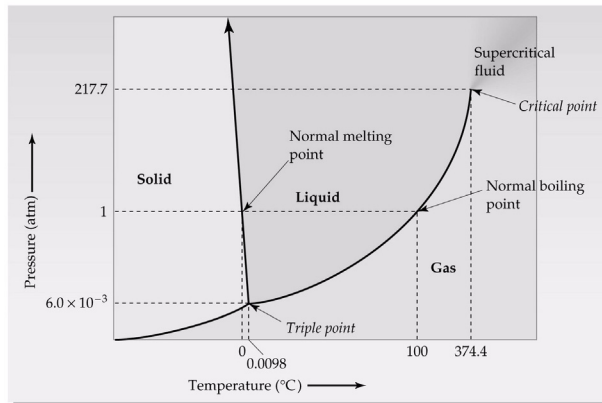


Figure 3-3: Phase diagram of water (from [54])

As can be seen in Figure 3-3 no liquid water can exist below a pressure of 6 mbar. This is then the minimum pressure required in the system to allow the capillary transport to take place. It can also be seen that the boiling point of water drops when the pressure gets lower, so very low pressures above the triple point can be expected to lead to problems of water loss due to boiling. Some results of the tests performed in a vacuum chamber to assess these issues are given in section 4.4.1. Based on those tests, a minimum pressure level of 30 mbar was chosen as the baseline for the system.

3.1.4 Behaviour of the porous material

ZAL-15 is a porous material containing 85% Al_2O_3 and 15% SiO_2 [99]. The material's microstructure consists of Alumina fibers bonded together with Silica. The Alumina fibers

have different sizes with thickness in the order of several μm , as can be seen in Figure 3-4. ZAL-15 is the trade name for flat board version of the material; the same material, at the same density, in various cylindrical and tubular shapes is sold as ALC (by the company Zircar Ceramics in the USA).

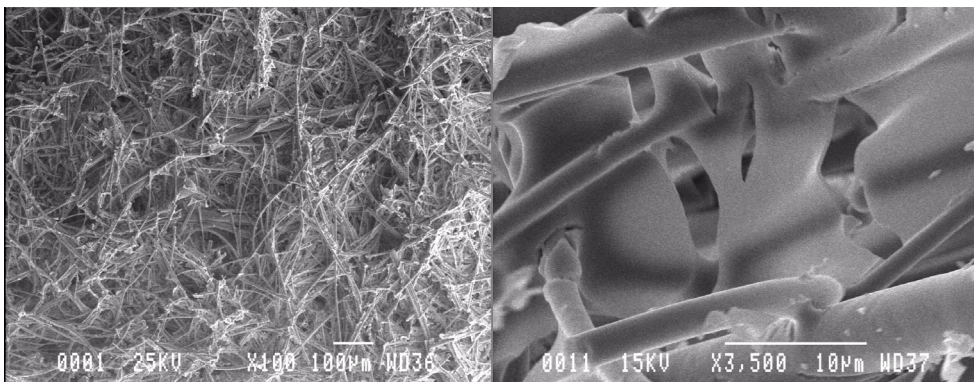


Figure 3-4: Scanning Electron Microscope images of ZAL-15, at magnifications of 100 and 3500, with typical length indicators in the pictures.

The capillary action depends on this microstructure. As can be seen in the image, the structure is not uniform on a microscale, so an analytical treatment of capillary forces is not attempted. The porosity of the ZAL-15 is 93% according to manufacturer's data. This is the theoretical maximum volume percentage of water it can contain. In reality, it can be expected that small bubbles of air will remain in the material so the actual saturation level will probably be slightly lower. Private conversation with an engineer of the material supplier made clear that they have not determined characteristics of the material like porosity and radiative properties.

water transport

When considering a three-phase system of a porous material, a liquid and a gas, the liquid phase can move in the porous material under capillary action for saturation levels down to the so-called irreducible saturation. Below that level of saturation, the liquid contracts under its surface tension into individual droplets, and the lack of a continuous liquid phase

prevents further capillary transport. Typically, this irreducible saturation is in the order of 10-15%. It depends on the interfacial tensions between the three phases and on the microstructure of the porous material. For rough or etched material surfaces it can be (close to) zero [72].

Here, no effort was made to determine these interfacial tensions, which can also be expected to be temperature dependent, because of the large effort that would go into such measurements, while still the microstructure of the porous material needed to be modelled for any prediction of irreducible saturation to be possible.

In operational use, a certain water transport velocity is required to supply the evaporation surface with a sufficient amount of water. The water transport in a porous material is given by Darcy's law [67]:

$$v_l = -\frac{K \cdot k_{rl}}{\mu_l} (\nabla p_l + (\rho_l \cdot g)) \quad (3.4)$$

where v_l is the liquid velocity,

K the material permeability,

k_{rl} the relative permeability for the liquid,

μ_l the viscosity of the liquid,

p_l the pressure field in the liquid, a combination of applied pressure and capillary pressure,

ρ_l its density and

g the acceleration (of gravity, or vehicle deceleration during re-entry).

So, the pressure and acceleration force work on the liquid, and these are scaled by material parameters that depend on the combination of materials. The material permeability is given by:

$$K = \frac{d_p^2 \cdot \varepsilon^3}{\beta \cdot (1 - \varepsilon)^2} \quad (3.5)$$

where d_p is the mean pore size,

ε is the porosity and

β is a constant.

Finally, k_{rl} is given by:

$$k_{rl} = \left(\frac{S - S_{ir}}{1 - S_{ir}} \right)^2 \quad (3.6)$$

where S is the saturation level, and
 S_{ir} is the irreducible saturation.

The pressure in the fluid is mainly described by the capillary pressure, which is given by:

$$p_c = \frac{\sigma \cdot F(S)}{\sqrt{\frac{K}{\varepsilon}}}$$
$$\text{where } F(S) = 1.417 \left(1 - \frac{S - S_{ir}}{1 - S_{ir}} \right) - 2.120 \left(1 - \frac{S - S_{ir}}{1 - S_{ir}} \right)^2 \quad (3.7)$$
$$+ 1.263 \left(1 - \frac{S - S_{ir}}{1 - S_{ir}} \right)^3$$

Here σ is the surface tension of the liquid. An other contributor to the pressure force can be a pressure difference over the thickness of the porous layer, which is not expected in the Enhanced Radiation Cooling System which will be backed by a closed support structure.

The function $F(S)$ decreases with increasing saturation level (see Figure 3-5). When the porous material is completely filled with liquid, there is no capillary pressure, because this depends on the interplay between the solid matrix and both the liquid and gas phases.

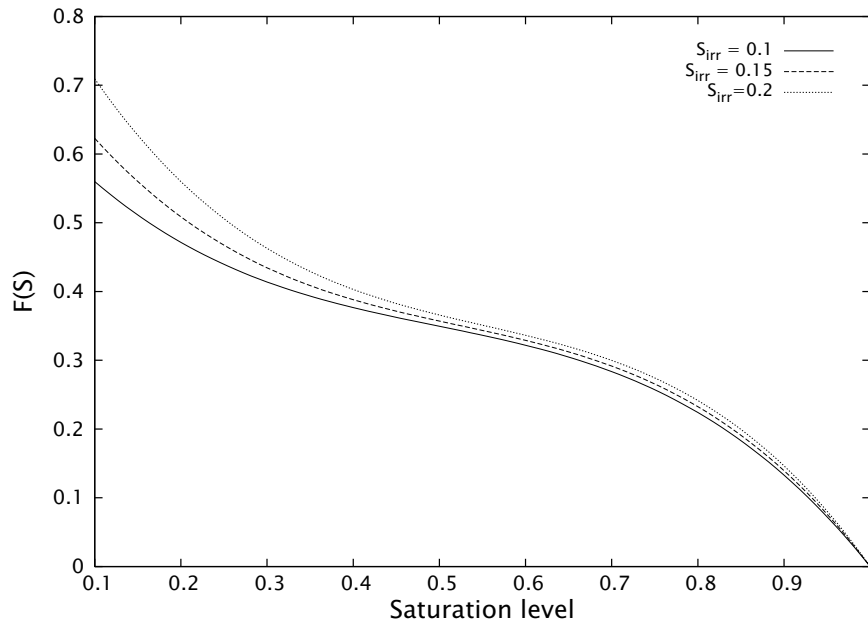


Figure 3-5: Function $F(S)$ plotted for 3 values of irreducible saturation

In operation, water evaporates at the surface of the porous material, leading to a local gradient in saturation level, with an accompanying gradient in capillary pressure, which will ensure the water transport to the surface according to equation 3.4.

So, in the expression for fluid velocity, parameter K depends on the materials, while $k_{r,l}$ depends on the actual saturation level. For reducing saturation level, the value for $k_{r,l}$ drops (Figure 3-6), so the fluid velocity drops.

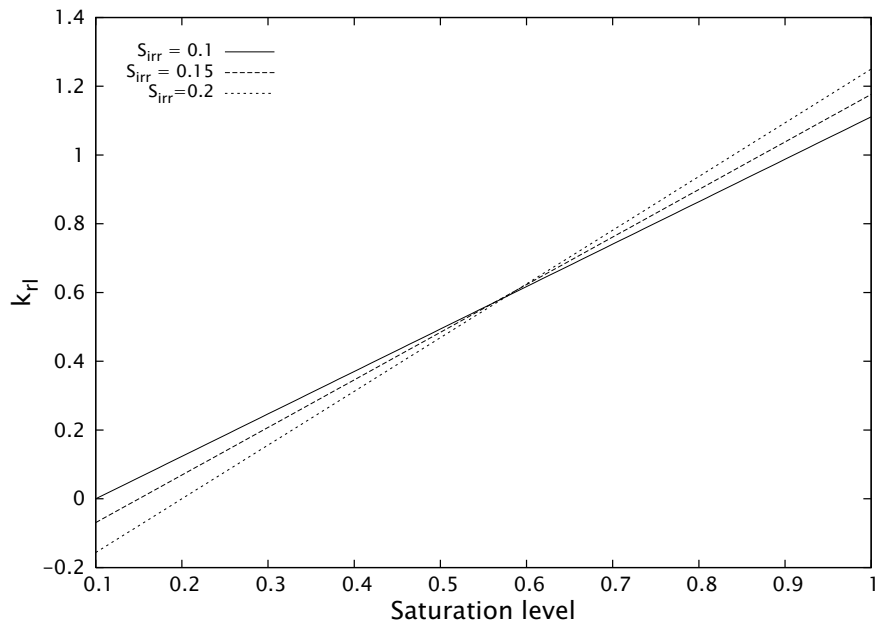


Figure 3-6: The function k_{r1} plotted for three values of irreducible saturation

At some point during operation, the fluid velocity drops below what is required to resupply fluid to the evaporation surface, so below the evaporation rate. That is the point where the surface of the porous material starts to dry out, which we call the ‘turnover point’. Putting an actual figure on the saturation at the turnover point based on this theory alone requires measuring the irreducible saturation, the mean pore size and the elusive constant β , which is a receptacle for all remaining unknowns. That full theoretical description was not attempted; rather the turnover point was measured experimentally to determine at what level of saturation it occurs.

After the turnover point, the porous material dries out from the heated surface downward. There is still an internal water transport, but this is slower than required to keep up with the evaporation rate. Because the saturation level in the still wetted part of the porous material keeps dropping, the descent of the evaporation plane in the material speeds up. This effect is countered by the fact that the energy radiated to the porous material is reduced because the

surface temperature increases and thus the radiation coupling reduces according to equation 3.3. This descending evaporation plane has been measured in tests.

Water retention

Water retention is an important aspect of the porous material behaviour. Under the g-loads that are experienced during re-entry, the water should not be forced out of the porous matrix. Under 1-g conditions, a certain amount of capillary rise is observed, in the order of 40cm (see chapter 4). This represents the ‘water column’ that can be supported under 1g acceleration and this water column will be smaller by ratio of the g-forces which act upon the system. These loads can range up to 15g for ballistic capsules like DART and Expert. The level of g-loads that can be withstood will give a maximum amount of material in the direction of the applied load that can be used; for larger lengths compartmentalization will be required. When the maximum supported amount of material is less than the local planned thickness of the ZAL-15, there is a problem.

Here the theory of capillary action in a thin tube is introduced; though the porous matrix of ZAL-15 has a very different structure, some insight might be gained from an analogy with a capillary tube, to see which parameters are involved and where improvements on performance might be possible. The behaviour of the combination of porous material with liquid and gas phase can be expected to be influenced by the following parameters (M.Kaviany in [72], ch.9):

Surface tension: this is linked to capillary pressure by

$$p_c = p_g - p_l = \sigma_{gl} \left(\frac{1}{r_1} + \frac{1}{r_2} \right) \equiv \sigma \left(\frac{1}{r_1} + \frac{1}{r_2} \right) \equiv 2H\sigma \quad (3.8)$$

where p_c is the capillary pressure,

p_g is the gas phase pressure

p_l is the liquid phase pressure

$\sigma_{gl} = \sigma$ = surface tension of the gas-liquid interface

r_1 and r_2 are the principal radii of curvature of the gas-liquid interface

H is the mean curvature of the interface: $H = \frac{1}{2} \left(\frac{1}{r_1} + \frac{1}{r_2} \right)$

Wettability: the ease with which the wetting phase (liquid) spreads over the solid phase; this is influenced by surface roughness and the presence of surfactants, among other factors.

Matrix structure: the structure of the solid phase.

Viscosity ratio: the ratio μ_g/μ_l influences flow rates through the interfacial shear stress.

Density ratio: ρ_g/ρ_l gives the relative importance of inertia forces for the two phases.

Saturation: the extent to which the wetting phase occupies the pore space. At low saturation, the wetting phase becomes immobile (or disconnected) while at high saturation, the nonwetting phase becomes immobile.

Temperature and concentration gradient further complicate the issue.

Capillary rise in a tube is given by [73]:

$$h = \frac{2\sigma \cos\theta}{m\rho gR} \quad (3.9)$$

where h is the rise,

σ is the surface tension of the gas-liquid interface,

θ is the contact angle between liquid and solid,

m is the mass of a molecule,

ρ is the liquid density (more exact would be: $\rho_l - \rho_g$),

g is the acceleration of gravity, and

R is the tube radius.

For $\theta = 0$, and using $\rho_l - \rho_g$, this can be rewritten as

$$a^2 = \frac{2\sigma}{mg(\rho_l - \rho_g)} = Rh \quad (3.10)$$

where a is called the capillary constant or capillary length of a liquid. For water this is 3.93mm at 0°C, falling to zero at the critical point.

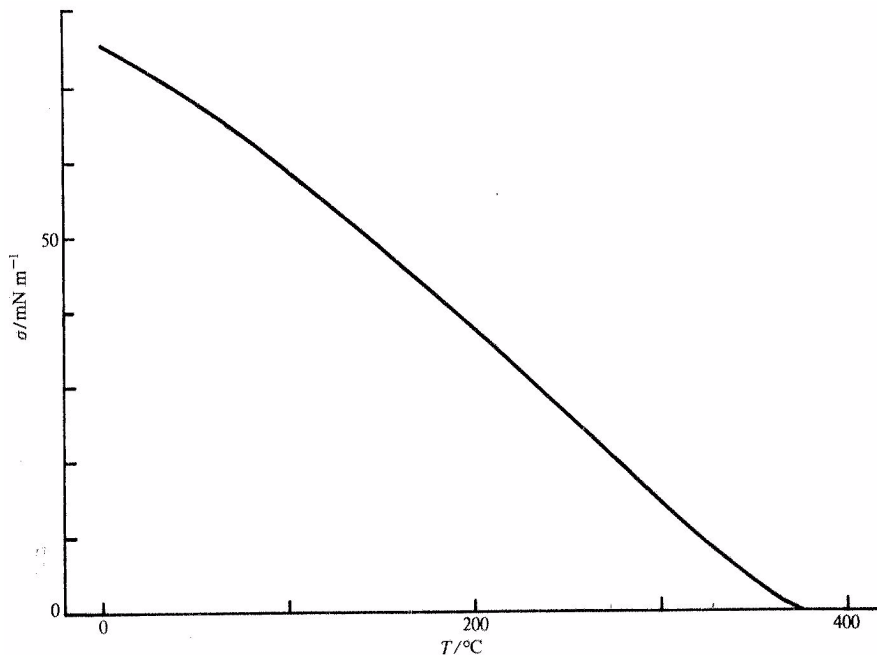


Figure 3-7: surface tension of water as a function of temperature [73].

It is observed that in ZAL-15 water will rise some 40cm under ambient conditions (room temperature, sea level atmospheric pressure); using a surface tension of 72 mN/m (see Figure 3-7), this implies an equivalent value of R for ZAL-15 of 0.037mm. Since R is also an unknown quantity here; in fact it is even an equivalent quantity because the ZAL-15 has a microstructure quite different from a cylindrical capillary tube, it makes sense to combine the quantity σ/R to describe the capillary behaviour of ZAL-15 and derive that from measurements. So, capillarity can be described as the rise of the water (or liquid) column under ambient conditions.

The surface tension of water is rather high [20], because at the liquid surface molecules lose potential hydrogen bonds directed at the gas phase and are therefore they are pulled towards the bulk liquid. At higher temperature the number of hydrogen bonds in the liquid falls, causing the reduction of the surface tension with temperature.

Tests have been performed of the water absorption in ZAL-15, of the amount of water it can retain and on retention of water under g-loads.

As for the radiation heat transfer properties of ZAL-15; the porous material will have an extinction coefficient (the sum of scattering and absorption of radiation by the medium) that is small compared to more solid ceramics. There is not yet a model for the radiative properties through scattering and reflection in porous media (see [72] pp 7.67).

Finally it must be remarked that there is an energy of adsorption that can also play a role in the behaviour of the two-phase flow problem in a porous matrix. This is an additional energy term because of the interplay between liquid and solid. At this point in time, we do not have a qualitative nor a quantitative description on this phenomenon for the cooled TPS. Future study should shed more light on this. It is expected though that this energy will lead to an increase in the performance of the system because more energy than simply the heat of evaporation of the water would be needed to remove the water from the porous medium.

3.1.5 PM1000 characterization

The properties of the skin material need to be known in great detail in order to be able to use it in design. The greater the uncertainties in material properties, the greater the margins that need to be applied in the design process to ensure a viable structure. The material properties as given by the supplier are not sufficient for a good design. Only limited data is available from the supplier, and the tests that were used to determine these properties are not described in detail, so little can be said about the accuracy of the data or the spread that can be expected.

Therefore, a number of tests have been performed, by the Dutch space industry in their earlier design programs with the material, and within the DART project, to determine some of the key parameters with greater accuracy than previously available, or for the first time.

The parameters of importance for operational use of the alloy are wide ranging:

- strength parameters (limit strength, ultimate tensile strength, stress-strain curves for a range of temperatures);
- thermal properties (thermal expansion, heat transfer, heat capacity)
- optical properties (emissivity and absorptivity, for which a range of definitions are available);
- chemical behaviour (oxidation resistance, resistance to other chemicals like salt, for a range of temperatures)
- fatigue properties, including mechanical fatigue, thermal fatigue and fatigue-related chemical effects.

Further increasing the range of parameters that need to be tested, the material is not isotropic, with the rolling or extrusion leading to noticeable non-isotropic properties. Therefore, the actual production process of the individual material samples needs to be known in detail. Not all of the material properties mentioned above have been studied; those that were are described in section 4.1.

3.1.6 Other possible material combinations

The enhanced radiation cooling system relies on a hot skin material and a cool internal background. This leaves open the possibility of using materials other than the ones used in the development so far (PM1000, ZAL-15/ALC Alumina and water). It is assumed that the cool background will consist of a evaporating coolant contained in a structure or porous material.

Parameters that can increase the performance of the system are:

- temperature of the outer skin: higher allowable temperature will lead to higher allowable heat flux (all else remaining the same)
- emissivity of the skin: high emissivity will increase radiation cooling and radiation coupling to inside
- emissivity of the wetted porous material: high emissivity (meaning also high absorbtivity) leads to high radiation coupling to the inside
- heat of evaporation of the coolant: higher heat of evaporation leads to less coolant mass flow
- evaporation temperature of the coolant: lower evaporation temperature leads to increased radiation coupling to the inside
- capillary characteristics of the porous medium and the coolant liquid.

Apart from these ones, the parameters influencing mass (like specific strength of the skin material and density of the porous material), reusability, maintainability, oxidation resistance, toxicity and others play a role, making a change in one of the component materials an undertaking which needs careful analysis of all these aspects. Nevertheless, an improvement in performance over the baseline system by improving on one or more of the parameters listed above is required for the change to make sense at all.

Skin material

For the skin material, improvement can be possible in mass, by using a higher specific strength material, and in temperature, by using a higher temperature resistant material. A gain in emissivity will be limited, since the emissivity of PM1000 is already high at 0.85 or more. An obvious candidate material for higher temperature and lower mass is a CMC

material like Carbon-Silicon Carbide (C-SiC). This material has the potential to be used to some 1870K (1600°C). Since the emissivity is about equal to that of PM1000 at 0.85, this gives a factor 2.4 increase in radiated thermal energy, all else remaining the same. Furthermore, the material has a higher specific strength than PM1000 (especially at high temperatures), leading to a reduction in mass for the skin.

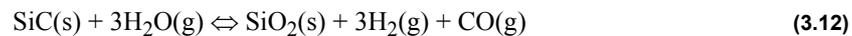
A problem with C-SiC materials is the oxidation resistance and damage tolerance. A coating is required to protect the material against atomic oxygen during re-entry, and this can easily be damaged by impact. Therefore, careful inspection is important, giving higher maintenance cost than PM1000. Nevertheless, the high temperature resistance would make this material applicable to a thermal load of up to some 1.2 MW/m² (with cooling). Of course, the amount of coolant used would increase, but this can be countered by reducing the cooled area by reduction of nose or leading edge radius.

The maximum rate at which the coolant can evaporate may be limited by the capillary transport in the porous material. This has not been determined, due to limitations in the test setup that do not allow testing at sufficiently high thermal loads. The turnover point will come earlier, with higher remaining water saturation level. The negative effect of this can be countered by using a relatively thin layer of porous material with continuous resupply from below through carefully spaced pipes.

Another problem with using C-SiC (or C-C) material can be a reaction between carbon and water vapour. There is an endothermic reaction between the two.



This reaction requires 122.6 kJ/kmol; it requires a high temperature (>800°C) to occur, which obviously is the case in this TPS application. Silicon Carbide also reacts with water [64]:



which reaction does not lead to mass loss, but then the SiO₂ will also react with water vapour:



The formation of these two gaseous products leads to a linear mass decrease. So, C-SiC will require a coating on the side exposed to water vapour to prevent degradation. For single or limited use applications, the mass loss of the skin material might be acceptably low to justify the use of the cooling system.

Porous material

Several options for porous materials were considered. Essential characteristics are:

- the ability to contain a large amount of water,
- the ability to retain the water under high g-forces,
- the ability to resupply water to the surface by capillary action,
- have a high emissivity, for good radiation coupling,
- have a low density,
- have low irreducible saturation.
- be chemically inert under operational conditions

As will be elaborated upon in chapter 4, the ZAL-15/ALC Alumina material was shown to be able to contain about 75% water by volume, retain it fairly well under g-loading, to an effective water column height of some 35-40cm, and exhibits good capillary transport behaviour. The emissivity of about 0.9 when wet leaves little room for improvement.

Carbon foam was also considered, but this will be sensitive to oxidation especially at elevated temperatures, and also the capillarity of the material is expected to be less than that of the Alumina. The aforementioned reaction of Carbon with water vapour at high temperature is also a significant and possibly a critical problem.

Metallic foams were briefly considered, but were not expected to give improvement over the Alumina material. It was not clear whether an open-cell foam with very a fine structure like ZAL-15 actually exists. Also, metallic foam can be expected to be less high-temperature resistant. This would certainly be the case for e.g. Aluminium foam, while Nickel foam has a negative mass impact due to the high specific density of Nickel.

In the end, the very good characteristic of the Alumina material have discouraged spending much effort on finding other materials. Some aspects remain to be checked; the strength of the Alumina material, especially its resistance against strong vibration and acoustic loads, needs to be determined.

From literature references of cooled TPS presented in chapter 2, it can be seen that a fibrous material was usually selected to contain the water, sometimes in combination with a gelling agent. It is expected that this gelling would leave a residue in the porous matrix, making

reusability problematical, limited to a few cycles. The X-20 TPS was expected to be used 4 times, and it is not clear if the water-wall would reach even that number without significant servicing, far beyond simple refilling with new water.

A possible option, that was not pursued (yet) is the use of a flexible fibrous Alumina material (i.e. an insulation blanket) in a honeycomb lattice covered with a fine mesh of high temperature metallic material. The mesh would only be for the purpose of supporting the porous material, and should block the radiation heat transfer as little as possible.

Coolant

The coolant should have a low evaporation temperature and a high heat of evaporation; water has the highest heat of evaporation of any liquid on a per-gram basis [20] because the hydrogen bonding in the liquid is still substantial (75%) at 100°C and all of these need to be broken. Improving on water in this respect is very difficult, if not impossible. The increase in hydrogen bonding at lower temperatures leads to even higher heat of evaporation (44.8 kJ/mol at 0°C vs 40.7 kJ/mol at 100°C). Related to this is the very high heat of sublimation.

A look at the tables of enthalpy of evaporation [1] will show that there are no substances which combine a higher heat of evaporation than that of water with a similar evaporation temperature (temperatures in the range of 0 to 150°C were deemed to merit some interest; lower than that will lead to handling difficulties, higher ones will lead to reduced heat transfer between outer skin and saturated porous layer). Combining this with the ease of handling of water, its non-toxicity and the low cost, make it clear that water is the ideal substance for this application.

Only the use of Carbon and the resulting problems with degradation by superheated water vapour can provide an incentive to look for other coolants. Nevertheless, the replacement coolant will almost certainly have a lower heat of evaporation than water. This avenue was not pursued in this study.

Because of the influence of surface tension on the capillary transport behaviour, a change in this property might lead to improvements in one of the characteristics influenced by it: filling speed, maximum achievable saturation level, water transport speed (and thus remaining saturation at the turnover point) and water retention under g-loads.

Equation 3.7 shows the relation of capillary pressure with surface tension. Since the water transport velocity depends on the gradient in capillary pressure, it scales linearly with

surface tension, and lowering the surface tension will also lower the maximum transport rate and therefore lead to a turnover point at higher remaining saturation level, an undesirable effect.

Surface tension can be increased by the addition of salt [20], where the ions increase the attractive forces between the water molecules and therefore the surface tension. These are so-called Chaotropes (disorder-makers), large single-charged ions like I^- , Cl^- , NO_3^- , NH_4^+ , Cs^+ , K^+ and Kosmotropes (order-makers) like Li^+ , Na^+ , H^+ and OH^- which are smaller ions with high charge density. It will be difficult to ensure a predictable and reproducible level of surfactants in the water when the system is heated and refilled repeatedly, since a distillation of the additives will take place. Some effort was made to experimentally study the effect of changed surface tension on the behaviour of the cooling system even though the operational usefulness was in serious doubt.

A look at endothermic reactions might be another option. It is possible that there exist substances which take up more heat than evaporating water in this way, but this was not studied. In literature, examples can be found of cooled scramjet structures which use hydrocarbon fuel for cooling. This fuel is cracked and takes up 8-10MJ/kg during the process [45]. A disadvantage is that a residue of carbon is left in the system.

Support structure

The material on the rear of the system, supporting the Alumina, is not exposed to high temperatures. This material should provide structural support for the Alumina, and be part of the air-tight enclosure of the system. Aspects to take into account when selecting a material are possible corrosion due to the water contained in the Alumina, and the joints to the side walls of the enclosure of the system. These side walls will be subjected to higher temperatures and therefore to thermal expansion and thermal stress.

The Alumina will need to be supported by and connected to the underlying material. A honeycomb sandwich core can be used to keep the Alumina in place. In addition, it can be bonded to the base material with a ceramic bonding agent. Together the honeycomb core and the bonding will fixate the Alumina on the base material. During production, the Alumina is heated to some 600°C. It is desirable to produce the ZAL-15 components in place, immediately on the base material with the honeycomb core.

If refilling during operation is required, holes can be drilled in the support plate into the cells, and refilling tubes brazed or bonded to the back side.

3.2 Engineering Model

3.2.1 Model description

To be able to make quick predictions of the behaviour of the cooling system, the temperature evolution and the water evaporation, an engineering model was built using a spreadsheet program. It uses a tabulated input heat flux and from that calculates the temperature of the skin, the wet porous layer and the evaporation of water. The input parameters are:

- temperatures at $t=0$ for ZAL-15 and PM1000;
- for PM1000: density, emissivity and thickness;
- for ZAL-15: density (assumed that of water), specific heat (idem), thickness, emissivity;
- for water: heat of evaporation, boiling temperature;
- environment temperature (for radiation from PM1000 to environment)
- time step size.

The following steps are performed in the model:

- Specific heat of the PM1000 is calculated based on the temperature:

$$C_p = 420 + 0.3833 \cdot T \quad (3.15)$$

- where T is in ° Celcius and the equation is based on the brochure values for PM1000.
- Heat radiated by the skin to space and to the ZAL-15 is calculated (right-hand side of equation 3.3).
- Summation of applied flux and radiated heat gives net heat into PM1000.
- Temperature change during time-step is calculated for PM1000:

$$\Delta T = \frac{\dot{Q}_{applied} - \dot{Q}_{out} - \dot{Q}_{in}}{C_p \cdot \rho \cdot t} \quad (3.16)$$

- where C_p , ρ and t apply to the PM1000 skin.
- For ZAL-15, when temperature is below boiling temperature, the temperature change is calculated. When temperature is at boiling temperature, it stays constant:

$$\begin{aligned}
 \text{if } T_{ZAL} < T_{boil} \quad \Delta T_{ZAL} &= \frac{\dot{Q}_{in}}{\rho_{water} \cdot \delta \cdot C_p(water)} \\
 \text{if } T_{ZAL} = T_{boil} \quad \Delta T_{ZAL} &= 0
 \end{aligned}
 \tag{3.17}$$

- where T_{boil} is the boiling temperature of the water (depending on the pressure) and δ is the thickness of the layer of water. Heat capacity of the ZAL-15 itself is neglected.
- When ZAL-15 is at boiling temperature, the amount of water evaporated by heat radiated inwards is calculated:

$$\begin{aligned}
 \text{if } T_{ZAL} < T_{boil} \quad \dot{m} &= 0 \\
 \text{if } T_{ZAL} = T_{boil} \quad \dot{m} &= \frac{\dot{Q}_{in}}{h_v}
 \end{aligned}
 \tag{3.18}$$

- Temperatures of PM1000 and ZAL-15 are increased with the calculated values. The model does not give a temperature gradient through the thickness of the ZAL-15 and the PM1000 is treated as a single layer. Measurements have shown however that the temperature inside the wet ZAL-15 during the operational phase (before drying out) rises to boiling temperature and then remains constant throughout the thickness. Approximating this by assuming a uniform temperature at all times is only a small deviation from reality.

By calculating the equilibrium temperature for PM1000 for the same heat flux, an immediate comparison with an adiabatic (perfectly insulated) wall is obtained. This model was implemented in an Excel spreadsheet. It can be used to quickly give an estimate of the performance of a section of cooled TPS under a given heating profile. Also, by changing some of the parameters, a sensitivity analysis can quickly be made.

3.2.2 sensitivity analysis

In the following example, the influence of the PM1000 skin thickness on the behaviour of the cooling system is shown. The applied heat flux profile is based on a heating profile for the Expert mission, scaled from the stagnation point heat load to an estimate for a point on the cone such that the peak heat load is about 250 kW/m^2 , the limit thermal load for uncooled PM1000. This is the expected peak heat load for the Expert flight experiment, described in more detail in chapter 5. Note that this heating profile is meant to be representative for a ballistic re-entry and a position on the vehicle at the limit of PM1000's

capabilities, it is not the heating profile that emerged from the Expert study phase-B. PM1000 emissivity is 0.85, ZAL-15 emissivity 0.91, boiling temperature for water is set at 300K, initial system temperature at 250K, outside temperature at 200K, ZAL-15 thickness at 5mm.

The aerodynamic heat load is plotted together with the energy radiated outward and inward by the PM1000, the sum of the two and the temperature.

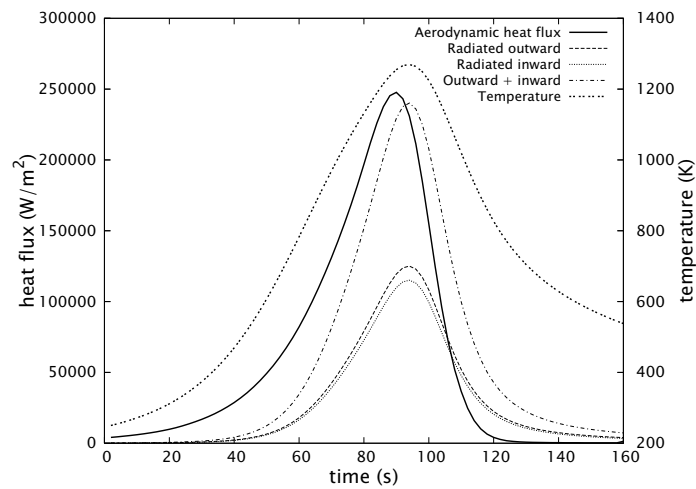


Figure 3-8: Heating predictions of the engineering model for a 0.5mm PM1000 skin

Here it can be seen that the energy radiated inward is almost the same as that radiated outward. The delay between the applied heat flux peak and the temperature peak is due to the thermal mass of the system. Uncooled PM1000 would peak at about 1500K under this load.

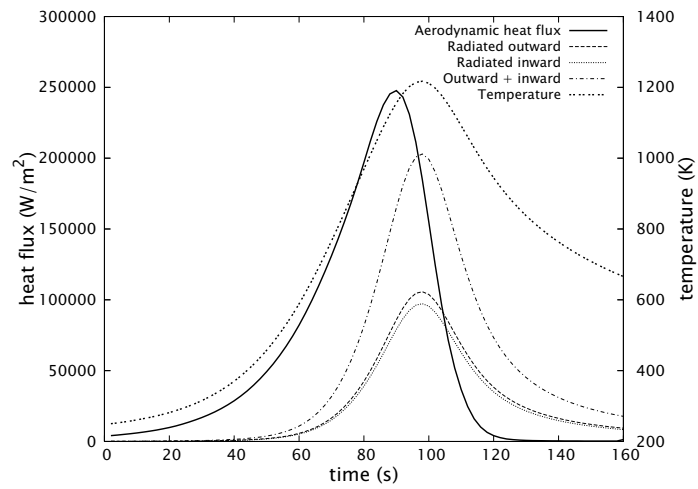


Figure 3-9: Heating predictions of the engineering model for a 1mm PM1000 skin

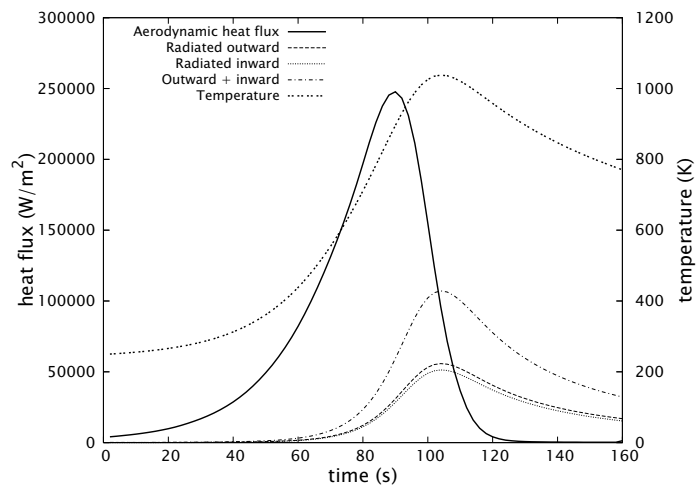


Figure 3-10: Heating predictions of the engineering model for a 2mm PM1000 skin

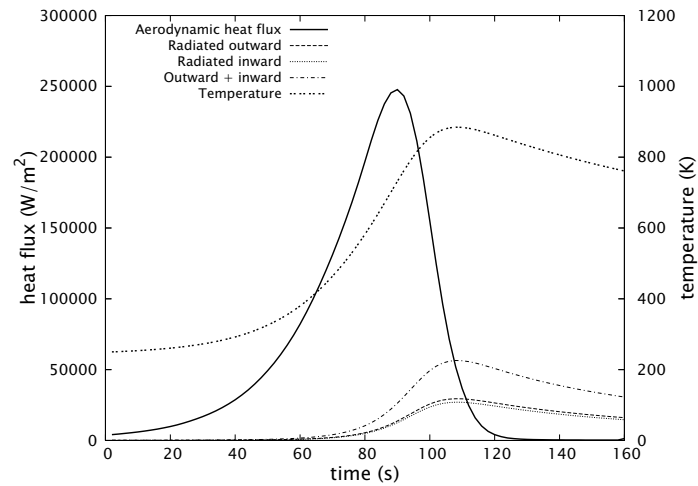


Figure 3-11: Heating predictions of the engineering model for a 3mm PM1000 skin

The influence of the thermal mass of the skin is clear from comparing these results: the maximum skin temperature varies from almost 1300K for 0.5mm to less than 900K for 3mm. The radiated energy drops from about 240 kW/m² to 60 kW/m².

Sensitivity of the system to the ZAL-15 emissivity is also interesting. It can be imagined that during repeated use, the optical properties of the ZAL-15 degrade. It was observed during tests that old and dirty ZAL-15 performs worse than new material. For operational use it is therefore important to keep the ZAL-15 clean by using purified water and preventing pollution from other sources. Settings are the same as in the above examples, with a 1mm PM1000 skin and varying ZAL-15 emissivity.

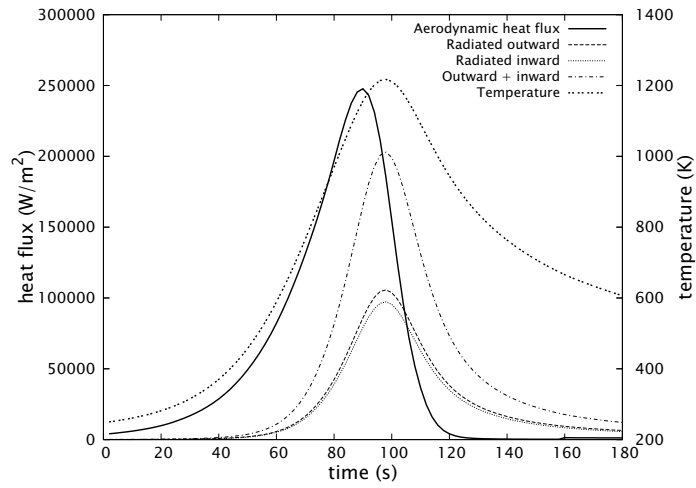


Figure 3-12: Heating predictions of the engineering model for 0.91 ZAL-15 emissivity

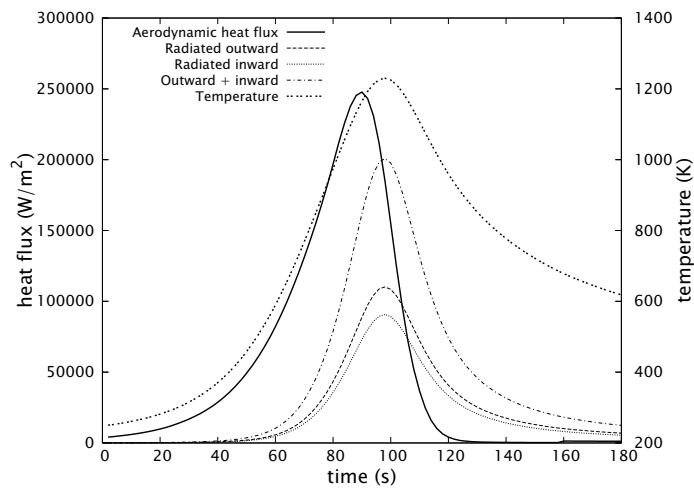


Figure 3-13: Heating predictions of the engineering model for 0.8 ZAL-15 emissivity

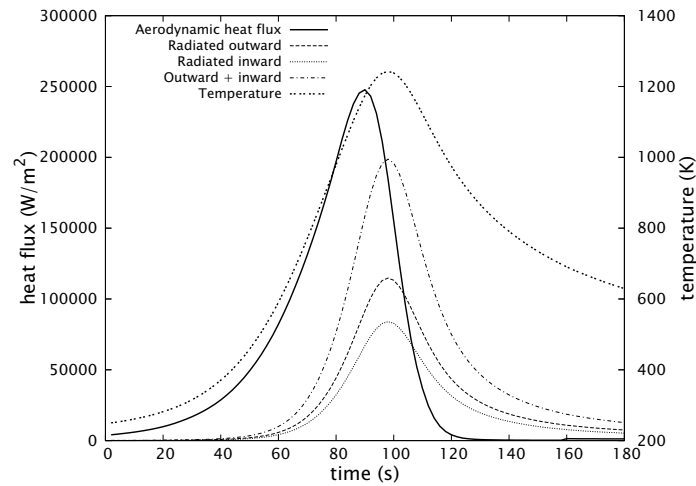


Figure 3-14: Heating predictions of the engineering model for 0.7 ZAL-15 emissivity

The differences in skin temperature are limited, peaking at 1242K for an emissivity of 0.7 and at 1217K for a value of 0.91.

3.3 Analytical Model of Vapour Flow

The vapour flow in the gap between skin and porous material will lead to some amount of convective heat transfer between the skin and the vapour, depending on the flow properties, velocity and vapour temperature. For a fairly simple geometry such as the large closed test model with a rectangular vapour cavity of 200 x 800 mm with constant gap width of 3 or 5mm, and an outflow opening at one short end, an analytical solution for the flow is possible [86]. This model is made for a 2-dimensional cross-section along the length of the model, as shown in Figure 3-15.

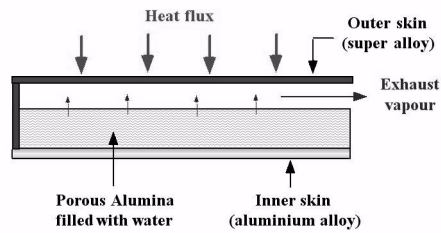


Figure 3-15: Sketch of the test sample which for which the analytical flow model was developed

It is observed that the flowfield shows similarity to a stagnation point (Hiemenz) flow for which a solution for the Navier-Stokes equations exists (see Figure 3-16 and Figure 3-17). Solving these flowfield equations gives a predictive model for the pressure and temperature fields inside the cavity and the velocity distribution of the vapour flow [86].

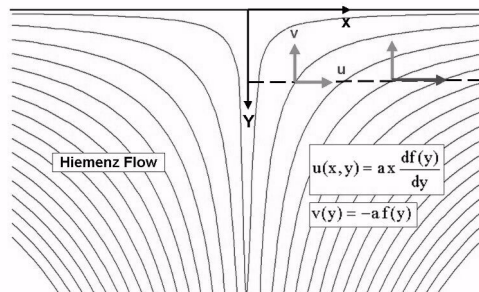


Figure 3-16: Hiemenz flow streamlines and the part of the flowfield that is expected in the test model

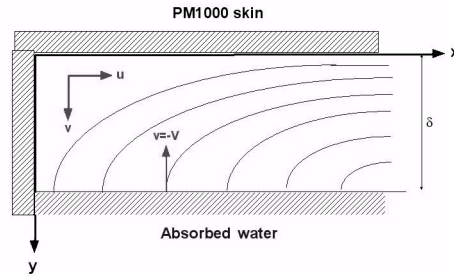


Figure 3-17: Sketch of expected flow topology in the gap of the test model and the coordinates used

The Navier-Stokes equations are given by

$$u \cdot \frac{\partial u}{\partial x} + v \cdot \frac{\partial u}{\partial y} = -\frac{1}{\rho} \cdot \frac{\partial p}{\partial x} + \nu \left(\frac{\partial^2 u}{\partial x^2} + \frac{\partial^2 u}{\partial y^2} \right) \quad (3.19)$$

$$u \cdot \frac{\partial v}{\partial x} + v \cdot \frac{\partial v}{\partial y} = -\frac{1}{\rho} \cdot \frac{\partial p}{\partial y} + \nu \left(\frac{\partial^2 v}{\partial x^2} + \frac{\partial^2 v}{\partial y^2} \right) \quad (3.20)$$

and the continuity equation by

$$\frac{\partial u}{\partial x} + \frac{\partial v}{\partial y} = 0 \quad (3.21)$$

The boundary conditions for the flow in the gap are given by:

$y=0:$	$u=0$	$v=0$	
$y=t:$	$u=0$	$v=-V$	
$x=0:$	$u=0$	$v=0$	$\frac{dp}{dx} = 0$
$x=L:$	$p=p_{ex}$		

Note that these are different from the classical Hiemenz flow.

The vapour velocity V of the evaporating water at the porous surface can be derived from the heat balance of the PM1000 skin, which consists of the applied heat flux, radiation to the outside and to the inside and the conductive heat transfer to the vapour:

$$\dot{Q}_{applied} - \dot{Q}_{rad-in} - \dot{Q}_{rad-out} - \dot{Q}_{cond} = 0 \quad (3.22)$$

where

$$\dot{Q}_{rad-out} = \varepsilon_{wall} \cdot \sigma \cdot T^A(x, 0) \quad (3.23)$$

$$\dot{Q}_{rad-in} = \frac{\sigma \cdot (T^A(x, 0) - T_{porous}^A)}{\frac{1}{\varepsilon_{wall}} + \frac{1}{\varepsilon_{porous}} - 1} = \rho_{water} \cdot h_v \cdot V \quad (3.24)$$

$$\dot{Q}_{cond} = -k \cdot \frac{\partial}{\partial y} T(x, 0) \quad (3.25)$$

To solve the Navier-Stokes equations, the assumptions for the Hiemenz flow are used, where a function f is defined which is independent of x and which defines the horizontal and vertical components of the velocity:

$$u(x, y) = a \cdot x \cdot \frac{d}{dy} f(y) \quad (3.26)$$

$$v(y) = -a \cdot f(y) \quad (3.27)$$

The constant a is to be determined, and is related to V and gap width t . Further, it is assumed that the pressure can be written as:

$$p(x, y) = p_t - \frac{1}{2} \cdot \rho \cdot a^2 \cdot (x^2 + h(y)) \quad (3.28)$$

Substitution of these assumed velocity and pressure functions in the Navier-Stokes equations and use of the boundary conditions allows for solving these to arrive at expressions for the velocity and pressure in the gap:

$$u(x, y) = 6 \cdot x \cdot y \cdot (t - y) \cdot \frac{V}{t^3} \quad (3.29)$$

$$v(x, y) = -y^2 \cdot (3t - 2y) \cdot \frac{V}{t^3} \quad (3.30)$$

$$p(x, y) = p_{ex} + \frac{1}{2} \rho \cdot a^2 \cdot (L^2 - x^2 + h(t) - h(y)) \quad (3.31)$$

where

$$a = \frac{2}{t} \cdot \sqrt{\frac{3vV}{t}} \quad (3.32)$$

$$h(y) = 2 \cdot \frac{v}{V} \cdot \frac{d}{dy} f(y) + f^2(y) \quad (3.33)$$

$$f(y) = y^2 \cdot (3t - 2y) \cdot \sqrt{\frac{V}{12vt^3}} \quad (3.34)$$

Equations 3.29, 3.30 and 3.31 fully describe the velocity and pressure in the 2-dimensional version of the gap flow. The results of the velocity are given in Figure 3-18 for a temperature of 1200°C and gap distance of 3mm, and the pressure distribution is given in Figure 3-19 for different temperatures and gap distance of 3mm.

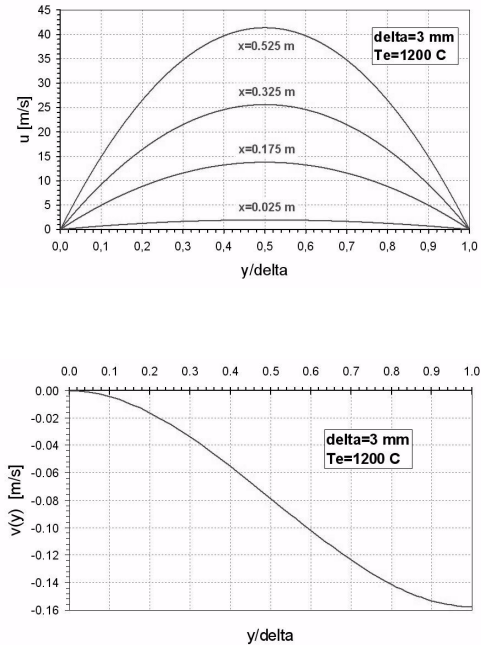


Figure 3-18: Velocity distribution in gap for 3mm gap distance and 1200°C skin temperature; horizontal velocity at the top and vertical velocity at the bottom.

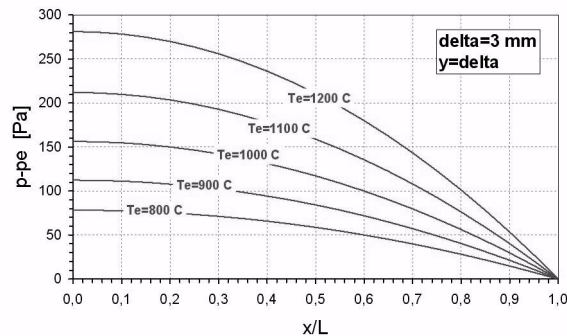


Figure 3-19: pressure in the gap for 3mm gap distance and different skin temperatures

3.4 Finite Element Models of Tests

Several FEM models of the test models were made to show that modelling the behaviour of the cooling system is possible and that the physics of the system is sufficiently understood. These models can be used to predict behaviour of the system and can help in understanding aspects of the tests that are otherwise unclear, like sneak heat flows (i.e. conductive heat transfer through side walls, radiation through gaps around the model).

Main goals of the use of FE models are:

- be able to reproduce the behaviour of experiments,
- be able to predict the behaviour of experiments,
- be able to predict the behaviour of new designs using Enhanced Radiation Cooling.

Also:

- give information on temperature distribution and thermal stress issues for new designs to use in the design process, and
- give temperature and thermal stress information on systems under conditions that can not be simulated in lab tests.

The reproduction of the actual detailed physics of the two-phase flow in the porous medium is not a goal.

3.4.1 Issues with Finite Element Modelling

The exact behaviour of the two-phase flow in the porous medium is too complex to be modelled in FE software. Therefore, a way has to be found to accurately represent the aspects of this physical process that influence the characteristics of the model that are of interest. The temperature distribution in the structure of the cooled TPS is to be reproduced with sufficient accuracy. This implies that all energy flows need to be modelled accurately. From the temperature field, the thermal stresses can be calculated, and for this the temperature dependent material characteristics need to be known with sufficient accuracy.

Modelling hot structures of PM1000 has been done before in the frame of the research of the Dutch Aeolus project. In this framework, the material model of PM1000 has been built, which is still being improved upon by adding results from new material tests. Modelling energy flows involving conduction, radiation, contact conductance and convection is not new in FE modelling, and this can be applied in the models of the cooled TPS.

A new aspect that needs to be modeled is the evaporation of water from the porous layer. This involves heating up the wetted ZAL-15 to the boiling point, from that moment on evaporating water at constant temperature up to the turnover point, and then the drying out of the ZAL-15. Since the capillary water transport can not at this moment be accurately modelled, a method has to be found to account for the evaporation of a part of the water at the surface of the ZAL-15 and the rest inside the material during the drying out phase. This is being done by defining a specified amount of water to be evaporated before the turnover point, and putting that into a layer of elements on top of the ZAL-15. The total potential latent heat of evaporation of this layer is tracked throughout the simulation run, and when it runs out, the drying out of the ZAL-15 can commence.

3.4.2 Convection modelling

Convective heat transfer is described by the formula

$$\dot{Q}_{conv} = h \cdot A \cdot (T_{wall} - T_{vapour}) \quad (3.35)$$

where h is the convective heat transfer coefficient, which contains all the complications of the physics involved. This will also depend on the geometry studied. A general expression for the heat transfer coefficient is

$$h = \frac{k}{L} \cdot C_1 \cdot Pr^{C_2} \cdot Re^{C_3} \quad (3.36)$$

where k is the heat conduction coefficient and L is the characteristic length. C_1 , C_2 and C_3 are constants and Pr is the Prandtl number, the ratio of molecular momentum and thermal diffusivities, given by

$$Pr = \frac{C_p \cdot \mu}{k} \quad (3.37)$$

with C_p being the specific heat of the vapour and μ its viscosity. Re is the Reynolds number, the ratio of inertial to viscous forces:

$$Re = \frac{\rho \cdot V_\infty \cdot L}{\mu} \quad (3.38)$$

The convective heat transfer coefficient can be made dimensionless, in the form of the Nusselt number, giving the ratio of convective heat transfer to conduction in a fluid slab of thickness L :

$$Nu = \frac{h \cdot L}{k} \quad (3.39)$$

It is the determination of the convective heat transfer coefficient, or the Nusselt number, that is the difficult part in modelling the convective heat transfer, and it should be determined based on the geometry under study.

The characteristic length is defined depending on the geometry: for a 1-dimensional flow along a plate it is the plate length, for 2-dimensional flow it is the area of the plate divided by its perimeter length. The convective heat transfer differs depending on whether the flow is turbulent or laminar. This in turn depends on the Reynolds number, with the critical number (above which flow can be expected to be turbulent) being about $2 \cdot 10^5$ for external flow and 2300 to 10000 (giving a range for transition to full turbulence) for flow in ducts. The two basic types of convection are natural and forced convection, and the Grashof number, giving the ratio between buoyancy and viscous forces, can be used to determine which type occurs:

$$Gr = \frac{g \cdot \beta \cdot (T_w - T_0) \cdot L^3}{\left(\frac{\mu}{\rho}\right)^2} \quad (3.40)$$

where g is the effective acceleration of gravity,

β is the volumetric coefficient of thermal expansion: $\beta = -\frac{1}{\rho} \left(\frac{d\rho}{dT} \right)_p$

T_w and T_0 are the temperature of the wall and the flow.

Natural convection occurs when $Gr/Re^2 \gg 1$; forced convection when $Gr/Re^2 \ll 1$ and mixed convection in between. In case of mixed convection, the Nusselt number can be obtained from the Nusselt numbers for forced and natural convection (subscripts F and N):

$$Nu^n = Nu_F^n \pm Nu_N^n \quad (3.41)$$

with the - sign when the flow is in the gravity direction and the + sign otherwise. The coefficient n is recommended to be 3 in literature, though some quote 3.5 or 4. A number of different Nusselt number correlations is given in literature; see e.g. [32] and [72]. The best one to choose depends on the characteristics of the problem at hand. We shall look at one here to show what parameters influence the convection cooling efficiency. This relation is called the Petukhov equation for flow between parallel plates:

$$\bar{Nu}_D = \frac{\frac{f}{8} \cdot Re_D \cdot Pr}{1.07 + 12.7 \cdot \left(\frac{f}{8} \right)^{\frac{1}{2}} \cdot \left(Pr^{\frac{2}{3}} - 1 \right)} \cdot \left(\frac{\mu_f}{\mu_w} \right)^n$$

$$f = (0.790 \cdot \ln(Re_D) - 1.64)^{-2} \quad (3.42)$$

$$Re_D = \frac{\rho \cdot 2t \cdot V_m}{\mu}$$

This equation is proposed for $0.5 \leq Pr \leq 2000$ and $10^4 \leq Re \leq 5 \cdot 10^6$. V_m is the averaged velocity between the plates. The viscosities μ_f and μ_w are evaluated at the freestream temperature and wall temperature respectively. The first part of the equation, without the viscosity terms, is plotted in Figure 3-20 and shows the way convection cooling increases

with increasing Prandtl and Reynolds numbers; fairly linear with Prandtl, and in a square root fashion for Reynolds, thus with velocity. Prandtl varies from 0.88 to 0.98 for water vapour between 300 and 1200K [72].

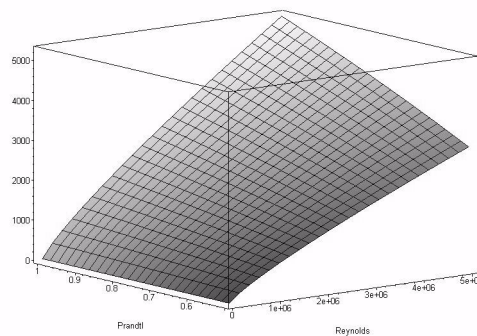


Figure 3-20: Petukhov equation without the viscosity term

The flow velocity which is used in the convection analysis can be derived from the evaporation rate, which is directly linked to the applied heat load. In combination with the actual geometry of the system under study relations for the averaged flow velocity can be derived, as shown in the analytical model of section 3.3.

In the large test model which has a length of 700mm, the value for Gr/Re^2 is 0.1 to 1 related to the plate length and about 0.05 related to the gap width. This suggests mainly forced convection, but the free convection aspects were also taken into account in the FE models because Gr/Re^2 is not that much smaller than 1 [32].

3.5 Other aspects of interest

3.5.1 Extended solar heating in space

When the enhanced radiation cooling system is used on a Space-Shuttle like vehicle, which can remain in space for extended periods of time (up to several weeks), it is important to know what the behaviour of the system is under extended solar heating. If the system heats up to over the boiling temperature and water starts to evaporate, the coolant that should be

used for re-entry will evaporate too early, or alternatively, more coolant mass is required to ensure sufficient supply for the entire mission. The heat balance can be calculated:

$$\dot{Q}_{applied} = \sigma \cdot \epsilon_{wall} \cdot T_{wall}^4 + \sigma \cdot \frac{1}{\frac{1}{\epsilon_{wall}} + \frac{1}{\epsilon_{porous}} - 1} (T_{wall}^4 - T_{porous}^4)$$

$$\Rightarrow T_{wall} = \sqrt[4]{\frac{\frac{\sigma \cdot T_{porous}^4}{\frac{1}{\epsilon_{wall}} + \frac{1}{\epsilon_{porous}} - 1} + \dot{Q}_{applied}}{\sigma \cdot \epsilon_{wall} + \sigma \cdot \frac{1}{\frac{1}{\epsilon_{wall}} + \frac{1}{\epsilon_{porous}} - 1}}} \quad (3.43)$$

which gives, with the following values:

$$\begin{aligned} \dot{Q}_{applied} &= 1260 \text{ W/m}^2 \text{ (Solar flux in Earth orbit)} \\ \epsilon_{wall} &= 0.85 \\ \epsilon_{porous} &= 0.91 \\ \sigma &= 5.668 \cdot 10^{-8} \text{ J/m}^2\text{sK}^4 \end{aligned}$$

This gives an equilibrium temperature for the outer wall as a function of the porous layer temperature (which is the boiling temperature of water at the pressure inside the system); see Figure 3-21.

The temperature difference between outer wall and porous layer (see Figure 3-22) is responsible for heating the porous layer and causing water evaporation. The amount of heat transported to the inside is shown in Figure 3-23.

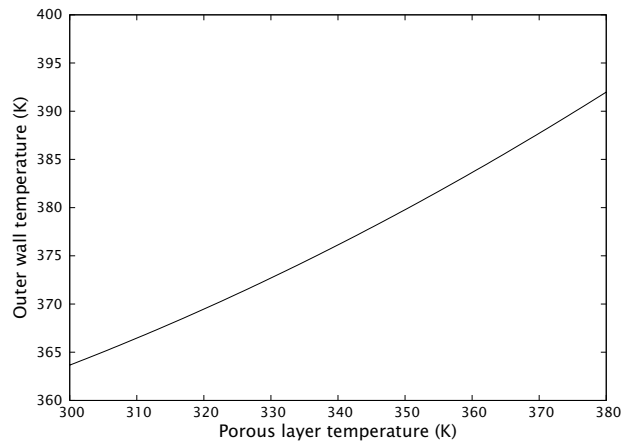


Figure 3-21: Outer wall temperature under solar heating as a function of evaporation temperature of water

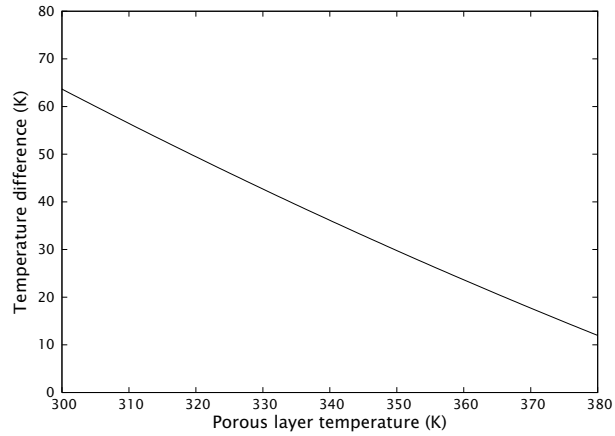


Figure 3-22: temperature difference between outer skin and porous layer for different porous layer temperatures under solar flux

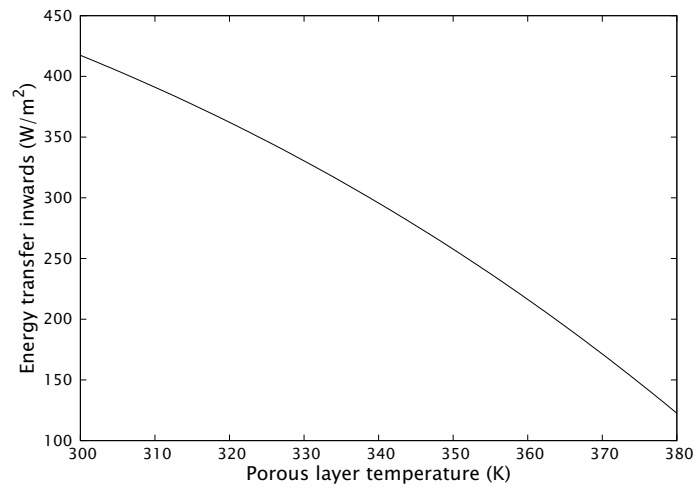


Figure 3-23: heat radiated to the inside as a function of porous layer temperature

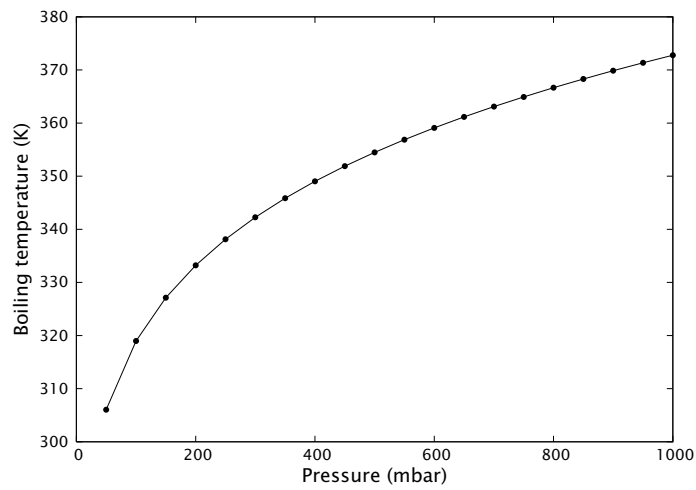


Figure 3-24: boiling temperature of water at low pressures [1]

Figure 3-24 shows the relationship between boiling temperature of water and pressure. Structural considerations are in favour of the lowest possible pressure inside the system, but at least triple point pressure must be maintained, otherwise no water vapour can exist. Triple point pressure for water is 611 Pa or 6.1 mbar [1]; 30mbar was chosen as the minimum pressure to be maintained inside the system. From Figure 3-23 and Figure 3-24 it can be concluded that for the low internal pressure that is required, there is always a heat flux to the interior of 300-400 W/m².

With a specific heat of 4.2 J/gK [1] it would take 1000 to 1400 seconds to heat up a layer of 10 kg/m² of water for 10 degrees. Melting water from ice costs 335 kJ/kg, so melting the 10kg/m² layer would add another 11,000 to 15,000 seconds (3 to 4 hours). Once the boiling temperature is reached, this heat flux would evaporate 0.13 to 0.18 g/s/m², or 468-624 g/hr/m². In reality, the spacecraft in low Earth orbit would be in eclipse about half it's orbit. Simulating this for a few orbits shows that the porous layer will reach boiling temperature of 300K, corresponding with a pressure of 30-40mbar, after seven orbits (see Figure 3-25).

The thermal equilibrium temperature of PM1000 with an emissivity of 0.85 exposed to the solar flux in Earth orbit (1260 W/m²) is 402K. Without cooling, this would be the limit temperature to which the outer skin would be heated.

Clearly, in case of a stay in space for days or weeks, something has to be done to prevent this slow boiloff. Two options seem possible:

- covering the outside with a high-reflective coating to reduce the heating of the outer skin. This would have to come off before or in the initial stage of re-entry, because then a high-emittance surface is required
- filling the porous layer with water only shortly before re-entry. This implies a large risk when the filling system does not work, and is surely a lot less attractive than having a system that is ready for operation without further operations being required.

Turning the spacecraft in such a way that the relevant surfaces are in the shade can be a possibility in some applications, but for a Space Shuttle-like mission this does not seem a feasible option. For short missions, like DART and EXPERT, with a time in space of less than half an hour, these problems will not occur.

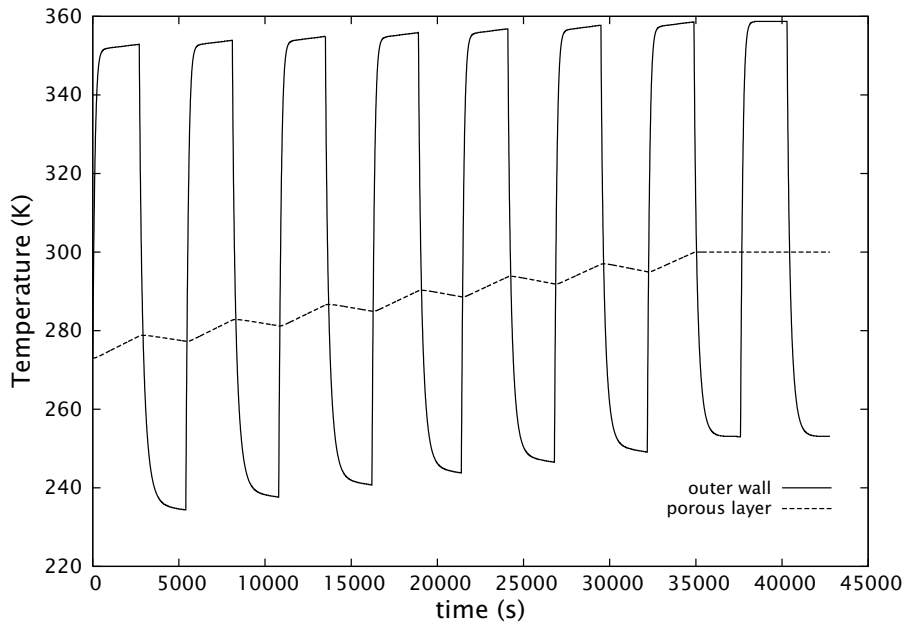


Figure 3-25: evolution of outer wall temperature and porous layer temperature in a 90 minute orbit, half of which is in eclipse, for water boiling point of 300K and initial temperature of 273K with liquid water.

3.5.2 Re-filling with water

Before re-entry, the porous medium must be filled with water. Two options are filling before the flight and filling during the flight, before re-entry. Also, continuous refilling during operation is an option, which is necessary when a thin layer of porous medium is used to save mass. The following advantages and disadvantages of these options can be identified:

On the Development of a Cooled Metallic Thermal Protection System for Spacecraft

	Advantages	Disadvantages
Filling before flight	<ul style="list-style-type: none"> - Check on ground possible - Least complicated; no filling valves operated during flight 	<ul style="list-style-type: none"> - Heaviest option - Needs to be airtight to prevent boiloff - Problems with solar heating
Filling before re-entry	<ul style="list-style-type: none"> - Possibility to reuse water from other uses? - No problems with solar heating 	<ul style="list-style-type: none"> - Pressure needs to be maintained above triple point pressure - If this fails, it could mean loss-of-vehicle
Continuous filling during re-entry	<ul style="list-style-type: none"> - Lightest option in case of long heating phase 	<ul style="list-style-type: none"> - Most complex option - Extensive tubing might be needed to supply enough water at all locations

A thorough risk analysis should be performed to determine which options can be built within acceptable risk limits. Different applications will be likely to need different solutions; the short mission without orbital phase of Expert will be best served with a pre-filled system, while a hypothetical use in a large manned future RLV will probably be better with a system that is refilled before re-entry and possible during re-entry as well. It can be noted that proposed reusable launchers with scramjet engines need complex active cooling systems for the engines, so the complexity of an active cooling system on an RLV is not necessarily a critical disadvantage.

When porous Alumina is re-filled with water it is important to know how fast water is spread through the material. It will likely not be possible to 'pour' water on the material, which is known to lead to extremely rapid filling. Therefore, tests were performed with supplying water to a strip of ZAL-15 through a thin hose connected to one side.

The tests were done in order to determine how much time it would take to fill the large lab model which contains some 3 liters of water. The goal was to get a ballpark figure for this filling time, to see whether it would be minutes, tens of minutes or hours. Also, an idea of the influence of inclining the ZAL-15 and filling it against gravity was checked. The results will

Chapter 3: Theoretical background of cooled metallic TPS

give an indication of the capillary pressure of water in ZAL-15 and they are reported in section 4.4.2.

Experiments with cooled metallic TPS

The experiments performed in support of the development of the Enhanced Radiation Cooling system are described in this chapter. First, the basic tests on the material are presented, after which the experiments on the cooling system are introduced. To start with there are tests on the basic operation of the system, tests to determine some critical parameters and finite element modelling to support these tests. Finally, some tests on other aspects of the system are shown, like water retention and absorption by the porous matrix.

4.1 Material testing

The material used for the TPS, PM1000, is characterized in only limited detail in the material brochures available from the vendor, and little is known about how these brochure values were obtained. Therefore, the required material parameters need to be determined in more detail in order to be able to reduce margins during design with this material.

The properties that are required are those that have an impact on the thermostructural behaviour: stress-strain curves for various temperatures, Young's modulus, thermal conductivity, heat capacity and emissivity, all as a function of temperature. A very important one is the catalicity of the material in hypersonic dissociated flow, since this has a large influence on the resulting heat load. Apart from this, for future operational applications, also the chemical (oxidation) behaviour of the material, also under the influence of e.g. salt, are of importance.

Some of these material characteristics have been measured in a number of test campaigns at Delft University of Technology, NLR, the University of Leuven (B) and the von Karman Institute. Earlier tests have been performed in the Dutch national Aeolus programme. The results of those tests are used in the Finite Element models, but are not reproduced here.

The results of the tests performed in the research programme on TPS at Delft university and University of Leuven will be presented here.

4.1.1 Strength and physical properties

Tests have been performed to assess the stress-strain curves for PM1000 for a range of temperatures, Young's modulus for a range of temperatures and the hardness of the material. Also, the emissivity, coefficient of thermal expansion and heat capacity were measured.

Stress-strain behaviour

A limited amount of data is available on this, in the form of plots of yield and ultimate strength versus temperature in the material brochure, and some stress-strain curves measured in the Aeolus programme. Also, some literature data is available on the very similar material MA754 from Special Metals in the USA, a material that is identical to PM1000 in composition, if not in the details of the production process.

Measurements were performed at the University of Leuven in Belgium [92]. A limited number of samples was available for tests in a test bench with a vacuum oven integrated in the setup which allows for temperatures up to 1400°C. Tests were performed at fixed strain rate while the force was measured with a force cell and the temperature with a Type S thermocouple. The temperatures at which the tests were performed were 850°C, 1050°C and 1300°C. Three samples were tested at each temperature at 0.008mm/s strain rate and an additional three at 1300°C at 0.0008mm/s.

As expected, the yield and rupture stresses decrease with increasing temperature. Also the rupture strain decreases. Lower strain rate leads to lower yield stress and rupture strain. This is in line with the behaviour of MA754. The staggered trend of the stress-strain curves is a result of the test method, not a real material property. The results are reasonably in line with the data in the PM1000 material brochure [56] (see Table 4.1).

Temperature (°C)	$\sigma_{0.2}$ (MPa)	σ_u (MPa)	Rupture strain (%)
700	310	412	17
900	216	238	10
1100	131	145	5
1300	92	95	3

Table 4.1 : Supplier data on yield and ultimate stress and rupture strain

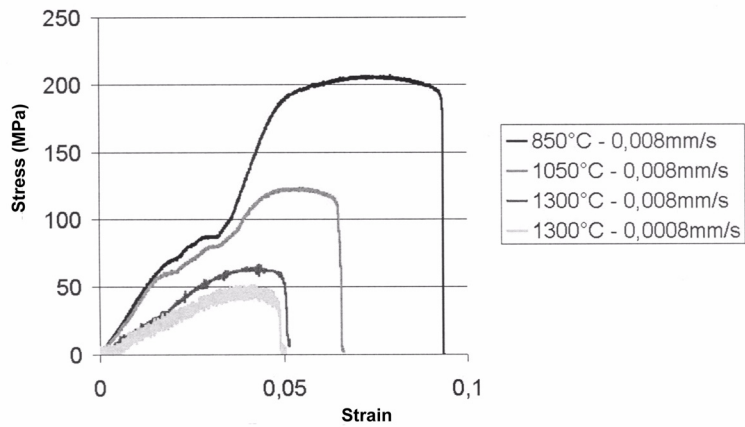


Figure 4-1: Stress-strain curves for PM1000 for different temperatures and strain rates

Looking in more detail at the individual sets of three measurements for the different temperatures shows the spread in the results (see Figure 4-2).

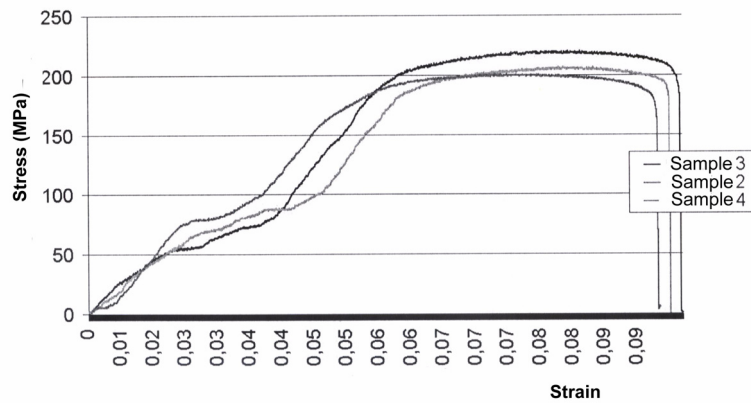


Figure 4-2: Stress-strain curves for three identical tests at 850°C

The odd strain scale in Figure 4-2 is due to the measurement method being converted to real strain from measured strains, i.e. removing some test-setup specific influences. In any case, it is clear that the spread in measurements is substantial with for example 5% strain being reached at 100 MPa in one test and 150 MPa in another. The accuracy of the individual tests was estimated to be to 10 MPa or better.

Young's modulus

Measuring Young's modulus at high temperatures in a tensile testing machine is tricky, because of e.g. visco-elastic behaviour and the need for high-temperature resistant extensometers. Another option was therefore used, the Impulse Excitation Technique. Here, a small bar of material is excited and the vibration frequency measured. The resonance frequency depends only on Young's modulus, density and dimensions of the sample [92]. It must be noted that this method required a homogeneous single-phase material, so without oxide coating. Therefore, the tests are performed in an inert atmosphere.

Three samples of 100x10x3mm are used and eight of 60x10x3mm. The size of the samples has an impact on the accuracy of the measurement, because the vibration characteristics depend strongly on the thickness of the sample.

The E-modulus can be obtained from the bending and from the longitudinal modes; the G-modulus from the torsion mode.

The material is not homogeneous; it is rolled in two directions, and a difference is expected between the rolling direction and the intermediate directions. Therefore, the samples were cut in rolling direction (4 samples; 3 of 100mm and 1 of 60mm length) and under 45° with the rolling direction (7 samples, all of 60mm length). The results are given in Table 4.2

Supplier data quotes a value of 210 GPa for the E-modulus at room temperature and does not give temperature-dependent values. The 210GPa appears to be a worst case value for the rolling direction when we look at the experimental data in Table 4.2.

The temperature dependence of the E-modulus was determined by heating the samples at 2°C per minute and measuring at one minute intervals, so every 2 degrees.

From the resulting data a linear regression was taken for two intervals: 25°C to 900°C and 950°C to 1150 or 1200°C. These are given in Table 4.3.

Chapter 4: Experiments with cooled metallic TPS

	sample #	E-modulus (GPa)		G-modulus (GPa)
		bending mode	longitudinal mode	torsion mode
In rolling direction	1 (large)	210 ± 16	214 ± 6	92 ± 2
	2 (large)	213 ± 10	217 ± 4	90 ± 1
	3 (large)	212 ± 20	218 ± 7	91 ± 3
	7 (small)	212 ± 2	217 ± 1	91 ± 0.5
45° with rolling direction	4 (small)	248 ± 5	246 ± 2	86 ± 1
	5 (small)	226 ± 5	226 ± 2	83 ± 1
	6 (small)	247 ± 2	245 ± 1	73 ± 1
	8 (small)	234 ± 5	234 ± 2	65 ± 0.5
	9 (small)	232 ± 4	238 ± 2	71 ± 0.5
	10 (small)	234 ± 3	240 ± 1	68 ± 0.5
	11 (small)	232 ± 2	237 ± 1	63 ± 1

Table 4.2 : Test results for E-modulus and G-modulus tests at room temperature

	sample #	E-modulus relations (GPa)	
		25 - 900°C	950 - 1150/ 1200°C
In rolling direction (to 1200°C)	1 (large)	214 - 0.07·T	-
	2 (large)	218 - 0.07·T	244 - 0.1·T
	3 (large)	222 - 0.07·T	237 - 0.1·T
	7 (small)	219 - 0.06·T	-
45° with rolling direction (to 1150°C)	4 (small)	251 - 0.08·T	279 - 0.11·T
	5 (small)	240 - 0.07·T	250 - 0.08·T
	6 (small)	251 - 0.08·T	274 - 0.11·T

Table 4.3 : E-modulus as a function of temperature

Figure 4-3 shows the regression functions plotted together to show the spread in the data and the difference between the rolling direction and the 45° direction.

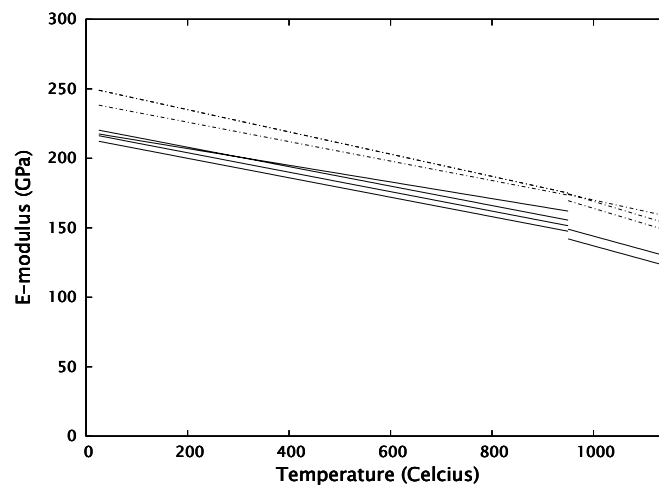


Figure 4-3: plot of the E-modulus linear regressions from Table 4.3 with the data in rolling direction as solid lines and the data under 45° as dashed lines.

Average yield stresses were determined for 850, 1050 and 1300°C at a strain rate of 0.008 mm/s are given in Table 4.4.

Temperature (°C)	Strain (%)	Yield stress (MPa)	Supplier data (MPa)
850	10	200	≈ 270
1050	7	120	≈ 160
1300	5	60	≈ 100
1300 (0.0008mm/s)	4.5	45	

Table 4.4 : Yield stress for three temperature levels, compared with brochure data from supplier

Here they are compared with the data from the supplier, which was measured at a strain rate of $1 \cdot 10^{-3} \text{ s}^{-1}$, which is four times higher than the strain rate of the tests performed here, which is at least a partial explanation of the difference.

It can be noted here that in brochure data, the exact circumstances of the measurements and the details of the material are rarely given, so interpretation of these data is difficult at least, and they should be used to get a first indication of material properties only.

Conclusions on material properties data

Based on the experiments performed and comparison with supplier brochure values, the main conclusion must be that there are sometimes large deviations between experimental values and brochure values, without a clear explanation. The lack of data on the details of the tests and the material samples used in the suppliers brochure make it very difficult to determine what causes these deviations.

A quite large programme of material characterization is required to define the material with high confidence, and the precise state of the test samples should be included with the test results. This also means that many tests need to be repeated for different base conditions of the material (rolled sheet, bar, in or perpendicular to rolling direction etcetera). Only a small start of this was done in the frame of the research on the cooled TPS at TU Delft thus far.

4.1.2 Environmental and oxidation tests

Samples of PM1000 have been exposed to salt water spray according to ASTM (American Society for Testing of Materials) standards [27]:

- ASTM B117-73 (salt spray / fog testing): spraying the test samples with a 5% NaCl in water solution at 35°C from 24 to 800 hours.
- ASTM B287-62 (Ascectic Acid Salt Spray / fog testing): spraying the samples with a 5% NaCl and 15% HCl in water solution at 35°C for 168 hours.

Table 4.5 shows the test matrix for the environmental tests. A reference series was not pre-oxidised and then subjected to salt spray for different exposure times, followed by high-temperature testing. A second series was pre-oxidised and subjected to salt spray for the same exposure times followed by high-temperature corrosion, the third to similar test followed by Vickers indentation test. Finally two series were subjected to the same pre-oxidation, followed by accelerated (Ascectic Acid) salt spray test and high-temperature corrosion and for one series the Vickers test.

Series	Pre-oxid.	Salt spray	Ascetic Acid Salt Spray	High temp	Vickers indent.
R1-R7	-	24/180/240/360/ 480/700/800 hrs	-	0.5 hrs	No
A1-A7	1 hr	24/180/240/360/ 480/700/800 hrs	-	0.5 hrs	No
A8-A14	1 hr	24/180/240/360/ 480/700/800 hrs	-	0.5 hrs	Yes
B1-B7	1 hr	-	24/48/72/96/120/ 144/168 hrs	0.5 hrs	No
B8-B14	1 hr	-	24/48/72/96/120/ 144/168 hrs	0.5 hrs	Yes

Table 4.5 : : test matrix for environmental tests on PM1000 [27]

The pre-oxidation was performed by heating at 4.8°/s to 1200°C, maintain that temperature for 60min and cooling down at 20°/s, all in air atmosphere.

The high-temperature corrosion test consists of heating to 1170°C at 4.8°/s and keeping that temperature for 30 minutes, then cooling down at 10°/s.

The PM1000 brochure from the supplier gives data for corrosion by the mass gain curve measured under cyclic heating to 1150°C in 1-hour cycles. This mass gain is parabolic, and levels off at about 1.6 mg/cm² after 80 hours.

Test data from TU Delft tests come out at lower values: the mass gain follows a similar curve but at lower level, reaching 0.35 mg/cm² after 25 hours at 1200°C. The Plansee data indicates more than 1 mg/cm² at that time.

SEM (Scanning Eletron Microscope) examination of the sample shows that the surface contains mainly Chromium, in the form of Cr₂O₃ oxide which has a cauliflower-like appearance.

4.2 Basic Operation Tests

4.2.1 Test setup & model description

For the proof of concept tests, a setup was built in which two patches of TPS were placed, consisting of PM1000 skin with a piece of ZAL-15 Alumina board at several millimetres behind, was made (see Figure 4-4 and 4-5).

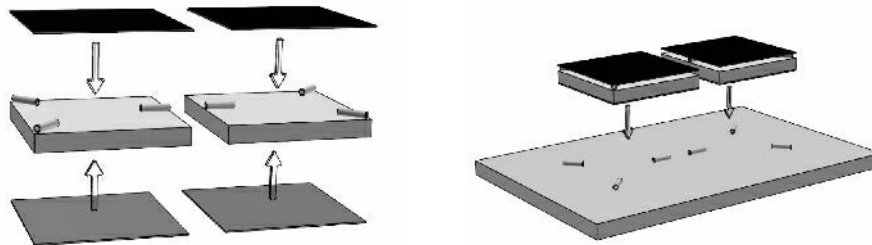


Figure 4-4: Left: the test samples, with from top to bottom the PM1000 sheets, the ZAL-15 board with Silica spacers and Aluminium support plates. Right: samples placed on Alumina board support on Silica spacers

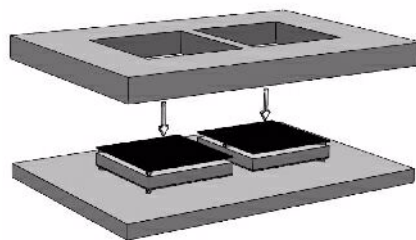


Figure 4-5: Alumina frame placed around test samples

The space between the ZAL-15 Alumina and the PM1000 skin is maintained by three small 5mm diameter Silica cylinders. The same are used to separate the samples from the Alumina board support underneath.

The surrounding frame prevents direct heating from the sides and closely fits the test samples, without actually touching them. This frame, and the support board, are made of ZAL-45 Alumina board, similar to ZAL-15 but with a higher density of 0.72 g/cm^2 . The test samples are $100 \times 100\text{mm}$ in size and the ZAL-15 is $\frac{1}{2}$ " (12.7mm) thick. The PM1000 is 1mm thick.

The test samples are heated by a single array of heater lamps, consisting of 10 quartz lamps of 1000W each, giving a thermal radiation of about 400kW/m^2 . The power supply to the lamps is regulated, and can be controlled via a feedback loop from one of the thermocouples in the test setup.

For mass measurement of the wetted ZAL-15 sample, a cutout is made in the underlying ZAL-45. The ZAL-15 is supported on a stack of ZAL-45 blocks on a aluminium beam which in turn is supported by two dynamometers. These dynamometers can be used to measure the weight by measuring their deformation with strain gages. The aluminium beam is necessary to place the dynamometers away from the heaters which would distort the measurements by inducing an asymmetrical thermal deformation on the sensors. An accuracy of a few grams can be attained, which will average out to higher accuracy over a full measurement run.

4.2.2 Proof of concept tests

At the very beginning of the development of the enhanced radiation cooling system, basic operating tests to show the amount of cooling were performed.

A heating profile based on the expected re-entry heating profile of the DART vehicle was applied to the test sample, controlling the temperature of the uncooled sample. Monitoring of the cooled and uncooled samples gave an indication of the cooling effect that was reached.

Test results

The temperatures measured in one of the very first heating tests are shown in Figure 4-6. Here a heating profile was imposed that simulates the heating during a ballistic re-entry. From simplified theory a temperature ratio equal to the fourth root of 1.92 can be expected, since the cooled sample loses 92% more thermal energy than the uncooled one and this related to the temperature to the fourth power. This means a temperature ratio of 1.177, so

where the uncooled sample reached 1450K, the cooled one should reach 1231K, so a difference of 219K.

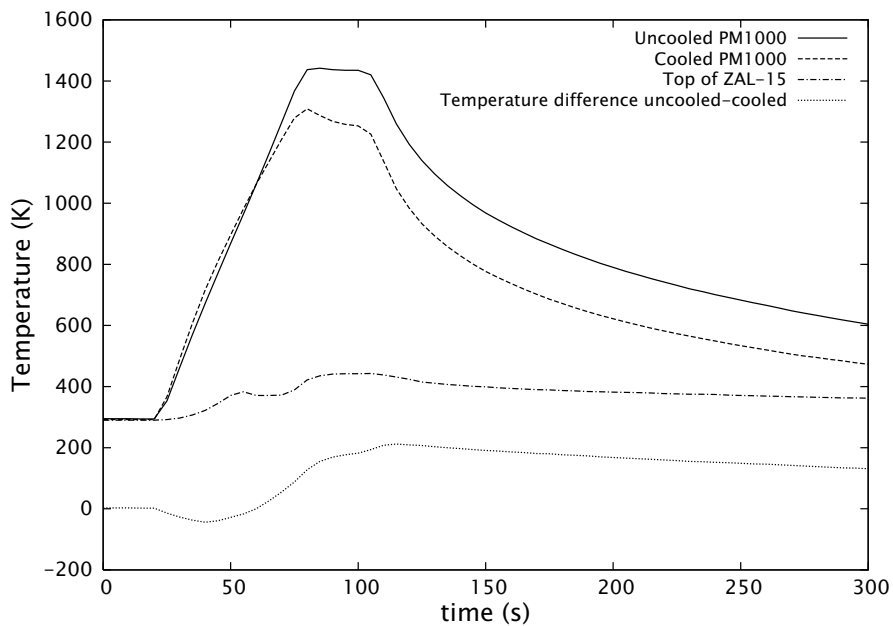


Figure 4-6: Temperature results of a heating test showing the difference between uncooled and cooled PM1000

The peak in temperature of the cooled sample where the uncooled one shows a plateau of constant temperature is due to the peak in applied power that can also be observed there, which is due to the way in which the temperature profile is enforced by the control loop. The cooled sample temperature drops off to a value close to the expected 1231K, with a maximum difference between the two of 200K. The temperature of the ZAL-15 can be observed to exceed 100°C (373K) at about 80 seconds. This is due to an imperfect contact between the thermocouple and the ZAL-15, maybe caused by thermal stress that resulted in deformation of the thermocouple wire. It was observed in more or less extreme extent in many of these tests, but it has little or no influence on the measurements.

Engineering model comparison

In order to make engineering model predictions on the test shown before, the applied heat flux has to be recovered from the actual test data. This heat load can be approximated from the measured temperatures of the uncooled sample by defining a heat balance between applied heat load, heat radiated away and heat radiated to the interior. This will neglect the thermal mass effect of the PM1000 and heat loss to the sides (to the frame). Trying to include these two effects in the calculation of the heat load is not succesful because of the low sampling rate of the temperature measurement.

Calculating the heat load in this way and putting that into the engineering model leads to the results shown in Figure 4-7. The shape of the graphs is somewhat different from the real test, because of the neglected thermal mass in the determination of the heat load. It can be seen that the level of temperature difference predicted matches the experiment quite well.

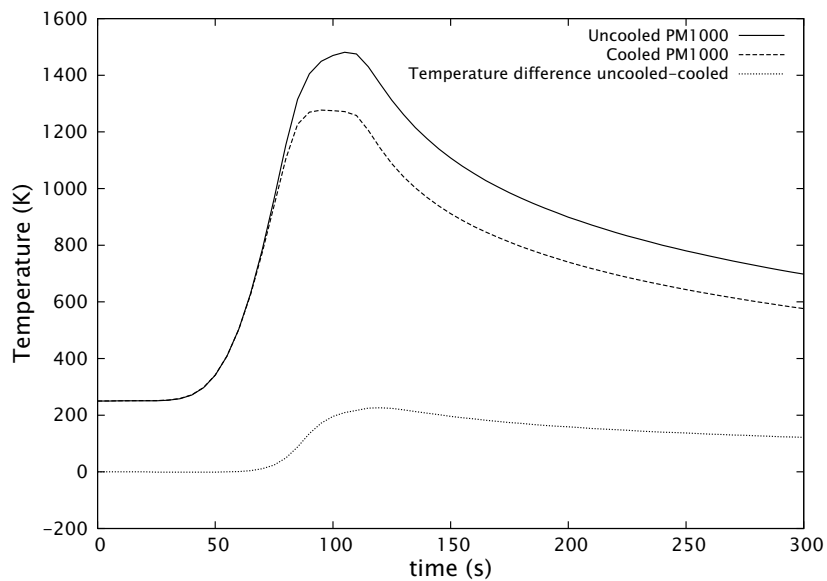


Figure 4-7: Engineering model predictions for test shown above

4.2.3 Drying out of ZAL-15

Theory predicts that at some point, the water transport to the evaporation surface breaks down, and that the surface will start to dry out. The top of the ZAL-15 layer will heat up and the radiation coupling with the PM1000 will decrease, leading to a temperature increase in the PM1000 as well. The ZAL-15 will dry out from the top down, leading to progressive layers through the thickness to show a sudden temperature increase when the drying front passes.

Test results and engineering model predictions

The results of a test with three thermocouples inside the ZAL-15 and one on top and below are shown (see Figure 4-8 below). The applied heating profile consists of a linear heating phase and a constant temperature phase.

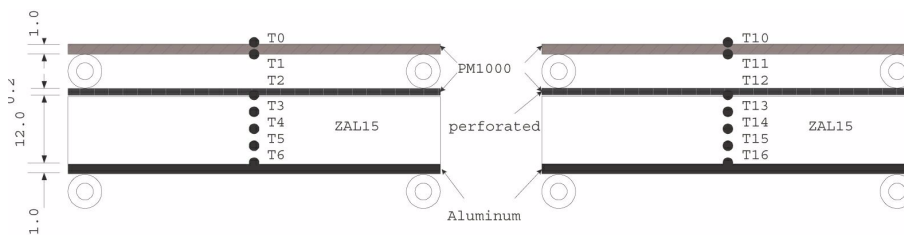


Figure 4-8: location of sensors in the two samples, one dry and one saturated with water

Figure 4-9 shows the results of a test run until drying out of the ZAL-15. It can be seen that the ZAL-15 dries out from the top downward as expected from theory. The time intervals become progressively shorter, which is also in line with the expectations, because water transport still continues at a rate lower than the evaporation rate, so remaining saturation in the still wetted part of the ZAL-15 continues to drop while it is drying out.

The prediction of the engineering model for the uncooled PM1000 is off by 35 to 57 degrees and the heating peak is shifted in time. This time shift is due to the way the applied heat load is reconstructed from the experimental measurements. The temperature difference is due to the neglecting of the thermal mass of the insulation of the uncooled part. The engineering model does not contain the drying phase, so the results are limited to the operational phase of the heating test, up to 435 seconds.

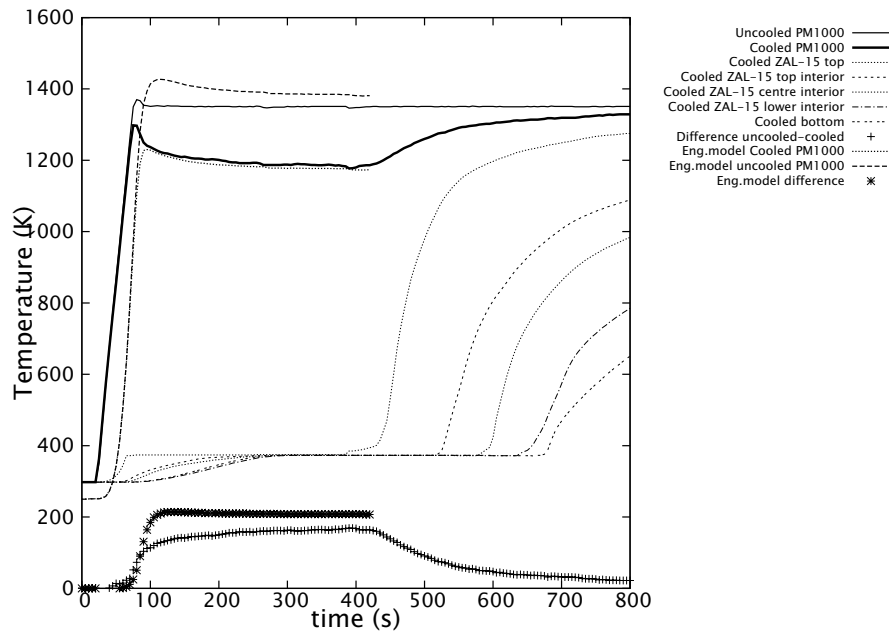


Figure 4-9: Results and engineering model predictions for a drying-out test run (colour version of figure in appendix B as Figure B-1)

FE model comparison

These FE results are for a test where a 0.2mm perforated sheet of PM1000 was placed on top of the ZAL-15 to see whether this would give equally positive results as uncovered ZAL-15. This could later be used to make a sandwich of ZAL-15 and PM1000 to increase robustness. The outcome of this test did not encourage further efforts, but the complete finite element results are available only for this test, so this is used here as an example.

The initial model of the basic test setup was made in PATRAN THERMAL [50], later this model was translated to ABAQUS [32], which was also used for all later models.

A 2D finite element model including convection was developed [32] which gives good results for the phase before the drying out of the ZAL-15. Heat fluxes included in the 2D model are radiation outward from the PM1000, radiation inward, natural convection on the PM1000 outside and mixed convection in the cavity between PM1000 and ZAL-15.

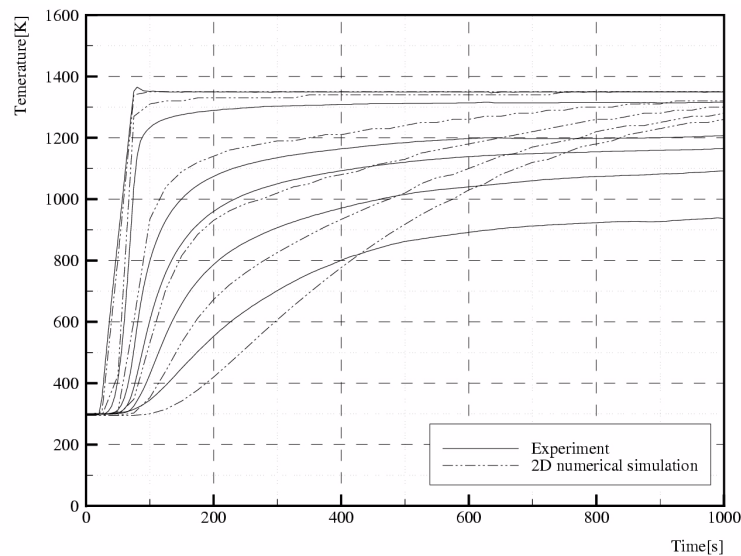


Figure 4-10: 2-Dimensional FE results compared with measured test results [50], showing the temperature through the thickness of uncooled ZAL-15 versus time. Top to bottom the six lines indicate top of the ZAL-15, four positions inside and the bottom.

It can be seen in Figure 4-10 that the temperature evolution of the 2D FE model in dry conditions is quite different from the measured values in the test. The achieved accuracy of the model with respect to the important system parameters as observed in the experiments is given in Table 4.6 and these are much better. The temperatures of the surface of the ZAL-15 are in good correspondence with test results.

It is clear that this finite element model (using 8 elements along the width and one through the thickness of PM1000, aluminium support and evaporation layer and 80 through the thickness of ZAL-15) predicts the behaviour of the experimental setup with very good accuracy. This gives confidence in the modelling of the physical phenomena in the finite element model.

	T=1350K	T=1425K	T=1500K
Turnover point time	+2.50%	+0.50%	+0.20%
Dry-out time	<+6.50%	<+4.80%	<+3.60%
Peak temperature	+0.07%	+0.56%	+1.93%
Temperature difference	+0.59%	+0.14%	+0.27%
Final PM1000 temp	-1.11%	-0.70%	-0.67%

Table 4.6 : performance of the finite element model of the experiment [32]

	T=1350K	T=1425K	T=1500K
$\dot{Q}_{\text{conv outside}}$	8.70	9.39	10.07
$\dot{Q}_{\text{conv inside}}$	31.91	36.79	41.67
$\dot{Q}_{\text{rad outside}}$	79.03	99.76	124.57
$\dot{Q}_{\text{rad inside}}$	69.23	87.39	109.13
\dot{Q}_{total}	188.86	233.33	285.44
\dot{Q}_{applied}	188.10	233.30	283.60

Table 4.7 : Contribution of different heat fluxes in FE model (all in kW/m²) [32]

The different heat fluxes in the finite element model at the point where the temperature difference between cooled and uncooled sample is maximum are shown in Table 4.7. The importance of the convection part in this model is clear, making up 15-20% of the heat loss by the PM1000. The sum of all terms is very close to the applied heat flux that was derived from the uncooled sample temperature measurements.

A 3D finite element model was made of the test setup consisting of one half of the real setup, because of the symmetry (see Figure 4-11). The supporting plate of ZAL-45 and the ZAL-45 frame with cutouts are modelled as one piece of material, so neglecting any possible contact resistance between them. Since thermal conductivity in the porous material is a combination of radiation and conduction in solid phase and air in the pores, this is not expected to have a large impact. The ceramic cylinders between the ZAL-15 and the PM1000 are not modelled. The outside and bottom of the model are assumed adiabatic, as are the sides of the cavities

around the ZAL-15 and the sides of the ZAL-15. In real tests, fibrous insulation was placed here, reducing the heat transfer and making this assumption acceptable.

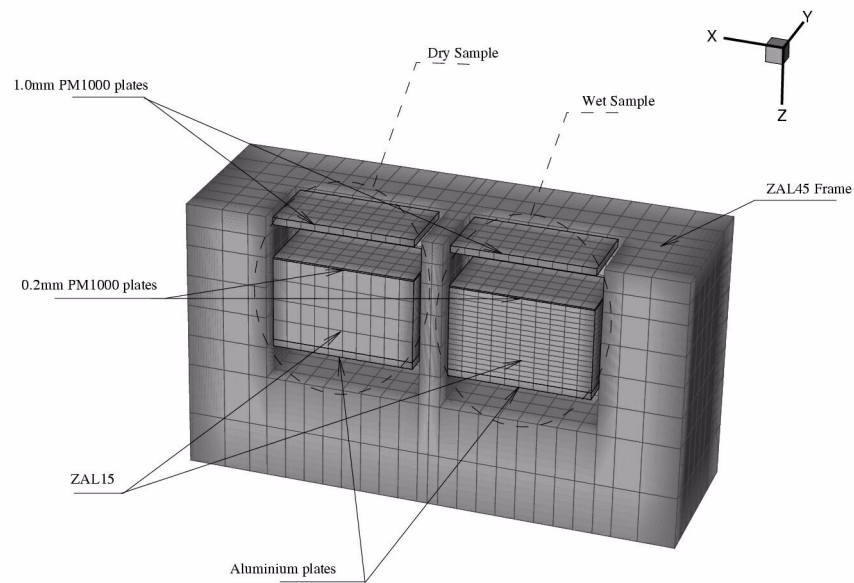


Figure 4-11: The FE model of the test setup, with vertical scale stretched by a factor of five

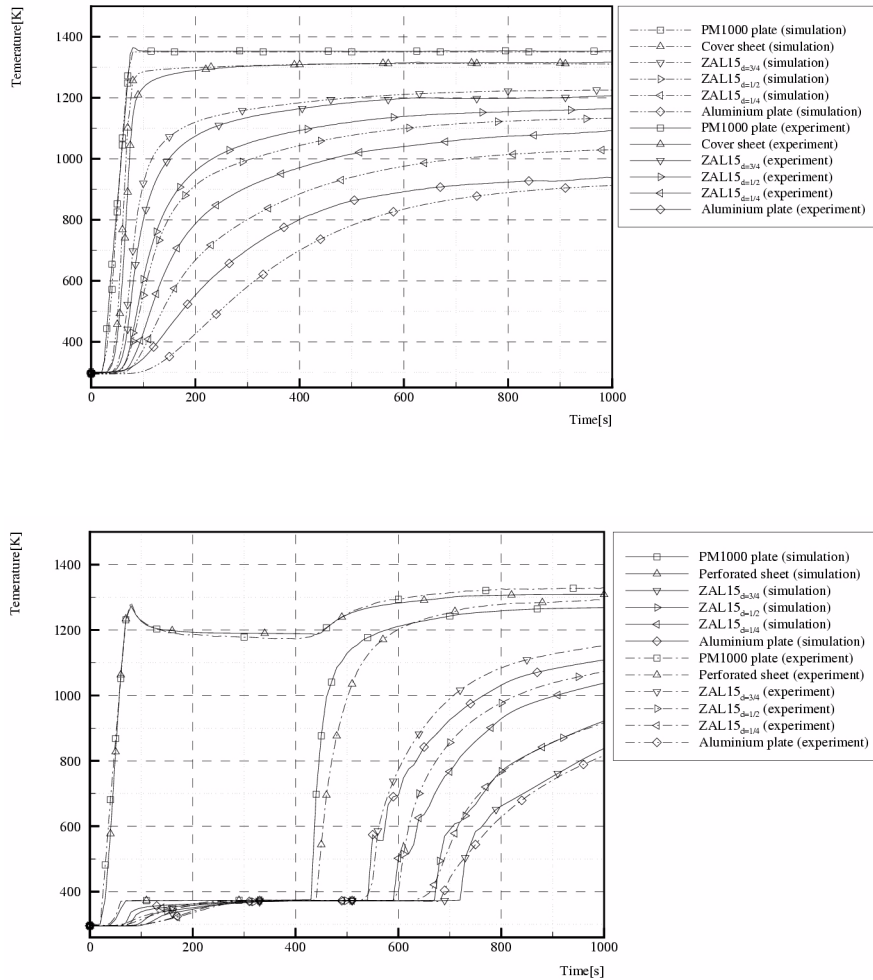


Figure 4-12: Comparison of test and FE analysis for heating test for dry part of sample (top) and wetted part of sample (bottom). Points through the thickness of the sample at the center. From [50].

Analysis of the results shown in Figure 4-12 shows a good correlation between measurement and FE model. It must be noted that the amount of water that evaporates before the turnover point is put into the model by hand, this is not predicted by the Finite Element model. The temperature distribution in the complete model at several points during the test is shown in Figure 4-13 and Figure 4-14. The fact that the heat transfer from the sides of the frame to the sides of the ZAL-15 is neglected will lead to a deviation from physical reality; in the images the temperature distribution is still layered quite nicely, while it is expected that in reality more heat is added to the ZAL-15 through the sides, where the temperature of the surrounding ZAL-45 is much higher.

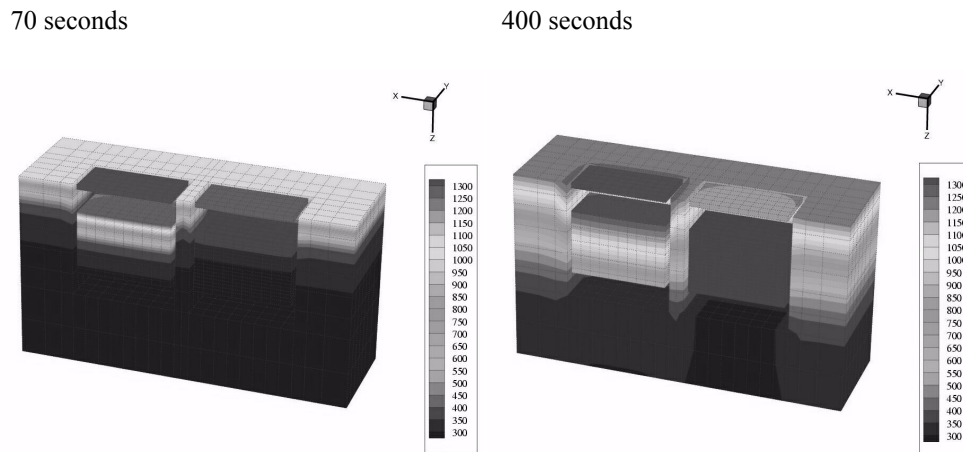
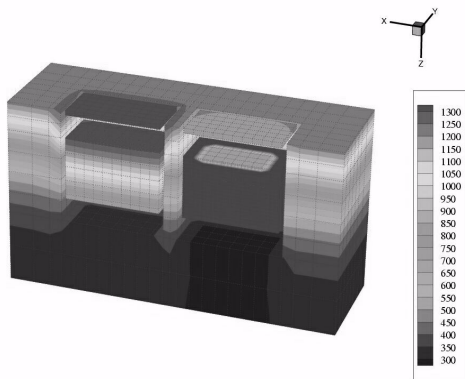
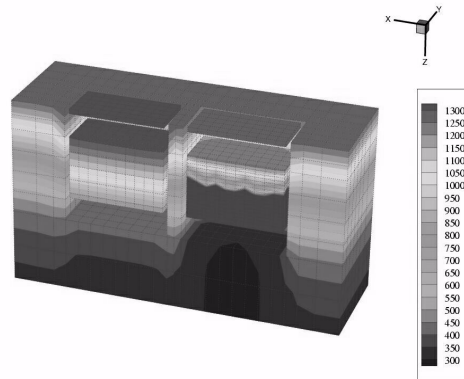


Figure 4-13: Temperature distribution in the test model at various times during the heating test (continued in Figure 4-14). Colour version of the figure can be found in appendix B as Figure B-2. From [50].

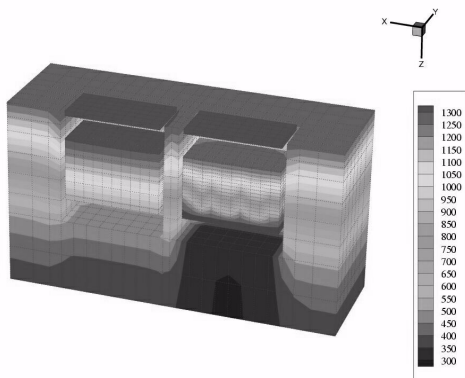
440 seconds



590 seconds



730 seconds



1000 seconds

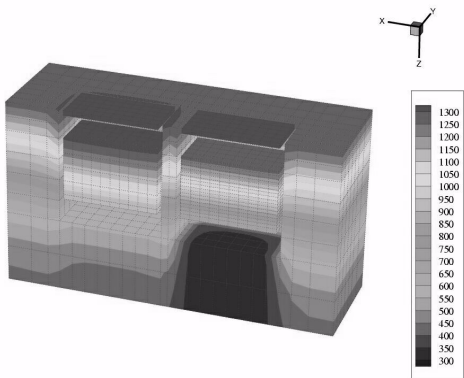


Figure 4-14: Temperature distribution in the test model at various times during the heating test (continued from Figure 4-13). Colour version of the figure can be found in appendix B as Figure B-2 and Figure B-3. From [50].

The following tables show a comparison of the 3D model with experiments similar to Table 4.6 and Table 4.7.

	T=1350K	T=1425K	T=1500K
Turnover point time	+2.80%	+0.90%	+0.90%
Dry-out time	<+10.50%	<+6.80%	<+7.30%
Peak temperature	-1.11%	+0.42%	+0.93%
Temperature difference	+0.15%	-0.07%	+0.40%
Final PM1000 temp	-0.44%	-0.21%	-0.20%

Table 4.8 : performance of the finite element model of the experiment [32]

	T=1350K	T=1425K	T=1500K
Q_{conv} outside	12.39	13.31	14.23
Q_{conv} inside	32.15	36.90	41.56
Q_{rad} outside	80.75	100.62	123.62
Q_{rad} inside	67.22	83.73	102.84
Q_{total}	192.51	234.56	282.25
$Q_{applied}$	188.1	233.3	283.6

Table 4.9 : Contribution of different heat fluxes in FE model [32] (all in kW/m²)

Comparison with the 2D model also shows that a careful and complete model of the 3D situation is important for a correct prediction of the temperature evolution in a quantitative sense. For a more basic qualitative analysis, simplified models are still useful.

Performance of a frozen sample

It was observed that exposure to vacuum will lead to freezing of the water in the porous layer. This raised the question of what would be the performance of the system in a heating test with a frozen piece of ZAL-15. To determine this, several tests were performed with a sample frozen in a household freezer. This gives an initial temperature of the sample just below freezing at the start of the tests.

The standard setup with a dry and a wetted (and frozen) sample was used. It was heated to 1450K at 20K/s and controlled via the uncooled sample. Temperature was kept level until the turnover point was observed; at that point the heaters were shut down manually.

Here the results from that test with a frozen sample is given (Figure 4-15) together with a test with a non-frozen sample (Figure 4-16) under the same conditions.

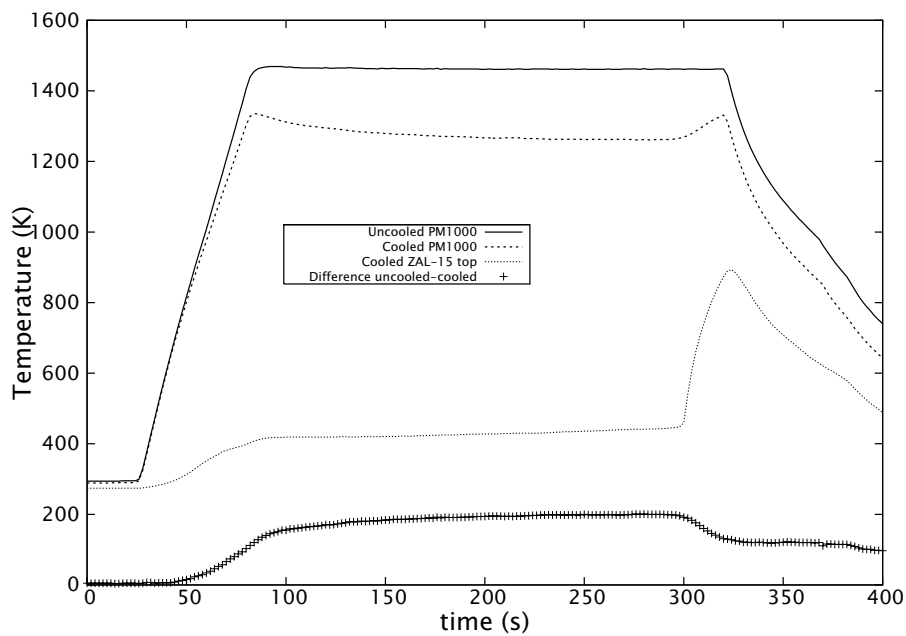


Figure 4-15: Heating test with a frozen sample of ZAL-15 showing the difference in temperature between the cooled and uncooled samples

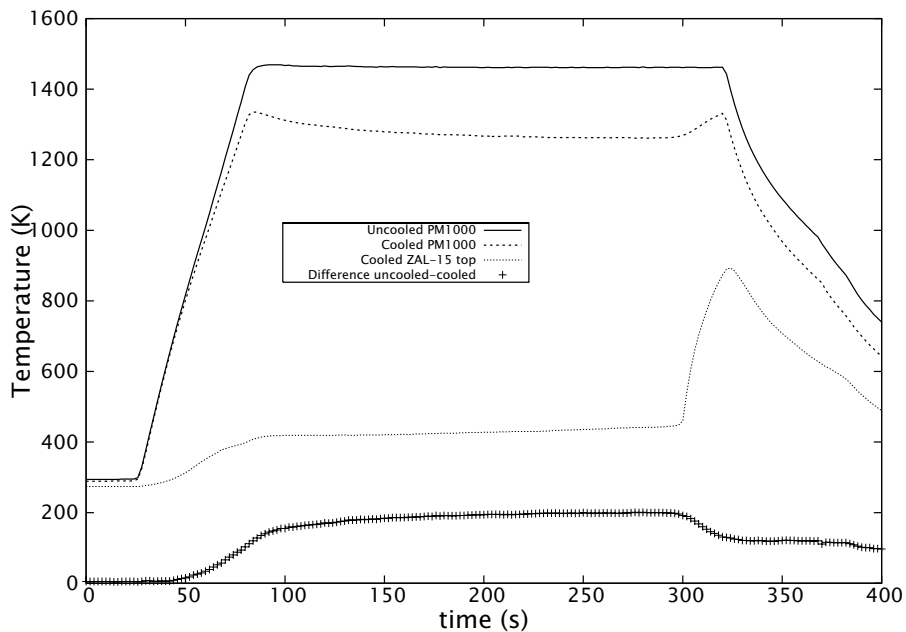


Figure 4-16: Heating test under the same conditions as the one with the frozen sample of ZAL-15 but with a non-frozen piece of ZAL-15

For the non-frozen sample the time to the turnover point is 250 seconds, for the frozen sample 274 seconds. The temperature difference between uncooled and cooled PM1000 is 232 degrees for the unfrozen sample and 199 degrees for the frozen sample. It can be concluded that the frozen sample performs slightly less than the unfrozen one, possibly because of a difference in emissivity of the ZAL-15.

In any case, the fact that the water in the ZAL-15 is frozen at the start of the test does not pose any problems in the water transport, so the water melts quickly enough to supply the evaporation surface at the top of the ZAL-15 with sufficient water. The temperature reading of the ZAL-15 of the frozen sample shows that the temperature of the bottom of the ZAL-15 is 0°C at the start of the test, and starts to slowly heat up immediately, suggesting that the ice quickly melts.

4.2.4 Determination of the turnover point and critical saturation

From the theory of flow of a liquid through the porous medium it has become clear that a full analytical model based on that theory requires the determination of a number of parameters related to the materials involved in the process and their interactions. Each one of these parameters would require a laborious experimental campaign and would introduce a separate measure of uncertainty in the results. Therefore, a more pragmatic approach of measuring the desired parameters of the system at once in simulated operational conditions is selected.

One of the most important parameters which define the operational behaviour of the Enhanced Radiation Cooling System is the level of saturation at which the cooling breaks down. This gives the amount of water that is used effectively, and the amount that is 'dead weight'. The variation of this parameter with porous layer thickness and with applied heat load is to be determined.

A range of tests was performed varying the following parameters:

- The temperature of the uncooled sample was set at 1300, 1400 and 1500K.
- A ZAL-15 sample of 12.7mm, 19.2mm and 25.4mm (1/2, 3/4 and 1 inch) thickness was used.

Every set of temperature and ZAL-15 thickness settings was run 3 times to check the repeatability of the tests. The 12.7mm ZAL-15 was a piece of material that was cut about 2 years prior to the test, while the thicker samples were from new material cut shortly before the tests.

The heating profile applied was controlled by a feedback signal from a thermocouple on the uncooled PM1000 sample. This temperature was controlled to follow a temperature profile with a heating phase at 20 degrees per second up to the specified temperature and then kept constant until the readout of the temperature of the wet ZAL-15 indicated the turnover point, shortly after which the heaters were shut down manually.

The repeatability of the tests was usually quite good, except a few cases where apparently not the same amount of water was put into the model.

The results of three tests with a 19.2mm (0.75 inch) thick sample of ZAL-15 are shown in Figure 4-17, with the uncooled PM1000 controlled to 1500K. The differences in cooled PM1000 temperature and in time to turnover point are very small. The mass measurements of these same tests show slightly more spread, as shown in Figure 4-18.

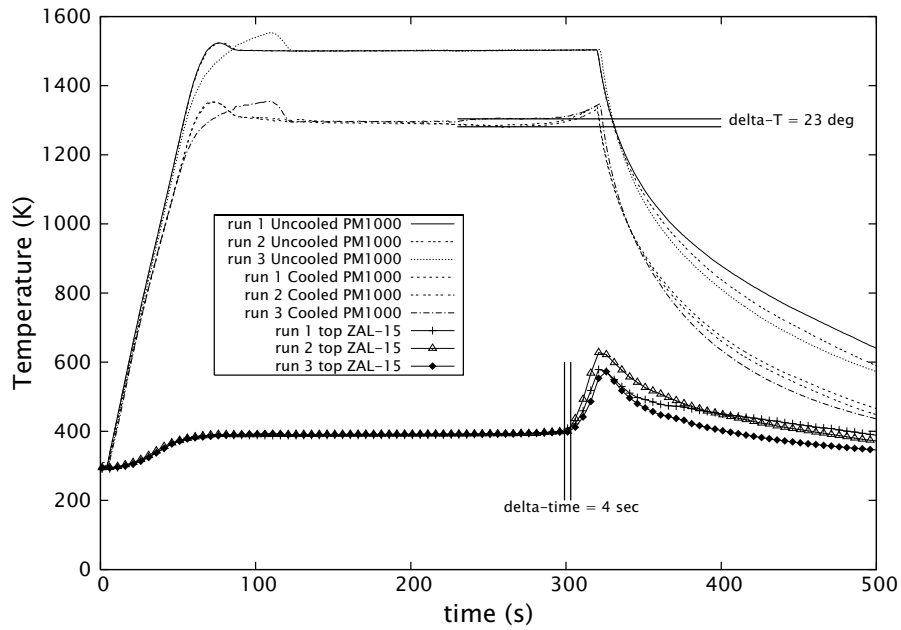


Figure 4-17: Repeatability of tests; 3 runs with 19.2mm (0.75 inch) thick ZAL-15 to 1500K for the uncooled PM1000. Colour version in appendix B as Figure B-4.

The results of all test runs together show the relation between the critical saturation level and the approximate temperature of the uncooled sample. Since the temperature of the uncooled sample is controlled, that of the cooled sample can change somewhat during the test, as can be seen in Figure 4-18 so an average number is used in Figure 4-19.

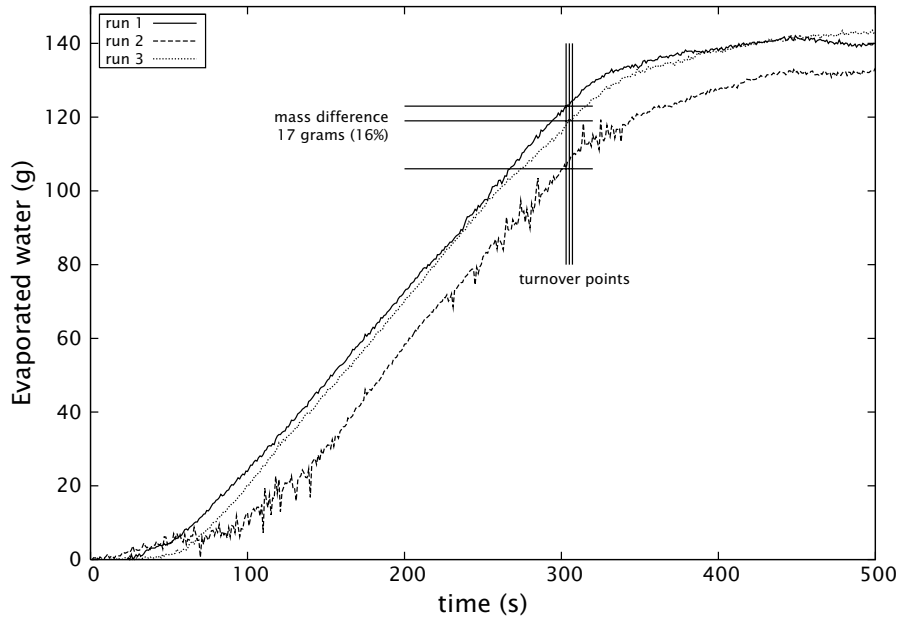


Figure 4-18: Mass measurement of the test runs shown in Figure 4-17. Colour version in appendix B as Figure B-5.

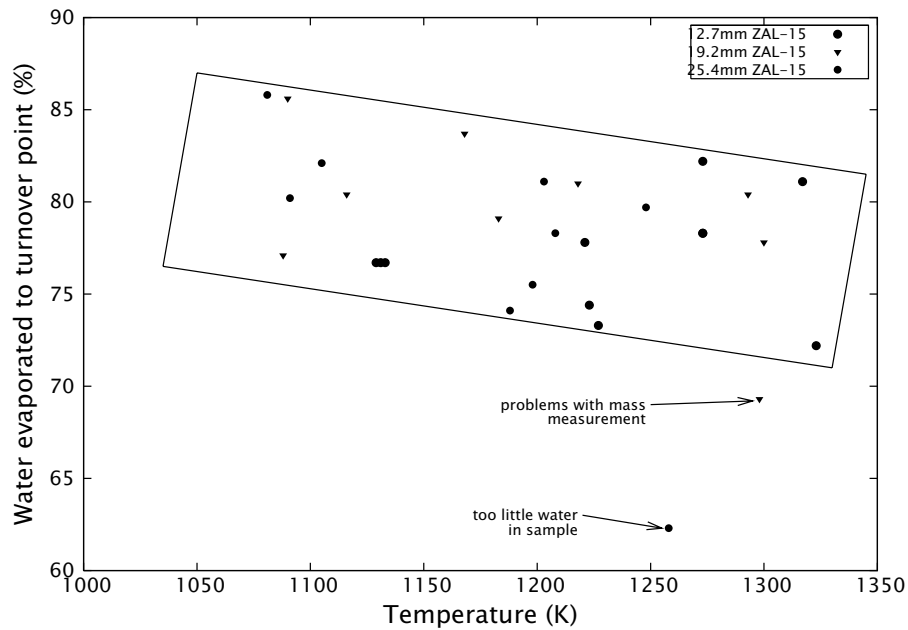


Figure 4-19: Critical saturation level for all runs. Colour version in appendix B as Figure B-6.

It can be seen that there is a bandwidth of about 10% in the critical saturation level and that there is a linear decrease in the amount of water that evaporates before the turnover point with increasing temperature (or applied heat load). All in all, the useful amount of water in the ZAL-15 ranges from a minimum of about 70% at 1300K to a maximum of up to 87% at 1050K.

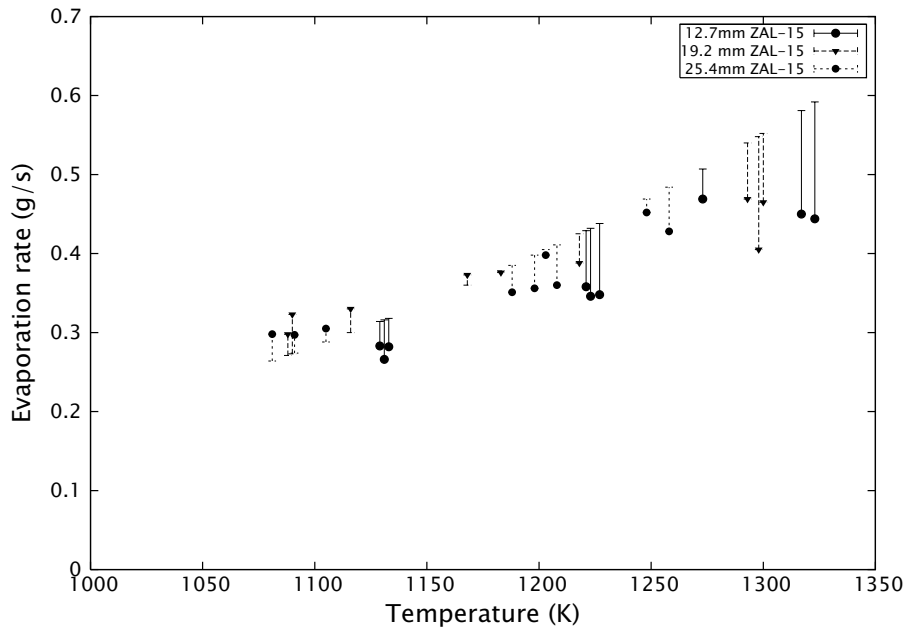


Figure 4-20: Evaporation rate as a function of temperature, data collected from all runs. Error bars indicate expected evaporation rate based on 1-dimensional engineering model. Colour version in appendix B as Figure B-7.

The evaporation rate for all runs is given in Figure 4-20 with the same average temperature level as used before. When comparing the measured evaporation rates with those expected from the 1-dimensional engineering model, it seems that the change of evaporation rate with temperature is much lower than expected. This is partly due to convection cooling of the PM1000 by vapour, which increases with increasing vapour flow. The 12.7mm thick ZAL-15 runs consistently show lower evaporation rates; this is probably due to degraded optical properties of this piece of material which had been lying in the lab for more than a year, as opposed to the thicker samples which were cut from new material.

4.2.5 Changing the surface tension of water

Because of the role the surface tension of water plays in the capillary transport in the porous material, an effort was made to change the surface tension of water and see what the results are on the behaviour during a heating test.

It was attempted to increase the surface tension by adding salts and colouring agents, but measurements of the surface tension by measuring the shape of a droplet of water were not encouraging, in that very little change was observed (see [87] for a full report on these tests).

Lowering the surface tension was done by adding a soap-like additive, with the trade name Nonidet P40 containing the working agent Alkyl-phenol-ethylene-oxide.

The interfacial tension was measured by measuring the contact angle of a droplet of the liquid on a glass plate with a special machine. The colouring agents were obtained from the Chemistry Faculty of Delft University and were supposed to increase the surface tension. The results in Table 4.10 show that only adding a large amount of soap will seriously alter the surface tension, so the soapy solution was used in heating tests.

Liquid	Interfacial tension (mN/m)
Demineralised water	72.3
same + 1% NaCl salt	71.8
same + 4% NaCl salt	71.2
same + colouring agent 1 (1 drop / 0.1 liter)	72.0
same + colouring agent 2 (1 drop / 0.1 liter)	72.2
same + colouring agent 3 (1 drop / 0.1 liter)	71.8
same + colouring agent 4 (1 drop / 0.1 liter)	70.9
same + Nonidet P40 (1 drop / 0.5 liter)	70.5
same + Nonidet P40 (6 drops / 0.5 liter)	67.7

Table 4.10 : Results of efforts to change the surface tension of water

A problem with this is that the ZAL-15 was refilled with the soapy solution after each test run, and it is clear that while the water evaporates, the soap remains behind, increasing the concentration after each run.

Also it was observed that the surface of the ZAL-15 developed a greyish sticky coating, probably of soap residue. Therefore, six runs with soapy water will mean six runs with increasing concentration of soap, so with progressively lower surface tension.

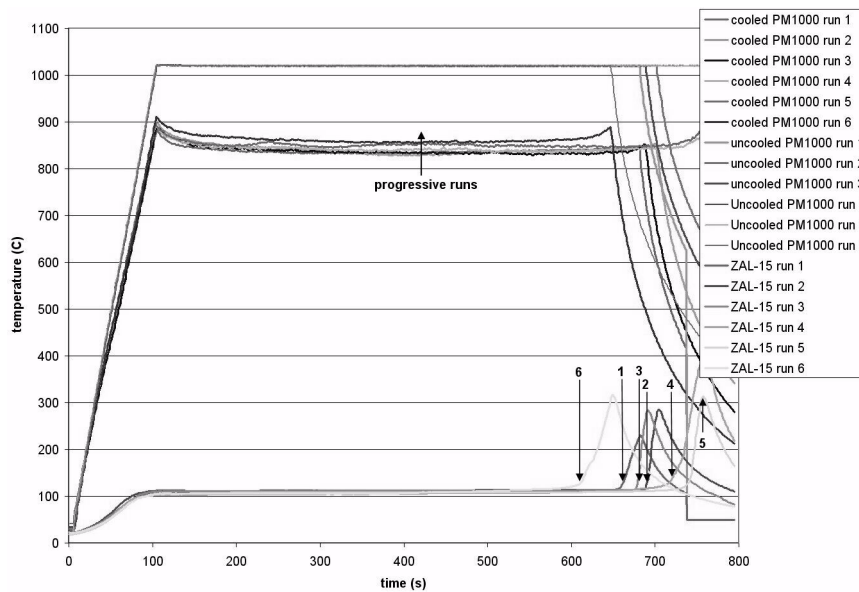


Figure 4-21: Comparison of six runs with reduced surface tension. Colour version in appendix B as Figure B-8.

Looking at the results of the six runs in Figure 4-21, it can be seen that for run 1-5, the time to the turnover point increases, and the temperature of the cooled PM1000 increases as well. In other words, the cooling effect decreases, probably due to the residue on the surface of the ZAL-15 reducing the emissivity of the material. Run 6 probably had too little water since the turnover point is unexpectedly early.

4.2.6 Conclusions of basic operation tests

The basic tests, even though performed with a very simple model and a test setup with limited possibilities, have clearly shown that the Enhanced Radiation Cooling System works in reality as was expected based on theory.

The tests have been compared with a one-dimensional engineering model and with two- and three-dimensional finite element models. These show that the models give a good comparison with the tests, but also that for reliable correlation a fairly large finite element model is required, which still needs some input data (notably, the amount of water evaporated before the turnover point) to give accurate results. Therefore, predicting the behaviour of a new layout with the data currently available on material properties and critical saturation can not be expected to give an accuracy better than 10-15 percent.

Several methods have been studied to improve the material characteristics of the ZAL-15 (mainly the emissivity at the surface) and the water (through the surface tension) but these have not led to improvements. The combination of materials performs very well, and considering the characteristics that have been measured, very little room for improvement remains based on theory, let alone what can be reached in reality.

4.3 Large lab model tests

A larger model was designed to study the effect of convection and to show the design of a closed system.

4.3.1 Model design and test setup

An 800 by 250mm box was designed in which various thicknesses of ZAL-15 can be used and with varying gap dimensions between the ZAL-15 and the heated skin plate. To reduce cost of the model, all components except the skin were constructed out of high-temperature resistant stainless steel. Two views of the model are shown in Figure 4-22 and an exploded view in Figure 4-23.

The model is built around a welded steel frame of a 3mm thick U-profile beam. A steel plate is screwed to the bottom of this frame and this supports the ZAL-15 plate. Holes for thermocouples and pressure measurements are drilled into this bottom plate. The thermocouples project through the bottom plate into the ZAL-15 to just under the upper surface of the porous material to measure the temperature as close to the surface as possible. From the pressure measurement holes, holes are drilled through the ZAL-15 as well, into which small hollow Alumina cylinders are placed to provide a pressure port through to the upper surface of the ZAL-15. An adapter is bolted to the bottom of the steel plate to hold a tube to the actual pressure sensor (see Figure 4-24).

On top of the steel frame, a separate spacer frame is placed which allows us to change the gap width between the ZAL-15 and the PM1000 by changing frames of different thickness. An Alumina paper seal is placed between the frame and the spacer frame and between the spacer frame and the PM1000 cover plate.

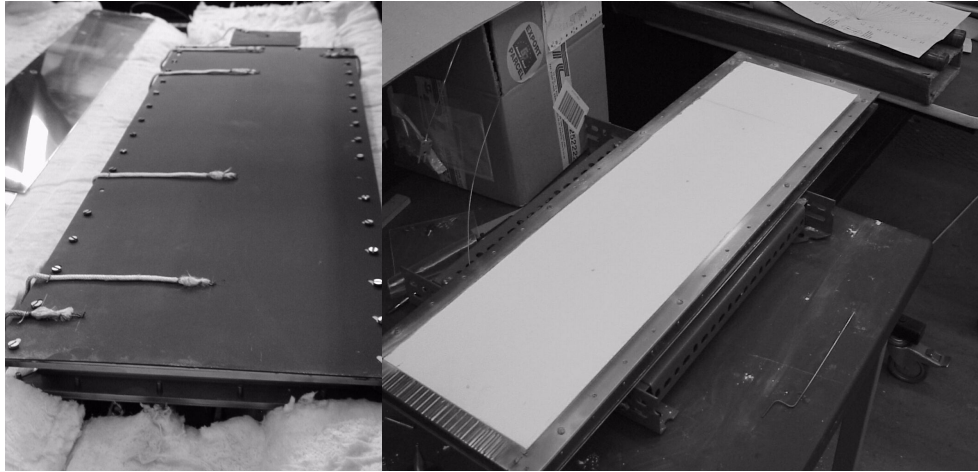


Figure 4-22: Two views of the large model; closed on the left with the themocouples on the PM1000; open on the right showing the ZAL-15 inside

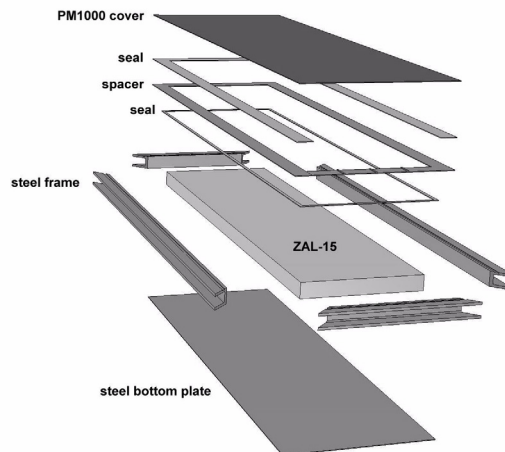


Figure 4-23: Exploded view of the large test model.

Three thickness grades of ZAL-15 were used, $\frac{1}{2}$ " , $\frac{3}{4}$ " and 1" (12.7, 19 and 25.4 mm) and the gap width was varied from 1 to 3 and 5mm. When heated from 0°C to 1300°C, PM1000 expands by about 2%, so the PM1000 plate is held on to the model by U-shaped clamps around three sides (not the outflow side) to allow it to slide to accommodate the thermal expansion. An earlier version used slotted holes through which the plate was bolted to the steel frame, but this did not work, so it was replaced by the clamped variant. Thermocouples are welded on the PM1000 at four points along the centerline and in two corners, one upstream and one downstream. Two control thermocouples are used to control the two halves of the heater array, and are located midway along the length equidistant from the centerline (see Figure 4-24 right).

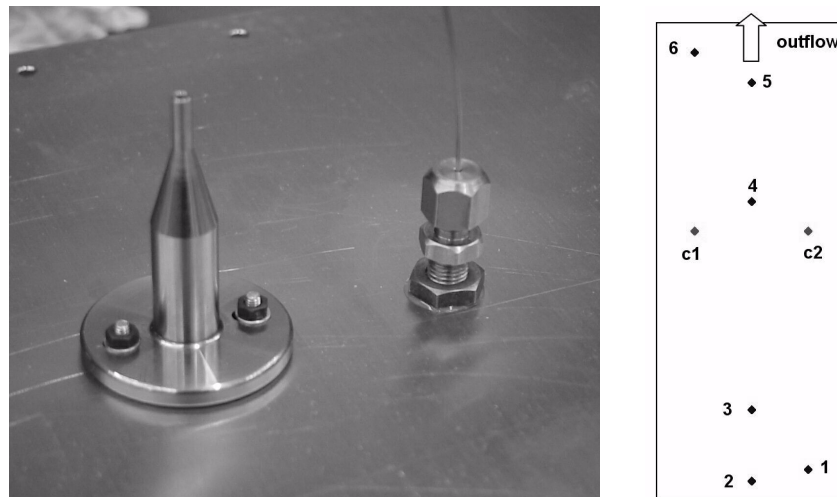


Figure 4-24: Sensor attachment for pressure sensing tube and attached thermocouple (left picture) and the locations of the temperature sensors on the model, with c1 and c3 being the control thermocouples.

The test model is mounted in a frame that is designed to measure the weight of the model throughout the test. This is done with four small dynamometers. In order to keep these dynamometers away from the hot part of the test setup, since temperature gradients would disturb the measurement, a bridge of about 2 meters in length carries the test model and is supported on its corners by the four dynamometers. Care must be taken to mount the dynamometers in such a way that they are loaded in the intended direction only, and that thermal distortion of the frame and bridge do not cause bending of the sensors in other ways.

To do this, the bridge is placed on the dynamometers on small pointed cones to make it closer to being statically determined. Of course, 3 points rather than four would make the system statically determined. The flexibility of the bridge ensures that it is always resting on four dynamometers. If the bridge would be stiff enough to carry the model on three supports out of the four, it could flip from one to the other, introducing noise in the measurements. A diagram of the test setup is given in Figure 4-25.

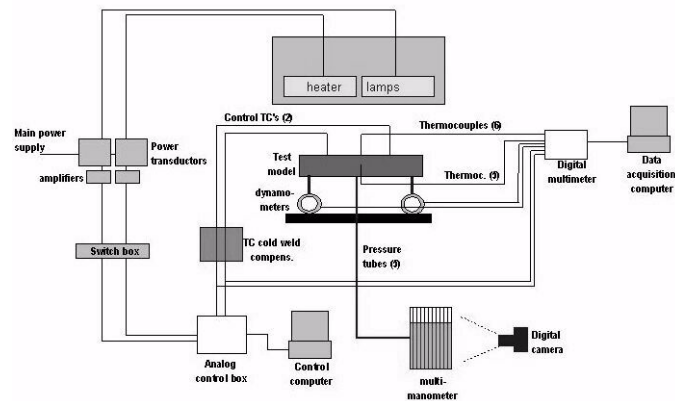


Figure 4-25: diagram of the controls and sensors of the test setup

4.3.2 Objectives and expected results

One of the main goals of the test is to show the influence of convection on the temperature of the model. The analytical model of section 3.3 is used to predict the temperature and pressure distribution along the length of the model in a 2-D cross section. The point of transition from laminar to turbulent flow in the model is something we want to measure. Finally refilling the model, and eventually continuous refilling during operation, is an objective. Numerous problems with building the model and test setup and with performing the actual tests have led to none of these objectives being reached within the time limits of this PhD study.

The pressure will drop along the length of the model from the closed end to the outflow opening. This pressure will cause a flow to the outflow opening with increasing velocity in that direction. The flow will cause the convection cooling which will lead to lower temperatures from closed to open end.

There are several factors which complicate matters. The model is placed under the heater lamps with the outflow opening under one end of the lamps, to minimize water vapour damage to the lamps. This also means that the thermal load at that end of the model is less than under the center of the heater array. Also, the steel frame of the model is a significant thermal mass that will cause the temperatures at the edge to be lower.

4.3.3 Test results

The actual tests have been much more troublesome than was initially expected, and the amount of useful results is limited.

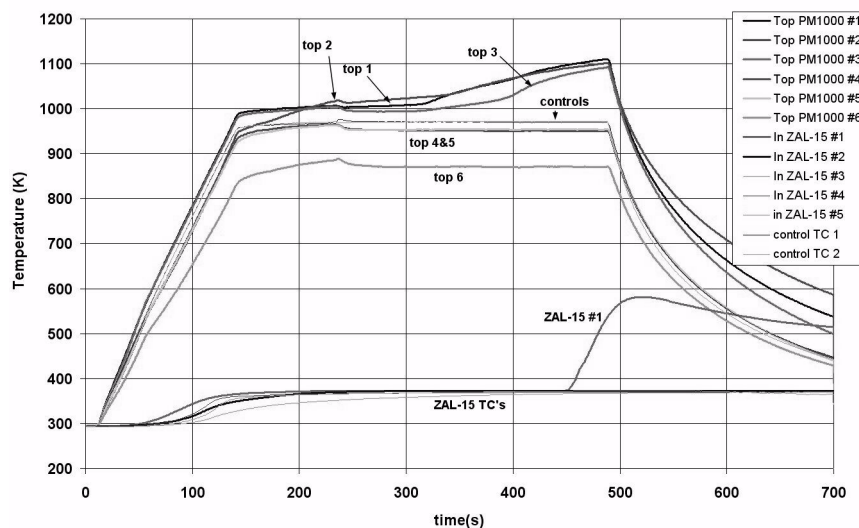


Figure 4-26: temperature measurements of test run with large model. Colour version in appendix B as Figure B-9.

Figure 4-26 shows the temperature readings of a test run with the large model where the model was heated at 5°/s to a temperature of 700°C and kept at that temperature for 400 seconds.

The readings from the different thermocouples are in line with the expectations that the temperature should drop off towards the outflow opening (so with progressively higher

number of the thermocouples). The ZAL-15 readings show the expected 100°C until at one point it starts to dry out. This is actually one of the corners furthest away from the water filling point, so there the saturation level is not what it should be. This thermocouple is placed inside the ZAL-15 from underneath, and should be as close as possible under the surface without breaking through. It is not possible to determine the depth precisely, so these measurements are actually at a small distance underneath the surface. This means that the surface of the ZAL-15 will dry out somewhat earlier than indicated by these readings, which is probably the reason for the temperature increase of thermocouples 1, 2 and 3 from 300-400 seconds.

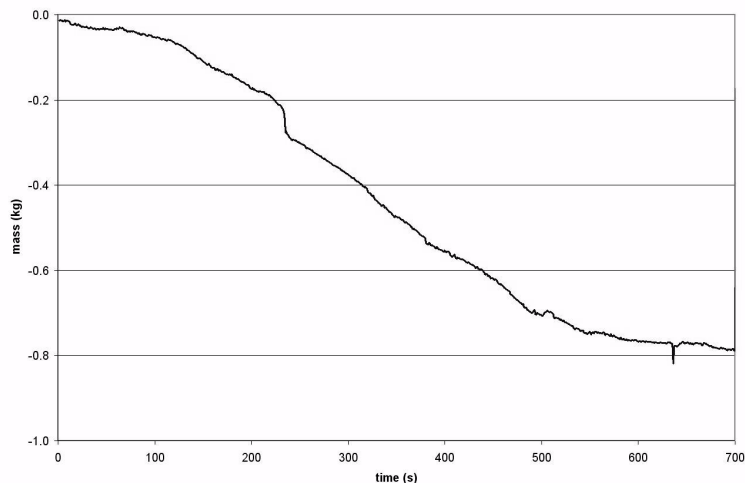


Figure 4-27: mass measurement of test run shown in Figure 4-26

The mass measurement of this test run shows a fairly linear decrease in mass of about 1.7 g/s during the highest temperature part of the measurement run. This is actually quite a bit less than what would be expected; for an average temperature of the skin of 950K, an evaporation rate of 2.6 g/s would be expected. This could be partly due to the skin temperature falling off towards the side of the model because of the thermal mass of the frame, so the average temperature is lower than one would guess from the thermocouple readings.

4.3.4 Finite element model

Like for the small test models, a finite element model has been made of this test model. A full representation of the convection inside the model has been made [78]. The FE model is able to reproduce the physical behaviour that is expected, similar to the previous small FE models.

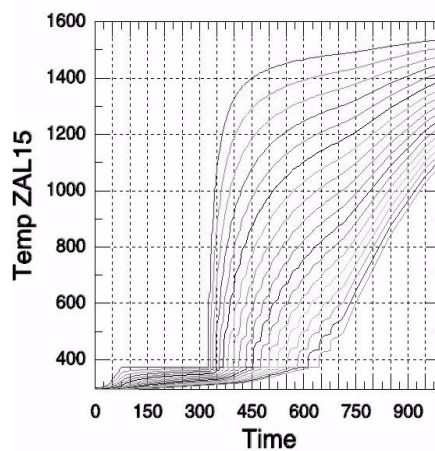


Figure 4-28: temperature predictions for the ZAL-15 in the FE model. The lines from top to bottom show temperatures for the nodes from top to bottom in the ZAL-15.

Figure 4-28 shows the temperature history of the ZAL-15 for a number of nodes through the thickness. It clearly shows the expected behaviour of heating to 100°C, followed by a period of constant temperature, followed by the progressive drying out and heating up.

A view of the model is given in Figure 4-29 showing the temperature field during the later stages of drying out of the model. Note that this is a phase that would not be reproduced in an actual test, because the high temperatures that can be reached by the steel components of the model might damage it. It gives an indication of the heat transfer through the steel frame leading to heating up of the ZAL-15 from the sides in addition to the radiative heating from the top by the hot PM1000 cover plate. The figure gives an indication of the size and complexity of the FE model.

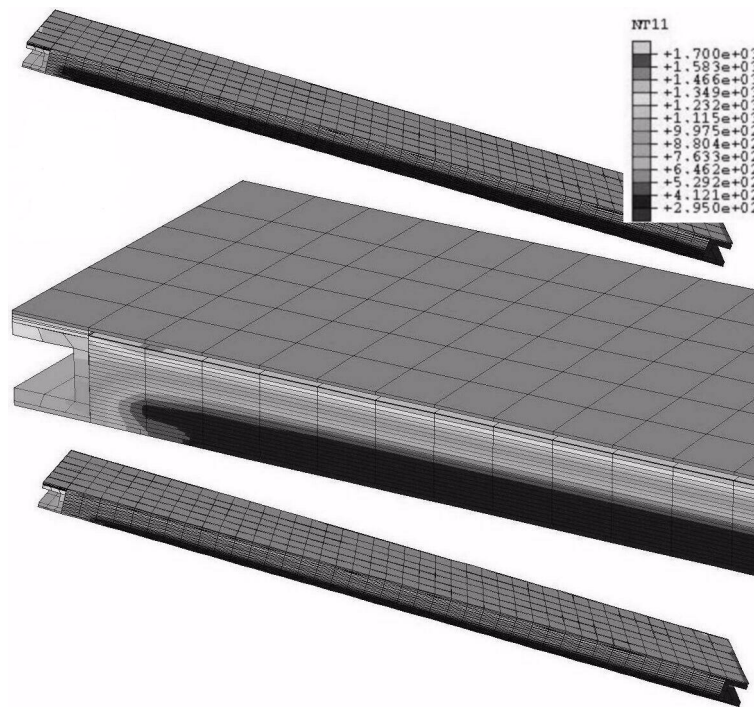


Figure 4-29: the FE model of the large closed model, consisting of half the real model because of symmetry. Temperature fields at two points during the drying out phase of a test run. Colour version in appendix B as Figure B-10.

4.4 Other tests

4.4.1 Vacuum chamber tests

The behaviour of wetted ZAL-15 exposed to low pressure was tested in a vacuum chamber where the pressure was progressively reduced from atmospheric pressure to about 5 mbar. Pressure drop down to 8-9 mbar is quite rapid, from there on the pressure slowly drops down to about 5 mbar where it remains constant, indicating the limits of the vacuum pump which is able to cope with the water vapour escaping at that point but is not able to reduce the pressure further. A number of tests were performed where the amount of time the sample

was exposed to the 5-6mbar pressure level was varied. The test was performed at room temperature.

Water loss during vacuum exposure

It was observed that water started to boil at about 25 mbar, which led to some water loss by sputtering. After that, the remaining water freezes. The samples were weighed before and after vacuum exposure to determine the amount of water lost. The test sample was 100x100x12.7mm in size and contains about 100 grams of water before the test.

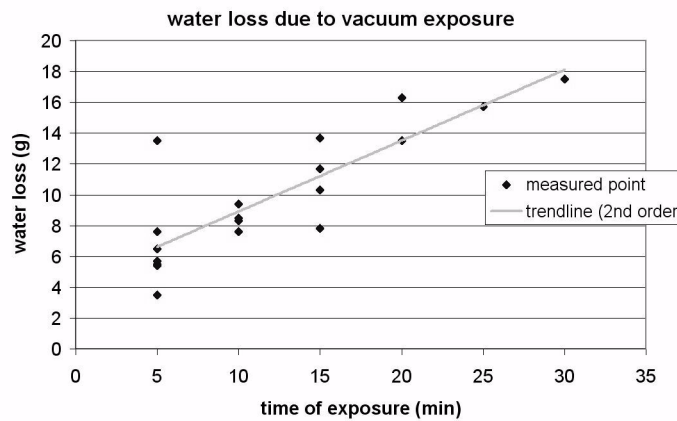


Figure 4-30: results of vacuum exposure tests of wetted ZAL-15. Initial water content was about 130 grams

The results of the tests (see Figure 4-30) show that water is lost continuously during exposure to vacuum. Because the sample is frozen, the water is lost through sublimation. After 20 minutes exposure to vacuum, already some 10% of the initial water content is lost.

Damage to ZAL-15 due to freezing

Because water expands on freezing, it was expected that this could lead to damage to the porous and brittle ZAL-15 material. Therefore, the test sample used in the freezing tests was examined in the Scanning Electron Microscope to look for changes in the microstructure.

Comparing a sample that was once frozen and then used in a heating test with a non-frozen sample gives the following result:

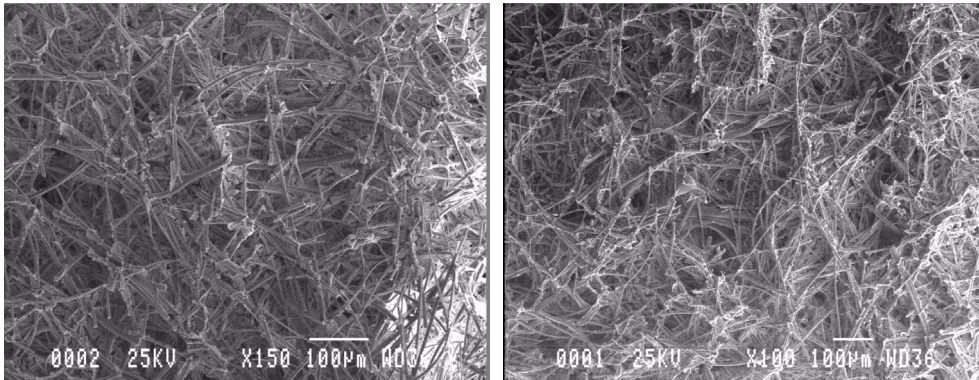


Figure 4-31: comparison of ZAL-15 that was not frozen (left), and ZAL-15 that was frozen once and then used in a heating test (right).

Close study of Figure 4-31 seems to indicate some parts in the right image where a macroscopic cavity could be discerned where the fibres are pushed aside by the freezing water, but this is far from clear. Considering the performance of this sample in the heating test it was concluded that freezing does not have a detrimental effect on the behaviour of the ZAL-15 in an operational sense in the cooling system. The size of the sample did not change after freezing and thawing.

A closer examination of the sample that was frozen 20 times was performed to see whether repeated freezing and thawing damages the ZAL-15. Comparison of the SEM image of the sample that was repeatedly frozen (Figure 4-32, lower right picture) with images from not-frozen samples (Figure 4-32, upper two and lower left pictures) show the same kind of structure: Al₂O₃ fibres with SiO₂ binder connecting them. The Silica is cracked in all images, this is clearly not due to the freezing. It was therefore concluded that freezing does not have any noticeable impact on the structure of the ZAL-15.

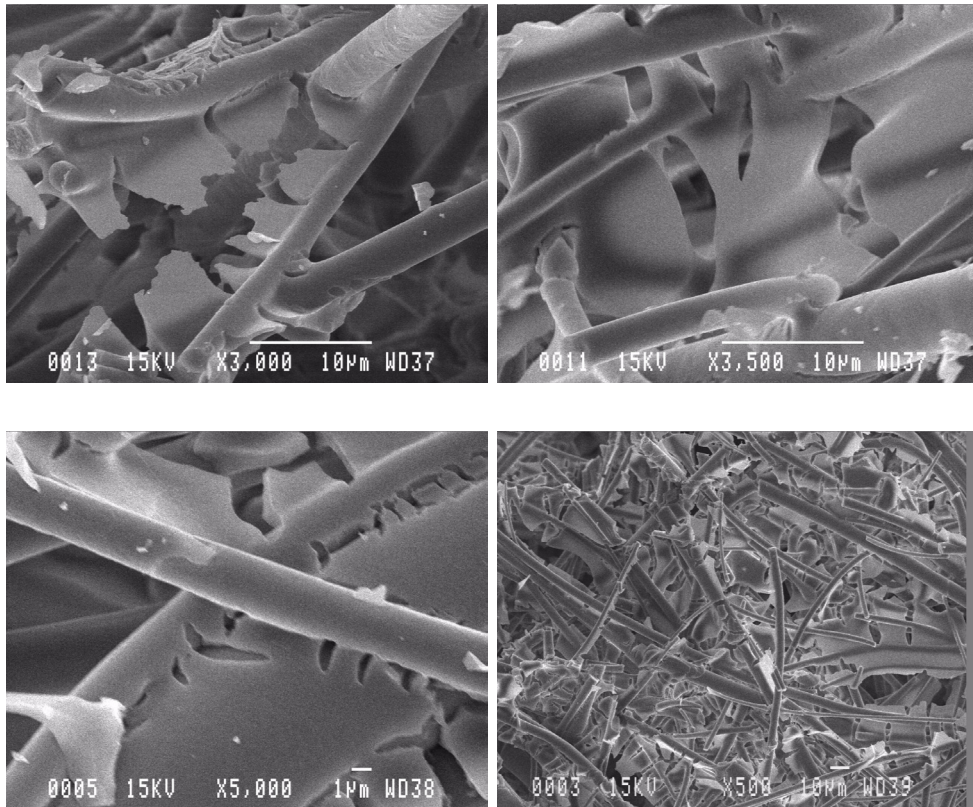


Figure 4-32: SEM images of ZAL-15; not frozen, 3000x magnified (top left); not frozen 3500x magnified (top right); not frozen 5000x magnified (bottom left) and 20 times frozen and thawed, 500x magnified (bottom right).

Conclusions from freezing tests

Despite the fact that freezing, even repeatedly, does not damage the structure of the ZAL-15, and the fact that a frozen sample performed as well in a heating test as a non-frozen sample,

the amount of water loss during exposure to vacuum shows a need to prevent vacuum exposure in operational use. When used in a Space-Shuttle like vehicle, and when the ZAL-15 would be exposed to vacuum, this exposure would be many hours to days in duration, which would lead to sublimation of a large part, or even all, of the water contained in the ZAL-15.

Because the boil-off starts at about 25 mbar at room temperature, a minimum pressure must be maintained in the system to prevent this boil-off, and a pressure level of 30 mbar is advised. This pressure can be maintained with a small pressure relief valve in a closed system.

4.4.2 Water filling tests

filling time

When porous Alumina is re-filled with water it is important to know how fast water is spread through the material. It will likely not be possible to ‘pour’ water on the material, which is known to lead to extremely rapid filling. Therefore, tests were performed with supplying water to a strip of ZAL-15 through a thin hose connected to one side. The test setup is shown in Figure 4-33.

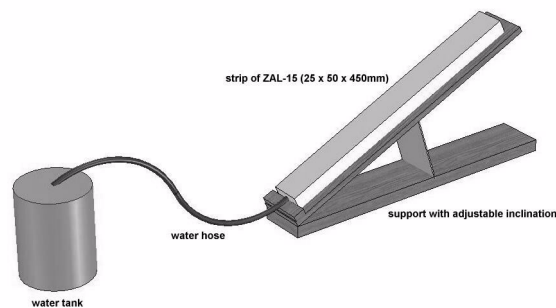


Figure 4-33: test setup for determining water dissipation speed in ZAL-15

The tests were performed under three angles: horizontal, vertical and 30° from horizontal. The time for the water to reach specified distances along the length of the strip of ZAL-15 was logged, and each setup was repeated once or twice. The results are presented in Figure 4-34. After testing with demineralised water, the test was also performed with water

with surface tension reducing additives (soap) in the horizontal and vertical position. These results are shown in Figure 4-35.

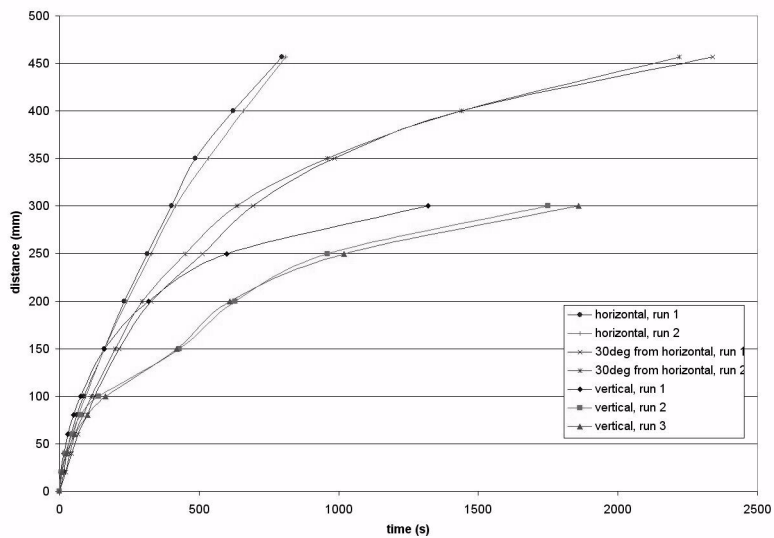


Figure 4-34: water transport in a strip of ZAL-15 under three angles with the horizontal. Colour version in appendix B as Figure B-11.

These results show that in the vertical sample, with water penetrating the material under capillary forces against gravity, it rises to about 30cm. This shows the limit of the capillary forces in the material, which is an important factor when designing a system for use in a re-entry vehicle undergoing deceleration of several g's. The thickness of a layer of ZAL-15 can not be more than this 30cm divided by the number of g's that are encountered, otherwise the water will be expelled by inertial forces. Compartmentalization of the ZAL-15 by mounting it in a honeycomb can solve this.

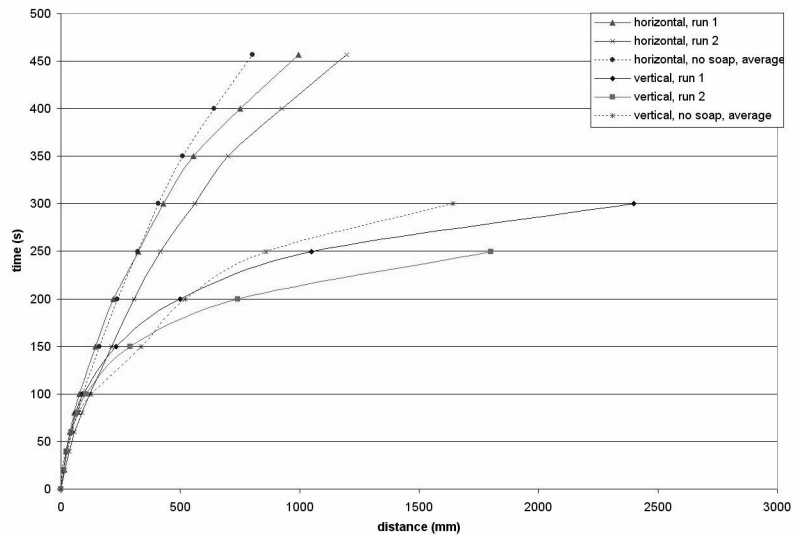


Figure 4-35: water transport in a strip of ZAL-15 for water with reduced surface tension, horizontal and vertical, compared with the average of the transport velocity for pure water. Colour version in appendix B as Figure B-12.

Reachable saturation level and reproducibility

The test sample used for the repeated freezing tests was weighed after each refill. The mass variation over the different filling cycles is shown in Figure 4-36. The amount of water in the sample varies from 76 to 84 percent of the ZAL-15 volume. No special care was taken in filling the ZAL-15, this was simply done by holding it under an open tap. Experience with the large closed model has shown that filling that large model from one small filling port in the center of the model does not give good results, in that the corners of the model are not filled completely. Attaching the filling tube close to the ends of the model appeared to solve this problem.

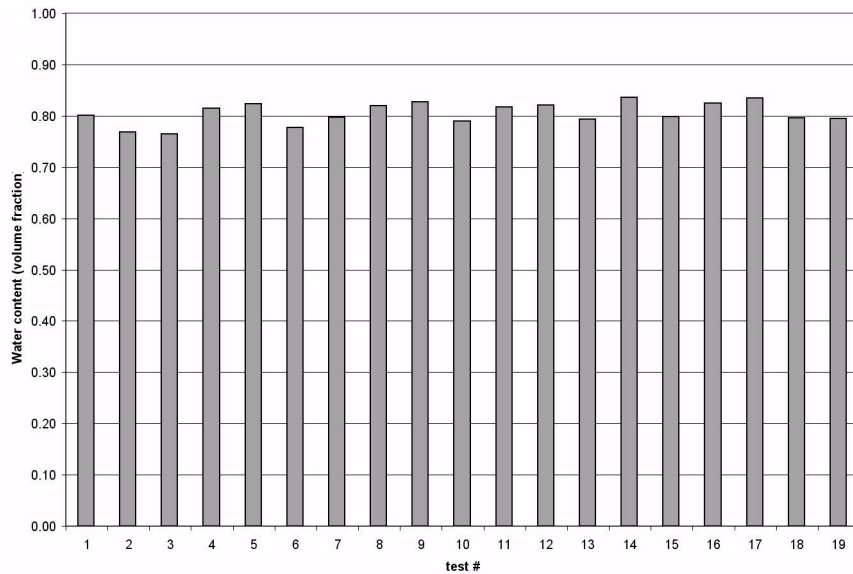


Figure 4-36: water content of ZAL-15 for 19 subsequent filling cycles.

So, in conclusion, about 80 volume-% of the ZAL-15 can be expected to be filled with water when this is done carefully and from multiple locations.

An operational system where the ZAL-15 is enclosed in a honeycomb core support structure would require a filling system where there is a filling point for every cell, which can simply be constructed by welding/soldering filling tubes to the support structure of the ZAL-15 with a hole connecting every cell to one of these pipes; forcing water into these filling pipes will then fill all of the ZAL-15.

4.5 Conclusions of the tests

The tests performed on the Enhanced Radiation Cooling system and the materials used therein had a number of goals:

- determining whether the cooling system works,
- determining how well the cooling system works (determining defining parameters),
- finding out if there are any critical problems with the materials
- supporting the development of a theoretical description of the system.

That the cooling system works, and works at high efficiency, was quickly determined in the very first series of tests. A cooling effect close to the theoretical maximum was identified.

Further tests to define the critical parameters like critical saturation level at different heating rates both gave data on these parameters, as well as supported the development of the theoretical description of the behaviour of the system.

Supporting tests on the material properties of PM1000 and ZAL-15 were performed, where especially for PM1000 a large number of tests are still required to get a thorough and complete description of the material under all operational parameters. This is a test campaign that goes far beyond the scope of this thesis and the cooled TPS development however, being of great importance to the broader hot structures technology development activities in the Netherlands and on ESA's Expert project.

Tests on ZAL-15 showed that the material is able to hold water very well, gave limits to the g-loading it can withstand and showed that a minimal pressurization of the cooling system is required in case of exposure to vacuum. No critical issues with the materials were identified on the basis of the tests that were performed. One type of test that still needs to be done is a vibration test on ZAL-15 to determine whether it is damaged by high vibration levels.

Finite element models of the test models were developed which gave good confidence in the ability to model this cooling system in such a way that it can be used for design.

Designing with cooled metallic TPS

In this section some designs with the cooled metallic TPS will be presented, starting with the DART re-entry vehicle that was the original reason for developing cooled metallic TPS. Furthermore, a flight experiment for cooled TPS will be described and some possible future applications, namely a cooled leading edge and a cooled TPS tile will be briefly treated to show what designing with the enhanced radiation cooling system would entail.

5.1 DART: the Delft Aerospace Re-entry Test Vehicle

The cooled metallic TPS that is the subject of this thesis was developed for the DART project, aimed at developing a small re-entry test vehicle at Delft University of Technology for scientific research in the field of aerothermodynamics and materials validation, specifically flying PM1000 in a real re-entry environment.

5.1.1 Goals of the DART mission

The goal of the DART mission was twofold:

- perform high-quality aerothermodynamic measurements to improve the knowledge base and calibrate ground based tools (CFD and wind tunnels),
- validate the use of PM1000 in a re-entry flight environment.

This had to be performed within the constraints of a university project: a need for low cost, especially for hardware and services that have to be bought outside of the university. This low cost requirement drives some choices:

- the vehicle will be launched by a very low cost launcher,
- the vehicle will be uncontrolled (ballistic re-entry),
- the vehicle will have a simple axisymmetric shape.

The only launcher that fits the requirement of low cost together with giving a reasonable payload capability is the Russian Volna, a former military missile. It is offered for suborbital flight including recovery of the payload on land. This also ensures that no de-orbit hardware is needed by the re-entry vehicle. On the downside, the re-entry offered by the Volna leads to rather high thermal loads because of the high entry angle. These high loads, coupled with the desire to use PM1000 for the outer skin, led to the need for cooling of the TPS.

5.1.2 Design of the vehicle shape & TPS

Because of the overriding requirement of low cost for the DART vehicle, a simple axisymmetric shape was selected, consisting of a sphere, cone and flare. Such a geometry can be defined by just a few parameters, like nose radius, cone angle, flare angle, length and base radius. Also, the aerodynamic coefficients for such shapes can be derived analytically, for small angles of attack, and the shape can be optimised fairly easily in an automated fashion.

A further advantage of a simple shape is that it will be easier to relate the theories on the physical phenomena to the actual measurements, which might be very difficult or even impossible for complex shapes. Also, the interest of the mission is not to reproduce flow phenomena related to a very specific shape but rather to look at the basic phenomena that can be applied to many shapes (like compression ramps).



Figure 5-1: early shapes of DART vehicle with 0.25m and 0.39m nose radius, 1.3m base radius and 1.6m length

From a vehicle shape, mass and re-entry conditions, a good approximation of the thermal loads can be derived using a Fay-Riddell like relation, and furthermore engineering formulas for the distribution over the surface. Because of the small size of the vehicle with an inherently small nose radius, the thermal loads get fairly high, far beyond what can be sustained by uncooled metallic TPS. Therefore, a water-cooled nose was proposed, where water is in direct contact with the outer skin. The thermal energy that is applied to the nose from the airflow is conducted through the thickness of the skin and immediately transferred to the water which will heat up and start boiling. The temperature will not rise above the boiling temperature, so the nose will be cooled by the water in this fashion. It is in fact the same principle that will protect an aluminium pot of water on a stove or fire, or even a thin plastic bag filled with water over a candle flame.

Since the heat load drops off quickly along the nose away from the stagnation point, the conical part of the vehicle does not require the 'heavy duty' direct water cooling that the nose does, and there the enhanced radiation cooling can be applied, that uses about half the amount of coolant of the direct water cooling (because half the thermal energy is radiated back into the atmosphere).

The known limits of the allowable heat load for nose and cone TPS together with the possibilities of the simple shape for automatic computation of important vehicle parameters were used by Mooij et al [85] for an automated optimization of the vehicle shape to a number of parameters, most notably that no strong shock wave-boundary layer interaction should occur on the flare, because that would lead to too high heat loads on a structure where direct water cooling is not applicable.

5.1.3 TPS layout: nose and cone

The direct water cooling system in the nose of the vehicle is quite straightforward in its operation, requiring only passive systems and few moving parts. The nose is a hemispherical metallic shape (see Figure 5-2) with a thin outer skin in PM1000 or possibly another material; the temperature levels are low because of the efficient cooling, so chemical resistance against the oxidative flow is a more important requirement than pure high temperature capability. The entire nose is a water tank where a filler body inside ensures that the volume of the tank is not too large, to prevent having to carry a very large amount of water. At the back of the tank a pressure valve allows for water vapour to escape at a predefined pressure. The re-entry deceleration will ensure that the water is pressed forward against the nose that has to be cooled. The water vapour is vented through a pipe to the base, keeping the boundary layer clean for aerodynamic measurements. In another application where these measurements are not important, venting the water vapour somewhere along the vehicle could provide some additional film cooling.

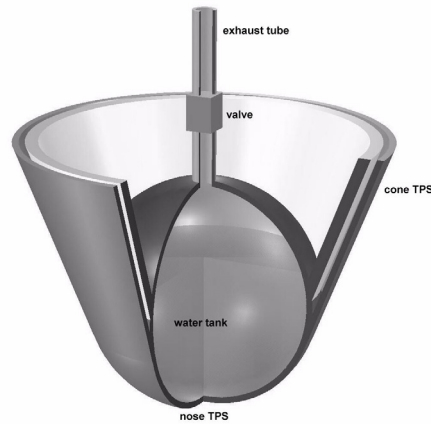


Figure 5-2: Sketch of nose cooling system with integral water tank

The cooling of the nose works as long as water is in direct contact with the outer skin. This means that the boiling of the water in the container must be nucleate boiling, rather than film boiling, in which case a vapour film forms between the wall and the water, blocking efficient heat transfer and allowing the wall to overheat. The point at which film boiling starts is called the critical heat flux for nucleate/film boiling and this depends on pressure and force of gravity/deceleration:

$$\dot{Q}_{max} = \frac{\pi}{24} \cdot \rho_v \cdot h_v \cdot \left(\frac{\sigma \cdot a_g \cdot (\rho_l - \rho_v)}{\rho_v^2} \right)^{\frac{1}{4}} \cdot \left(1 + \frac{\rho_v}{\rho_l} \right)^{\frac{1}{2}} \quad (5.1)$$

where ρ_v and ρ_l are the densities of vapour and liquid,

h_v is the heat of evaporation of the liquid,

σ is the surface tension,

a_g is the effective acceleration of gravity (so including vehicle deceleration).

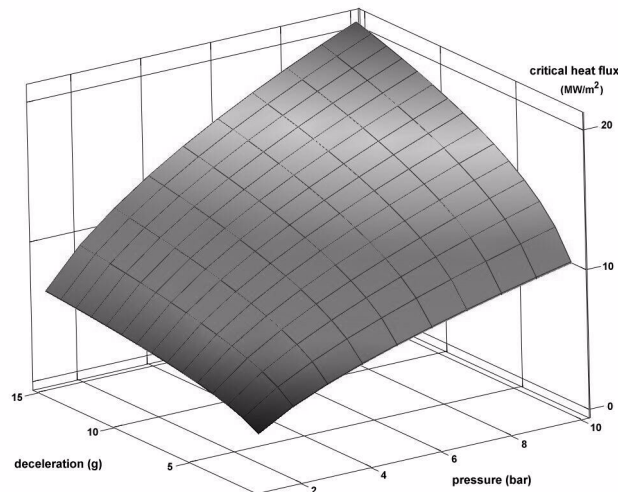


Figure 5-3: Critical heat flux as a function of pressure (1-10 bar) and deceleration (1-15g) for a spherical nose.

Figure 5-3 shows the critical heat flux as a function of pressure and deceleration. Considering that the deceleration of DART is quite high, up to 15g, and that a pressure of at least 5 bar can be maintained in the pressure vessel without a problem, a critical heat flux of more than 10 MW/m² is possible. In any case, the critical heat flux can be increased further by simple measure like changing the texture of the tank wall or stirring the fluid. This does not seem to be necessary for the DART mission however, since peak heating rates are in the order of 2-3 MW/m².

For the cone of DART, the Enhanced Radiation Cooling system was foreseen. The conical outer skin would be a single piece of PM1000 rolled into shape and welded along the joint on one side. Inside there would be a cone to support the ZAL-15, made from Aluminium, onto which the ZAL-15 can be mounted in several blocks. A small gap in between allows for venting the water vapour.

The connection between the nose and the cone is the most difficult part of the vehicle structure, because here the strongly cooled nose, the hot cone and the cold inner structure come together. A solution has been proposed where the nose connects to the inner structure and the cone connects to the nose only. There are two possible solutions for assembly:

putting the nose on the inner structure and sliding the cone over it, or integrating the nose and cone and lowering them over the inner structure together.

More recently, DutchSpace has developed an alternative solution for this for the Expert vehicle, where the nose is mounted on the inner structure separate from the cone, and the two are not connected. The cone is mounted on the inner structure via a second backwards facing cone.

5.1.4 Predictions of performance

Nose water usage

An estimate of the water needed for cooling the nose was made by simply integrating the applied heat load over time and over the nose surface, assuming that all this energy was used to evaporate water. The heat load over a hemisphere can be related to the heat load at the stagnation point by [9]:

$$\frac{\dot{Q}}{\dot{Q}_{stag}} = \cos^{\frac{3}{2}}\varphi \quad (5.2)$$

where φ is the angle along the hemisphere away from the stagnation point. This equation holds to $\varphi \cong 70^\circ$. A heating profile over time for the stagnation point is given by the trajectory analysis software used to calculate the re-entry trajectory. Integrating the heating rate over the nose area gives an integrated heat load for a part hemisphere from $\varphi=0$ to φ_{max} degrees of:

$$\begin{aligned} Q_{total} &= \int_0^\varphi \dot{Q}(\varphi) dA = \int_0^\varphi \dot{Q}_{stag} \cos^{\frac{3}{2}}\varphi 2\pi R \sin\varphi R d\varphi \\ &= -\frac{4}{5}\pi R^2 \dot{Q}_{stag} \cos^{\frac{5}{2}}\varphi \Big|_0^\varphi \end{aligned} \quad (5.3)$$

To determine the amount of water used during a given re-entry the engineering model is used to integrate the stagnation heat flux over the nose with the above equation. The angle to which the nose extends is 75° (for a cone half angle of 15°). While this stretches the applicability of equation 5.2 a bit, this has limited influence on the outcome because the heat load in that last part of the nose is very small compared to the more forward part.

The total amount of energy on the nose hemisphere is integrated and the temperature increase of the water in the nose is calculated; when this reaches boiling temperature the energy is used for water evaporation instead. The starting values used are:

- amount of water in the nose: 6kg,
- initial temperature of that water: 0°C,
- boiling temperature: 150°C (5 bar pressure).

The heat flux applied to the vehicle was calculated for a 150kg DART vehicle re-entering from 120km with 7000m/s at an entry angle of -5°.

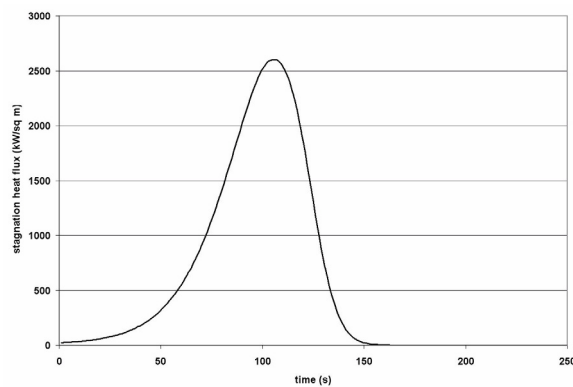


Figure 5-4: stagnation point heat flux history for 150kg DART used in calculation of water usage

This energy will heat up the water in the nose as shown in Figure 5-5 below.

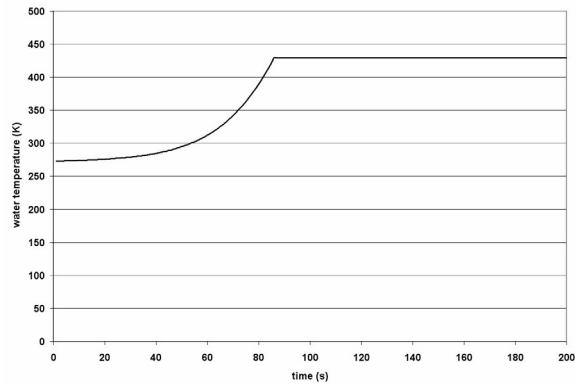


Figure 5-5: Temperature of the water in the nose of DART

As the water reaches boiling point, evaporation starts at a rate peaking at about 120 grams per second. Note that this is quite a substantial amount of water vapour, venting of which needs to be done with some care, so as to not disturb the vehicle stability or trajectory.

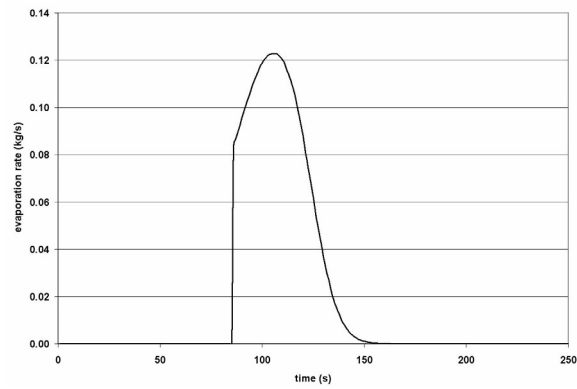


Figure 5-6: Nose water evaporation rate vs time

The total amount of water evaporated in the 25cm radius nose is 4.63kg for this re-entry. The amount carried on board would be more, but as little more as possible to conserve mass.

Cone water usage

The amount of water used in the cone is also determined with the engineering model for Enhanced Radiation cooling. The same heat flux as used above, assuming a heat flux of 11% of stagnation flux on the cone of the vehicle. Again, the heating phase of the water is simulated, taking a layer of 5mm water over the surface of the cone (which would require a porous layer thickness of about 7mm). Boiling temperature is set at 300K, taking account of the lower pressure in the enhanced radiation cooling system. The surface area of the cone that is cooled this way is 1.86m². PM1000 thickness is 0.5mm.

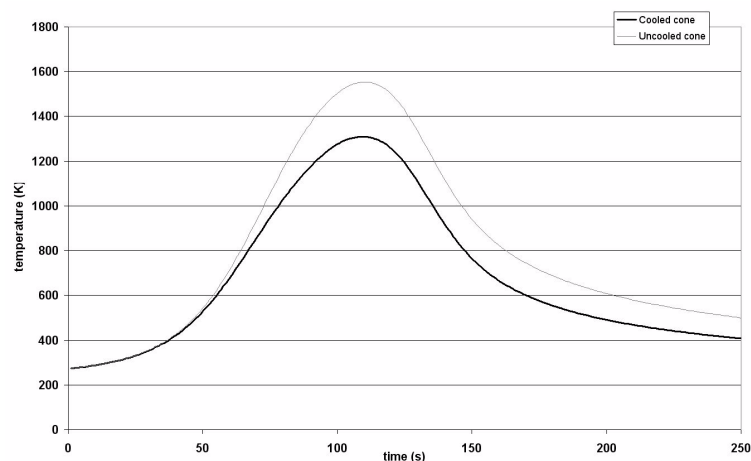


Figure 5-7: Cone temperature compared with uncooled cone temperature

The cone temperature is shown in Figure 5-7 together with the uncooled temperature at the applied heat flux. Here the uncooled temperature is calculated by balancing the incoming heat flux with re-radiated heat and stored heat only, so it is assumed that the inside is perfectly insulated. This will give a slight over-estimation of the real temperature, but considering that insulation material is meant to minimize the heat flux to the inside, the error will be small. The temperature difference between the cooled cone and radiation equilibrium is over 250 degrees in this simulation.

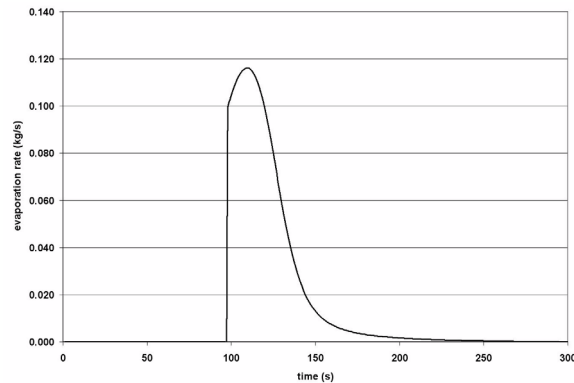


Figure 5-8: Water evaporation rate in the cone for the full 1.86m² surface

The total amount of water needed to cool the cone during this re-entry is 5.57kg; actually a layer of less than 3mm of water over the surface of the cone which has a surface area of 1.86m².

5.1.5 DART project conclusions

In the DART vehicle, using cooled metallic TPS allows us to reach the following:

- the design of a small low-cost vehicle,
- without resorting to expensive ceramic materials that are not available in the Netherlands,
- and ensuring a clean flow around the vehicle without e.g. ablation products.

Considering that use of metallic TPS was baselined as one of two major goals of the vehicles mission, the cooling systems are essential for reaching a viable design within the boundaries set by the top-level requirements. Water used for a 150kg vehicle re-entering at 7km/s with a peak heat load of 2.6MW/m² is less than 10.4kg (4.6kg in the nose, 5.7kg on the cone).

5.2 Flight experiment for cooled TPS

The Faculty of Aerospace Engineering of Delft University of Technology has been offered the chance to fly an experiment of the Enhanced Radiation Cooled TPS on ESA's Expert re-entry module. The design of this experiment will be presented here.

5.2.1 The Expert mission

Expert is an ESA program for a small re-entry test module to perform basic research in the field of hypersonic aerodynamics, flight measurement systems and, to a lesser extent, TPS materials. In this, it is a variation of the DART vehicle proposed by TU Delft earlier, but focussed more on aerothermodynamics and less on TPS.

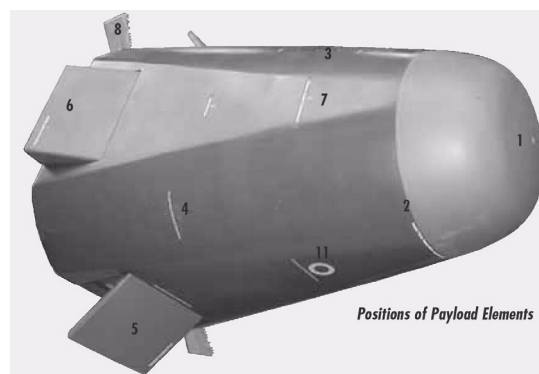


Figure 5-9: Expert vehicle with position of some of the payload; #11 is the cooled TPS sample

The rationale for flying such a mission is that it is not possible to recreate all aspects of hypersonic flow in ground test facilities (i.e. wind tunnels). Also, the theories used in computational flow solvers are not mature in all respects. Therefore, there is a continuing need for actual flight test data to validate wind tunnel and CFD results. It was considered to be useful to fly a rather simple generic configuration which gives results that are fairly easy to understand and applicable in a wide range of situations, rather than try to do measurements on flights of larger, more complex vehicles (e.g. Space Shuttle), where aerothermodynamic experiments are always of secondary importance and where the flow phenomena are much more complicated, making it more difficult to draw conclusions on the basic processes from them.

Expert is about 1.6 meters long, 1.05 meters in diameter and has a mass of some 350kg. The nose and fixed flaps are made of C-SiC, while the rest of the exterior is PM1000 of about 3mm thickness, to give a structure which is able to withstand the thermal loads without

requiring too much in the way of testing and analysis. The heat sink effect of the rather thick skin will ensure a relatively low temperature.

The Enhanced Radiation Cooling sample will be integrated in one of the flat side panels of the capsule. A diameter of 10cm in the outer face has been foreseen, being a good compromise between small size for low cost and impact on the vehicle and sufficient size for useful measurements.

The requirements to the payload are the following:

- the payload shall not endanger the vehicle or its main mission,
- the payload shall not induce substantial thermal stress on the surrounding skin,
- adding the payload shall not lead to a substantial increase in analysis or testing required from the main contractor or TPS subcontractor,
- the impact of the experiment in terms of mass, data handling/storage required and integration shall be minimal.

5.2.2 Design evolution

The basic design of the circular test sample is a shallow hat-shaped container of PM1000 closed with a steel plate on the inside. A piece of ZAL-15 is mounted on the steel plate so it sits inside the container when assembled. The flange of the container is shaped in such a way as to make for the simplest attachment to the re-entry module outer skin.

Initially, it was expected that the skin of the re-entry capsule side panels would consist of a PM1000/PM2000 sandwich. For that case, it was foreseen to include a ring flange in the sandwich surrounding the 10cm hole to which the experiment could be bolted. The design of Expert evolved towards a thin stiffened skin structure, with a skin thickness of 0.75 to 1mm. In this case, a dedicated ring stiffener surrounding the hole was required, to which to attach the experiment. In addition, radial stiffeners leading outward from the ring were needed to stiffen the skin panel around the hole.

Finally, the re-entry vehicle design underwent a cost-reduction and simplification cycle, which resulted in a 3mm thick outer skin which resulted in lower skin temperature and therefore required less analysis and testing and is easier to build. In this case, the experiment can simply be bolted directly to the thick skin, with little or no additional stiffening required.

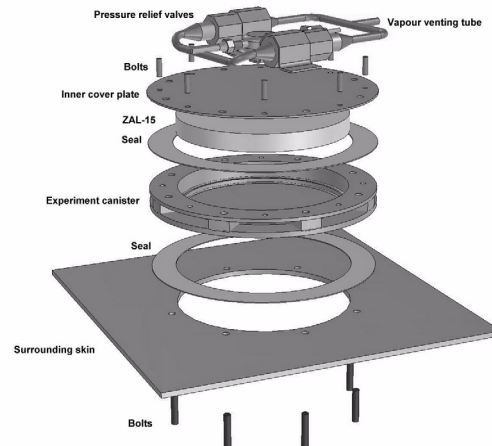


Figure 5-10: Exploded view of flight experiment design. The top of the image would be inside the vehicle, the bottom would be the outside.

The final version of the design is such that it minimises the impact on the vehicle architecture, limiting most interfaces to the TPS alone. Additional interfaces are the sensor leads to the on-board data handling unit and a vapour exhaust tube to vent the vapour to the base of the vehicle, so as to prevent changing the boundary layer flow that is of importance to other experiments on board.

5.2.3 Sensors and measurements

The goal of the experiment is to show that the cooled TPS works and that the predicted reduction in skin temperature is reached. For this some temperature measurements are needed. Since there will not be a suitable location on the vehicle that will have exactly the same thermal load and wall thickness to give an uncooled reference temperature, the cooling effect has to be reconstructed post flight from the data on the actual thermal load on the location of the experiment. The temperature on the inside of the experiment outer skin will be measured in the center point of the experiment. In addition, the temperature on top of and below the ZAL-15 will be measured, as well as the temperature in the outflow chamber (giving the vapour temperature).

Since an important aspect of the flight test is to show that a complete and self-contained system can be designed and built, which is able to stay under the required pressure during the pre-flight and flight phases, pressure sensors will be used to track the pressure evolution during the mission. Two miniature pressure transducers are baselined weighing just a few grams each.

5.2.4 Predictions of flight measurements

The engineering model has been used for predictions of the flight behaviour of the experiment, as well as for a quick sensitivity analysis on e.g. the skin thickness of the test sample.

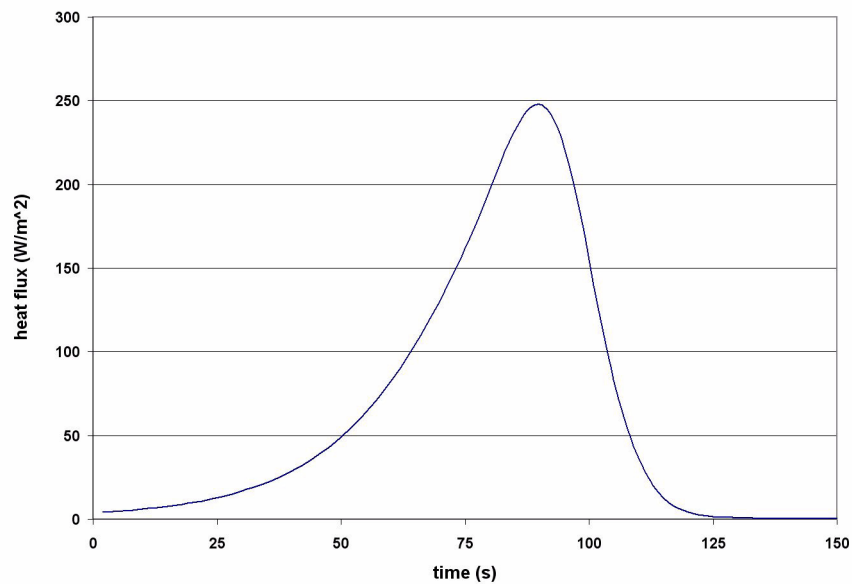


Figure 5-11: heat flux used for engineering model of flight test experiment

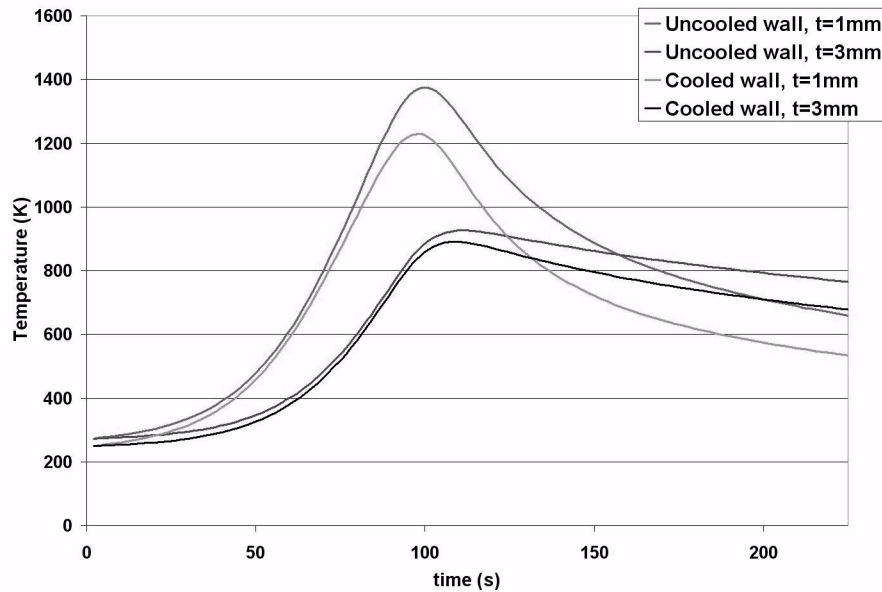


Figure 5-12: temperature predictions from the engineering model based of the heating profile shown in Figure 5-11 for flight test model for different skin thicknesses. Colour version in appendix B as Figure B-13.

The heating profile used in the predictions is based on a stagnation point heat flux history provided by the Expert main contractor, and scaled down to peak at about 250kW/m^2 , the limit heat flux for uncooled (thin) PM1000 (see Figure 5-11). Based on this heat flux, the temperature evolution of the 1D model is given in Figure 5-12 for a skin thickness of 1mm and 3mm. While for a thin 1mm skin the cooled skin is 145 degrees cooler than the surrounding uncooled skin, for a 3mm thick skin the difference drops to just 36 degrees. Obviously, this makes it harder to show the cooling effect in a clear and obvious way.

Making the skin of the test sample thinner than the surrounding skin would lead to a more defined cooling effect, but in that case the cooled skin would actually be hotter than the uncooled skin surrounding it, and this was not acceptable to the main contractor, because failure of the cooling could lead to a large risk to the vehicle. Also, the catalicity of PM1000 increases with increasing temperature, so when the test sample would be substantially hotter than the surrounding skin, this would become a patch of increased catalicity with resulting

elevated thermal load, further aggravating the problem, and potentially disturbing experiments downstream.

5.2.5 FE analysis of the test sample

Finite element analysis was performed in two stages on the design of the flight experiment. At an early stage, a very simple 2D analysis (see Figure 5-13) of an early design of the outer cover of the test sample was performed to get an idea of the level of thermal stress and shape distortion. At a later stage a much larger 3D model was made of a 1/8 segment of the experiment including outer cover, inner cover, porous layer and water, surrounding skin and fasteners. This model was used to predict the temperature response of both experiment and surrounding skin, bowing of the experiment and thermal stresses in the experiment casing. Based on these results, the skin thickness for the experiment was adapted to reach an outer skin temperature that is more in line with that of the surrounding uncooled skin, as per the wishes of ESA and the main contractors of Expert and the Expert TPS (Alenia and Dutch Space respectively)



Figure 5-13: Mesh of 2D model of experiment outer cover

The thermal stress at the point in time where it peaks is shown in Figure 5-14. In this model, the experiment cover is clamped at the flange at the right of the image and heated on the outer surface at the top of the figure. The thermal expansion of the hot part of the structure causes it to bow out; in reality the surrounding skin will also heat up and expand, pulling the experiment with it and reducing the shape distortion. This simulation is thus a worst case scenario.

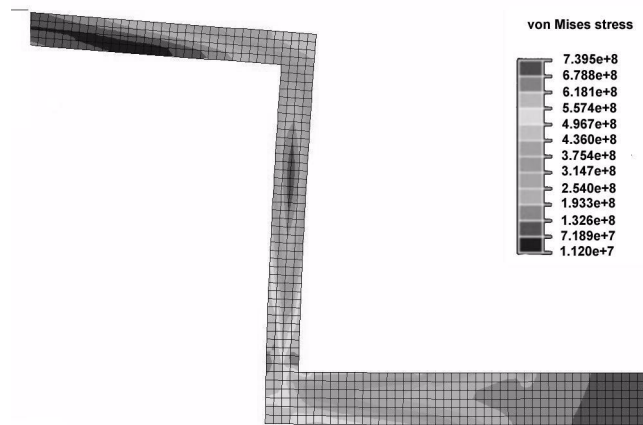


Figure 5-14: Von Mises stresses in experiment outer cover due to thermal stresses at time of maximum stress level. Colour version in appendix B as Figure B-14.

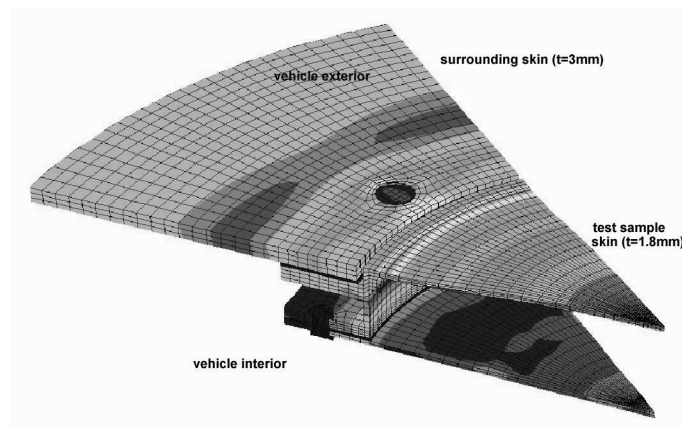


Figure 5-15: 3D Finite element model of flight experiment; stress field. Colour version in appendix B as Figure B-15.

A stress field output of the 3D model (1/8 of the model because of symmetry) of the flight experiment is shown in Figure 5-15. This model was used first to determine at what skin thickness of the experiment canister the temperature difference between the experiment and the surrounding skin was low enough to satisfy the prime contractor; later it is also used to predict the complete temperature distribution and stress distribution in the model under various loads. This finite element model will be validated by a lab test on a steel model.

The lab test will use the heating profile for the flight of Expert as provided by DutchSpace, the responsible for the TPS design for Expert. This heating profile is translated to a curve that can be used in the control system for the test equipment, i.e. a constant heating phase, a constant temperature phase and a constant cooling rate phase. This temperature profile was then translated again to a heating profile, which was used in the FE model to give a complete temperature history for the entire model, that can later be compared with the test results (see Figure 5-16 for the resulting heating history of the simulation).

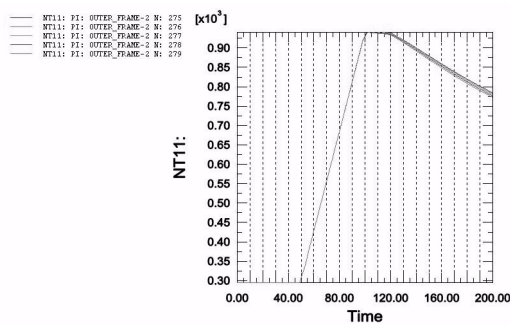


Figure 5-16: temperature history from FE model simulation of laboratory test showing temperatures of 4 nodes through the thickness at the center of the PM1000 (the ‘point’ of the FE model).

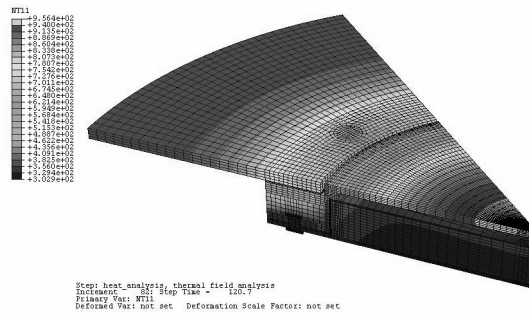


Figure 5-17: temperature distribution in model according to FE simulation of lab test. Colour version in appendix B as Figure B-16.

The result of the FE simulation shows that the desired result of reaching a more or less uniform temperature over the test sample and the surrounding skin has been reached for the applied 1.8mm thick skin on the model and 3mm on the surrounding plate (see Figure 5-17). It is also clear that a temperature drop of more than 400 degrees occurs at the location of the side flange of the model due to the increased thermal mass and the heat leak to the cooled ZAL-15 inside. This will lead to high thermal stresses that the structure will have to withstand.

5.2.6 Lab tests on the flight experiment

To check the predictions of the finite element model, a relatively cheap steel model was made of the flight test sample which is to be tested under the infrared heater lamps. The steel model of the flight experiment is similar in every way to the flight test sample, except for the material. To simulate the skin, a 3mm thick steel plate 300x300mm in size is used with the circular cut-out for the experiment in the center. Time constraints prevented performing these tests in time for including them in this thesis.

5.2.7 Qualification tests

For final qualification of the experiment, a test using the actual flight hardware is foreseen, where the flight version of the experiment is tested together with the flight version of the TPS panel in which it is to be integrated. The test philosophy of the TPS is to test the complete TPS up to a temperature of about 600-700°C and compare with a finite element model, then use that finite element model to extrapolate to the flight temperatures. Testing one small panel including the cooled TPS experiment to the actual flight temperature gives

an additional check that nothing unexpected happens above the test temperature (i.e. 600-700°C) for the complete TPS, so giving increased confidence in the design.

Apart from thermo-structural tests, vibration testing of the experiment is necessary, on the one hand to validate the structure and attachment, failure of which would mean loss-of-vehicle, and on the other hand to show the integrity of the sensors and the porous layer, failure of which would mean a failed experiment, but no danger to the vehicle.

5.3 Cooled leading edge

The leading edge of a re-entry vehicle is one of the thermally highest loaded regions of the vehicle. While metallic TPS can be applied to larger areas of a large re-entry vehicle like the X-33, the leading edges are subjected to thermal loads that are too severe for unprotected metals. However, the thermal load might be in the range for the enhanced radiation cooled TPS, allowing use of a metallic leading edge, with potential for increased robustness and maintainability.

5.3.1 Basic analysis of a cooled leading edge

By definition, the heating levels at which enhanced radiation cooling can be applied range from about 220 to 450-500kW/m² (for PM1000). When the heating rate on the leading edge is in this range, enhanced radiation cooled metallic TPS could be used. It must be noted that the geometry of a leading edge (approximated by a half cylinder) leads to a reduction of the view factor between the outer skin and the porous layer, which gets worse (lower) when the distance between the two increases. This reduces the allowable heat load compared to a flat plate geometry.

When the heating rate is lower than the maximum for the enhanced radiation cooling system, the margin can be used to reduce the leading edge radius which leads to lower drag, thus higher L/D and therefore better flying characteristics and lower heat fluxes.

The attractiveness of a sharp leading edge is shown by several studies into small-radius leading edges with e.g. high temperature heat pipe systems for cooling the tip of the leading edge (see e.g. [34]), and into the use of UHTC materials [74].

5.3.2 Design issues

The deceleration forces during re-entry work on the leading edge in a direction under varying angle to the local normal direction of the skin surface. Because there is a limit to the g-forces under which the porous layer can support water, depending on the geometry, care must be taken that the porous layer is compartmentalized in a suitable way to ensure that the water does not escape the porous layer due to deceleration.

A venting location for the water vapour must be selected, and this could be used to provide some film cooling at a suitable location, by venting behind the leading edge on the windward side for example.

5.4 TPS tiles with enhanced radiation cooling

5.4.1 Potential for use

The rationale for developing metallic TPS tiles using enhanced radiation cooling would be to replace part of TPS that would otherwise need to be made from ceramic materials like C-SiC or Silica tiles a la Space Shuttle. The benefit would come from much reduced maintenance effort on the metallic tiles and possibly a decreased risk of failure. A very detailed analysis and probably some flight experience would be required to be able to make a final judgement on the benefits of one type of tile over the others, complicated by the fact that different performance aspects need to be compared and traded off, with weight factors for aspects like cost and reliability to be determined.

On a large reusable launcher like the X-33 or Hopper, the largest area of windward TPS can be covered with uncooled metallic TPS but there is a region behind the nose and leading edges where the thermal load is such that something with higher temperature capability is needed. This is where cooled TPS would be applied. It might be possible to extend the use of enhanced radiation cooled metallic TPS all the way to the nose and leading edges if thermal loads there are low enough.

5.4.2 Design issues

Design of a tile of metallic TPS with enhanced radiation cooling is structurally similar to that of an uncooled tile. The NASA-Langley design of the ARMOR tile can be used as a reference, being the most advanced design currently built and tested. Differences between the cooled and uncooled tile are the following:

- The cooled tile has to be an airtight enclosure to ensure the minimum pressurization required for the enhanced radiation cooling to work. It is already desirable for an uncooled tile to be closed, because the internal fibrous insulation needs to be protected from (rain) water while on the ground or in atmospheric flight.
- The sidewalls of the cooled tile will have a greater temperature gradient because the lower part of the tile is forced to remain at low temperature by the water and the temperature gradient has to be accommodated in a small part of the sidewall. This will lead to serious thermal stress issues that require a very careful design, and which might lead to unavoidable occurrence of plastic deformation in small areas.

- A vapour venting system needs to be implemented, and a decision has to be made on where to vent the water vapour. It might be very beneficial to vent in the inter-tile gaps, and from there through the inter-tile seals on the outer surface into the boundary layer flow. This would give an additional film cooling on the outside, and also effectively pressurize the intertile gaps and in that way reduce the risk of hot gas incursion.
- A refilling system has to be integrated. This could consist of perforated pipes brazed or welded to the inside surface of the tile, underneath the porous material. Pumping water into these pipes would then allow the porous layer to absorb the water. These water pipes need to be connected to a network running under a large number of tiles, which should still be individually detachable. When this system only needs to work when on the ground, the design should be fairly straightforward. A possible system for in-flight water resupply will be more complex, but no show-stoppers are apparent; hydraulic systems operate continuously under much higher pressures in equally critical subsystems of aircraft and spacecraft.
- The problem of heating in space under solar heat input has to be solved. As shown in chapter 3, exposure to solar heating for about 1 day would raise the temperature of the TPS to such temperatures that water would start to evaporate. An obvious solution to this is to fill the system only just prior to re-entry (just prior being in the order of hours). The other option is to reduce the heat input in one way or another, by using a coating of some kind or by keeping the relevant parts of the vehicle shaded if possible.

5.5 Design issues - conclusions

Designs with the enhanced radiation cooling system have not progressed far enough to be able to conclude that operationally usable systems are feasible. On the other hand, no show stoppers were identified. Designing metallic TPS or hot structures is a difficult process that is still being learned at various industries and institutes around the world (e.g. in the Netherlands, at NASA-Langley, at EADS-ST in Bremen and others). Integrating enhanced radiation cooling in such a TPS seems to be an extra complication, but no critical problems have been identified. The higher standard of airtightness that is required for the system might be a significant complication, but even that is negotiable, when a refilling system is used which fills the porous material just before re-entry.

Whether the system is mass-advantageous is impossible to say without making a much more detailed design, and it is certainly very dependent on the specific application. When a re-entry is very prolonged, the amount of water that is needed adds up to a substantial amount. Direct mass comparison is difficult however, on the one hand because the system is aimed at TPS locations with quite specific and high heat loads for which little or no comparative data is available from existing projects, on the other hand because a mass optimization of a

vehicle using enhanced radiation cooling would result in a different shape and/or trajectory than a vehicle with conventional TPS.

The flight experiment is in an advanced stage of design, but is not representative for the structure of an operational TPS, being much too heavy in order to comply with the overall layout of the Expert capsule, which itself uses a non-optimised TPS because of the large uncertainties in the operational environments as well as to reduce development cost.

At the current stage of development, it can be said that the enhanced radiation cooling system is valuable for niche missions like DART (or Expert) where its specific characteristics allow for some specific type of mission or experiment (allowing an aerothermodynamic test flight without boundary layer pollution, in the case of DART). In order to determine the value of this system for larger operational launch/re-entry vehicles, a more elaborate design and test (flight) of a cooled tile or leading edge would be needed, and in parallel a design of a vehicle taking the cooled TPS into account from the outset, to see what the mass benefit or penalty is.

The overview of TPS and specifically metallic and cooled TPS has shown that the Enhanced Radiation Cooling system is unique, and that the flight experience with metallic TPS is very limited to date. Also it is clear from the literature that metallic TPS holds great promise in achieving a reduction in cost through increased robustness, reduced maintenance and lower production cost compared with ceramic and CMC materials.

Enhanced Radiation Cooling holds the promise of enabling the use of metallic TPS materials under higher thermal loads than would be possible without cooling. Where direct water cooling allows even greater thermal loads, it uses almost all incoming energy to evaporate water, where enhanced radiation cooling radiates half back to space. Thus, only half the amount of water is required. Also, a more uniform temperature over a vehicle is reached when part is covered with non-cooled TPS and part with enhanced radiation cooled TPS, reducing thermal stress and strain mismatch problems. Because enhanced radiation cooling was invented at the start of this research, the complete theory had to be built from scratch, and the experiments also started from the very first proof-of-concept tests, without prior knowledge to build upon.

The theoretical aspects of the thermal problems are in principle fairly well known, but the behaviour of the porous material with water and water vapour/air is something for which no complete theoretical model exists. A full quantitative theoretical model of the two-phase flow problem in the porous medium was not considered achievable within a reasonable amount of time; therefore averaged properties have been derived and measurements are used to determine key parameters of the behaviour of the cooled TPS. This is judged sufficient for design with this cooled TPS system. Another conclusion from the theoretical studies is that material properties of the metallic material (i.e. PM1000) are required with the maximum possible accuracy, while it is clear at the same time that a program of measurements for all

required material properties as a function of all relevant variables is a huge undertaking which takes a lot of time, effort and money. Parallel studies in the Dutch Aeolus programme have pointed out that great attention for detail is needed to understand all aspects of highly thermally loaded structures in PM1000. Very small regions of plastic deformation for example can radically change the stress distribution, meaning that in finite element analysis all non-linearities of the material properties and the physical problem have to be included to achieve reasonable results.

The Enhanced Radiation Cooling system has the potential of increasing the allowable thermal load for a given skin temperature by 92% based on the radiation heat transfer alone. An additional contribution from convection cooling can be gained when the geometry is right. Tests on small samples of the system showed that the cooling effect that was measured came very close to this theoretical performance, indicating that the system does work as expected. An important performance parameter is the amount of water that is used effectively for cooling. When the saturation of the porous medium drops below a certain level, capillary water transport to the evaporation surface is no longer sufficient and the porous material dries out, increases in temperature and the radiation coupling between skin and porous material breaks down, ending the cooling. The saturation level at which this occurs depends on the heating rate, which is directly linked to the required capillary transport rate. For a skin temperature of 1000 to 1200°C the so-called critical saturation level was measured to vary from a maximum of 77-87% at 1050K to a minimum of 70-80% at 1350K; the bandwidth of these measurements was about 10%.

When the saturated porous material is exposed to pressures below about 25 mbar the water will boil at room temperature, after which it will freeze and continue to sublimate. The water loss is substantial, at about 20% after 20-30 minutes at 6 mbar. To prevent this water loss, a minimum pressure of about 30 mbar must be maintained in the system when it is filled with water. Alternatively, it could be filled just before re-entry.

Extended heating by solar radiation in space was concluded to lead to significant water loss in the cooled TPS by heating the porous material to above boiling temperature for water at 30 mbar. Therefore, a filling system that fills the porous material with water just prior to re-entry is probably needed for applications involving extended time in orbit. Such a system would not be very complex when compared to other hydraulic systems that are currently in use in aircraft and spacecraft and that are as safety-critical as this TPS filling system would be.

The goal of this thesis research was to develop the Enhanced Radiation Cooling System to a higher Technology Readiness Level.

Chapter 6: Conclusions

- Since the cooling system was invented at the start of this research effort, the starting point is before TRL 1.
- The various experiments and studies that have been performed can now be given a TRL value.
- The basic operation tests would fit in TRL 3.
- The large closed model test would be TRL 4.
- The flight experiment would be TRL 6.
- Flying a cooled TPS tile as an experiment on an experimental or operational vehicle would be TRL 7.
- Flying a cooled TPS operationally on a vehicle would be TRL 8/9.

So, within the frame of this study, the Enhanced Radiation Cooling system has advanced from not-invented-yet to TRL 4, with work towards TRL 6 being fairly advanced.

To summarize, the following can be concluded on the Enhanced Radiation Cooling System:

- It has been shown in experiments that the allowable heat flux for PM1000 TPS can be increased by 80-90% by using EHRC.
- It has been shown experimentally that the amount of water available in the system that is used effectively for cooling varies from 75-85% at 1050K to 70-80% at 1350K.
- A physical description of the cooling system has been formulated based on literature studies and experimental observations that gives a good explanation of the phenomena that are observed.
- Finite element modelling based on the physical models has been successful in reproducing experimental results on the simple models with good accuracy.
- Based on literature surveys and limited comparative tests, it has been made plausible that the combination of materials used (water, ZAL-15, PM1000) is one that results in very high performance that can not easily be surpassed with other combinations. In this regard it must be noted that this is especially valid for water and ZAL-15; the metallic component of the system has in principle a number of competitors in other superalloys that could give very similar performance, but this has not been studied because of the role of PM1000 in the large Dutch research effort on hot structures and TPS.
- A number of design ideas has been put forward for operational use of this cooling system, but these are not yet worked out in real detail.
- Refilling the system during flight from a grid of water tubes underneath the porous material is not assumed to be a problem in principle, since hydraulic systems are in common use of aircraft and on the Space Shuttle for critical systems. The risk of failure of these systems is

well understood and methods are available or can be devised to mitigate these risks (e.g. redundancy).

Future research

For continued research, the following avenues of study can be advised:

- Continue a programme of material research to determine all relevant material properties of the materials used.
- A number of tests are still required on the material and components of the system; most notable a vibration test on especially the porous material. Test of the system under g-loading would also be very valuable, but it is difficult to imagine a high-temperature test in a centrifuge.
- As a next step in the enhanced radiation cooling TPS development, a closed TPS tile for laboratory tests can be designed, comprising extensive FE modelling followed by building the tile and testing it in the thermal test facility.
- After that, such a tile can be test-flown on a suitable re-entry test vehicle.
- Testing of alternative materials will be interesting; especially using the system with C-SiC is attractive because it would enable low radius nose and leading edge structures which would dramatically improve the flying characteristics of a re-entry vehicle. Questions that remain for such an application are how well the capillary transport in the porous medium would be able to cope with the much higher flow rates required and whether the potential chemical reactions of water vapour with Carbon and C-SiC lead to problems. Also, improvements might be possible in optimizing the porous material. The current material is not designed for this application, so it can be expected that the actual optimum porosity and microstructure are somewhat different from those of ZAL-15.

References

- [1] CRC Handbook of Chemistry & Physics (CD-ROM); CRCnetBASE, 1999
- [2] Metals handbook; American Society for Metals
- [3] Polytechnisch zakboekje [*poly-technical pocket book*] 39th edition; PBNA, Arnhem, 1981
- [4] P.K.Ackerman, A.L.Baker, C.W.Newquist; Thermal protection system; US Patent # 5,322,725; US patent office, June 1994
- [5] J.F.Alvis, J.V.Young; Protective means; US Patent 3,082,611; US Patent Office, Mar.1963.
- [6] D.Alwes; Development and flight demonstration of TPS and hot structures for reentry vehicles; in ‘proceedings of the 3rd European workshop on Thermal Protection Systems’; ESA WPP-141, ESA, Noordwijk, 1998.
- [7] R.A.Anderson, R.T.Swann; Sandwich panel construction; US Patent 3,090,212, US Patent office, May 1963.
- [8] J.Antonenko, M.Müller; High temperature insulations on the X-38 re-entry vehicle; in ‘proceedings of the 4th European workshop on TPS for Space Vehicles, Palermo, nov 2002’; ESA SP-521, ESA, Noordwijk, April 2003.
- [9] W.J.Bannink; Inleiding hypersonic aerodynamic (introduction to hypersonic aerodynamics); TU Delft reader, Delft, 1994.
- [10] S.R.Birjmohan, A.Maree, J.Offerman; Development test of a hot metallic rudder for the reusable re-entry vehicle X-38; 2nd international Symposium on Atmospheric Re-entry Vehicles & Systems; AAAF, France, March 2001.

- [11] R.B.Bland, F.J.Ewing; Cooling with endothermic chemical reactions; US Patent 3,067,594, US Patent Office, Dec.1962.
- [12] M.L.Blosser, C.J.Martin, K.Daryabeigi, C.C.Poteet; Reusable metallic thermal protection systems development; in 'proceedings of the 3rd European workshop on Thermal Protection Systems'; ESA WPP-141, ESA, Noordwijk, 1998.
- [13] M.L.Blosser; Advanced metallic thermal protection systems for reusable launch vehicles; PhD thesis, University of Virginia, May 2000.
- [14] M.L.Blosser, R.R.Chen, I.H.Schmidt, J.T.Dorsey, C.C.Poteet, R.K.Bird; Advanced metallic thermal protection system development; AIAA-2002-0504; AIAA, Washington DC, 2002.
- [15] M.L.Blosser; private email communications with author, 2003-2004.
- [16] J.Buursink, T.J.van Baten, E.Mooij, K.J.Sudmeijer; DART: the Delft Aerospace Re-entry Test vehicle; IAF paper IAF-00-V.4.07; IAF, Paris, October 2000
- [17] J.Buursink, T.J.van Baten; DART - a low cost reusable re-entry test vehicle; 2nd international Symposium on Atmospheric Re-entry Vehicles & Systems; AAAF, France, March 2001.
- [18] J.Buursink, T.J.van Baten; Status of the Delft Aerospace Re-entry Test vehicle; IAF paper IADF-01-V.5.08; IAF, Paris, October 2001.
- [19] Buursink, J.; High temperature alloys - literature study; Aeolus document AE-DUT-TN-02CCM01; TU Delft, 2002 (limited distribution)
- [20] M.Chaplin; Water structure and behaviour; online at <http://www.lsbu.ac.uk/water/index.html>; London South Bank University, May 2005 (website update referenced)
- [21] D.R.Chapman; An approximate analytical method for studying entry into planetary atmospheres; NASA TR R-11, NASA, Washington DC, 1959
- [22] R.Churchward; Examples of thermal protection systems for reentry vehicles; handout of presentation at Workshop on Thermal Technology for the Brazilian Reentry Program, Federal University of Santa Catarina, Brazil, November 2000.
- [23] C.Clay, H.Croop, M.Camden; TPS and hot structures for RLV / OSV; in 'proceedings of the 4th European workshop on TPS for Space Vehicles, Palermo, nov 2002'; ESA SP-521, ESA, Noordwijk, April 2003.
- [24] COI Ceramics; Oxide-oxide overview; web page www.coiceramics.com/cmdevelopment.htm (viewed Dec 2003)

References

- [25] W.D.Deveikis, R.Miserentino, I.Weinstein, J.L.Schideler; Aerothermal performance and structural integrity of a René-41 thermal protection system at Mach 6.6; NASA-TN-D-7943, NASA, Washington DC, 1975
- [26] M.Dogigli, K.Handrick, M.Bickel, A.Fröhlich; CMC key technologies – background, status, present and future applications; in ‘proceedings of the 4th European workshop on TPS for Space Vehicles, Palermo, nov 2002’; ESA SP-521, ESA, Noordwijk, April 2003.
- [27] A.El Abbadi; High-temperature corrosion of PM1000 and the influence of halogens on the Nickel based super-alloy; MSc thesis report, TU Delft, August 2004.
- [28] D.A.Ellis; Overview: the design of an efficient lightweight airframe structure for the national aerospace plane; AIAA-89-1406, AIAA, Washington DC, 1989
- [29] J.Fatemi, S.Birjmohan, M.Rijkeboer, M.Bakker; Analysis and testing of a metallic Thermal Protection System for RLV application; 4th international Symposium on Atmospheric Re-entry Vehicles & Systems; AAAF, France, March 2005.
- [30] W.P.Fischer, A.Gülhan, B.Esser, J.Faerber, N.Reger; Plasma-windtunnel tests on a new metallic TPS material; in ‘proceedings of the 4th European workshop on TPS for Space Vehicles, Palermo, nov 2002’; ESA SP-521, ESA, Noordwijk, April 2003.
- [31] D.W.Fox, R.M.Rivello; Airborne evaporative cooling system; US Patent 2,922,291; US Patent Office, Jan.1960.
- [32] D.García Yáñez; Numerical Modeling of an active cooling thermal protection system based on water evaporation; M.Sc. thesis report, TU Delft faculty of Aerospace Engineering, Delft, Dec.2002
- [33] M.Giegerich, K.Handrick, H.Hald; Flight test verification of current generation ceramic-based TPS; in ‘proceedings of the 3rd European workshop on Thermal Protection Systems’; ESA WPP-141, ESA, Noordwijk, 1998.
- [34] D.E.Glass, M.A.Merrigan, J.T.Sena, R.S.Reid; Fabrication and testing of a leading-edge shaped heat pipe; NASA-CR-1998-208720; NASA, Washington DC, October 1998.
- [35] R.Godwin (editor); Dyna-soar - hypersonic strategic weapons system; Apogee Books, Canada, 2003; ISBN 1-896522-95-5.
- [36] K.Hagihara, T.Nakano, Y.Umakoshi; Mechanical properties of C40-based ternary Mo(Si,Al)₂ and quaternary (Mo,Zr)(Si,Al)₂ silicides; Scripta Materialia, vol.38, No.3; Elsevier Science, 1998.

- [37] B.Harnisch, B.Kunkel, M.Deyerler, S.Bauereisen, U.Papenburg; Ultra-lightweight C-SiC mirrors and structures; ESA-bulletin 95, ESA, Noordwijk, August 1998.
- [38] Haynes International, Inc.; *High temperature alloys* and *Hastelloy corrosion resistant alloys* catalogues; Haynes Int.Inc., USA, 2000.
- [39] H.H.Hoadley; Surface cooling means for aircraft; US Patent 2,908,455; US Patent Office, Oct.1959.
- [40] P.A.Hogenson, M.J.Green, C.W.Carrol; Recent advances in ceramic TPS for commercial reusable hypersonic vehicles; in 'proceedings of the 3rd European workshop on Thermal Protection Systems'; ESA WPP-141, ESA, Noordwijk, 1998.
- [41] L.Innocenti, C.Dujarric, G.Ramusat; An overview of the FLPP and the technology developments in RLV stage structures for elevated temperature applications; in 'proceedings of the 4th European workshop on TPS for Space Vehicles, Palermo, nov 2002'; ESA SP-521, ESA, Noordwijk, April 2003.
- [42] D.R.Jenkins; Space Shuttle: the history of the National Space Transportation System (3rd ed.); Midland Publishing, Hinckley (UK), 200
- [43] D.J.Kinney, J.V.Bowles, L.H.Yang, C.D.Roberts; Conceptual design of a 'SHARP'-CTV; AIAA paper 2001-2887; AIAA, Washington DC, June 2001.
- [44] D.A.Kontinos, K.Gee, D.K.Prabhu; Temperature constraints at the sharp leading edge of a crew transfer vehicle; AIAA paper 2001-2886; AIAA, Washington DC, June 2001.
- [45] A.V.Korabelnikov, A.L.Kuranov; Thermal protection using endothermic fuel conversion; AIAA paper 2005-3368, AIAA, Washington DC, May 2005.
- [46] M.Lambert, F.Schäfer; Hypervelocity impacts on thermal protections. A review of the ESA work; in proceedings of the 3rd European Workshop on Thermal Protection Systems; ESA-WPP-141, ESA, Noordwijk, 1998.
- [47] R.Le Touche; Thermal protection or dissipation screen; US Patent 4,482,111; US Patent Office, Nov.1984.
- [48] R.Le Touche; Composite assembly forming thermal protection or dissipating screen; US Patent 4,592,950; US Patent Office, June 1986.
- [49] R.Le Touche; Thermal protection device using the vaporization and superheating of a rechargeable liquid; US Patent 5,330,124; US Patent Office, July 1994.
- [50] Lopes, C.; Concept design of an enhanced radiation cooling thermal protection system; M.Sc. thesis report, TU Delft faculty of Aerospace Engineering, Delft, Oct.2002.

References

- [51] G.Loizino-Lozinsky, V.Timoshenko; Lessons learned from the BOR flight campaign; in 'proceedings of the 3rd European workshop on TPS for Space Vehicles, Noordwijk, nov 1998'; ESA SP-426, ESA, Noordwijk, December 1998.
- [52] G.Marino, G.Russo, A.Denaro, G.Borriello; USV: flying test bed opportunity for TPS and hot structures; in 'proceedings of the 4th European workshop on TPS for Space Vehicles, Palermo, nov 2002'; ESA SP-521, ESA, Noordwijk, April 2003.
- [53] G.Mastrangelo, A.Ortona; Development and preliminary testing of uniform and gradient high temperature CMC materials; in 'proceedings of the 3rd European workshop on Thermal Protection Systems'; ESA WPP-141, ESA, Noordwijk, 1998.
- [54] F.McMurray; Chemistry; Prentice-Hall, 2004 (online edition at <http://wps.prenhall.com/wps/media/objects/602/616516/index.html>)
- [55] Metallwerk Plansee; Material data sheet ODS Superalloy
- [56] Metallwerk Plansee; Dispersion Strengthened High-temperature materials (brochure)
- [57] Miller, J.; The X-planes, X-1 to X-45; Midland publishing, Hinckley (UK), 2001
- [58] R.Monti, G.Pezzella, R.Savino, D.Paterna, Aesposito; Aerothermodynamic study of an advanced thermal protection system; in 'proceedings of the 4th European workshop on TPS for Space Vehicles, Palermo, nov 2002'; ESA SP-521, ESA, Noordwijk, April 2003.
- [59] R.Monti, G.Pezzella, D.Paterna; A low risk reentry : looking backward to step forward; AIAA paper 2005-3365; AIAA, Washington DC, May 2005.
- [60] W.D.Morris, N.H.White, C.E.Ebeling; Analysis of Shuttle Orbiter reliability and maintenance data for conceptual studies; AIAA paper 1996-4245, AIAA, Washington DC, 1996.
- [61] J.Muylaert, L.Walpot, H.Ottens, F.Cipollini, L.Marraffa, M.Caporicci, C.Stavriniadis; European experimental reentry testbed (EXPERT); in 'proceedings of the 4th European workshop on TPS for Space Vehicles, Palermo, nov 2002'; ESA SP-521, ESA, Noordwijk, April 2003.
- [62] NASA ECS (Engineering for Complex Systems); Technology Readiness Level chart; <http://ecs.arc.nasa.gov/other/TRL.htm>; July 2005
- [63] W.E.Neuenschwander, D.U.McBride, G.A.Armour; Shuttle TPS performance and analysis methodology; in 'Shuttle Performance: lessons learned'; NASA-CP-2283, NASA, Washington DC, 1983.
- [64] E.J.Opila, R.E.Hann; Paralineer oxidation of CVD SiC in water vapor; Journal of American Ceramic Society, vol.83, issue 7, pp.1761; July 2000.

- [65] J.J.Petrovic, K.A.K.Vasudevan; Key developments in high temperature structural silicides; *Materials Science and Engineering A* vol.261 (1999); Elsevier, 1999.
- [66] H.Pfeiffer, D.Roos; CMC body flap for NASA's X-38 test vehicle; in 'proceedings of the 3rd European workshop on Thermal Protection Systems'; ESA WPP-141, ESA, Noordwijk, 1998.
- [67] O.A.Plumb; Transport phenomena in porous media: modelling the drying process; in "*Handbook of porous media*"; K.Vafai (ed.); Marcel Dekker Inc, New York, 2000.
- [68] R.W.Powell, M.K.Lockwood, S.A.Cook; The road from the NASA Access-to-space study to a reusable launch vehicle; IAF paper IAF-98-V.4.02; IAF, Paris, October 1998.
- [69] D.Rasky, J.Salute, P.Kolodziej, J.Bull, D.Keese; The NASA SHARP flight experiment; ; in 'proceedings of the 3rd European workshop on Thermal Protection Systems'; ESA WPP-141, ESA, Noordwijk, 1998.
- [70] H.Reindl, T.Pichon; Analytical and test results of a feasibility study for a ceramic heatshield assembly; in 'proceedings of the 3rd European workshop on Thermal Protection Systems'; ESA WPP-141, ESA, Noordwijk, 1998.
- [71] J.Reuther, D.Kinney, S.Smith, D.Kontinos, P.Gage, D.Saunders; A reusable space vehicle design exploring sharp leading edges; AIAA paper 2001-2884; AIAA, Washington DC, June 2001
- [72] W.M.Rohsenow, J.P.Hartnett, Y.I.Cho (editors); *Handbook of Heat transfer* 3rd edition; McGraw-Hill, New York, 1998
- [73] J.S.Rowlinson, B.Widom; *Molecular theory of capillarity*; Clarendon Press, Oxford (UK), 1982.
- [74] G.Russo, G.Marino; The USV program and UHTC development; in 'proceedings of the 4th European workshop on TPS for Space Vehicles, Palermo, Nov 2002'; ESA SP-521, ESA, Noordwijk, April 2003.
- [75] D.Saunders, G.Allen, P.Gage, J.Reuther; Crew transfer vehicle trajectory optimization; AIAA paper 2001-2885; AIAA, Washington DC, June 2001.
- [76] J.W.Sawyer; Aerothermal and structural performance of a cobalt-base superalloy thermal protection system at Mach 6.6; NASA TN-D-8415, NASA, Washington DC, 1977
- [77] J.W.Sawyer, J.Hodge, B.Moore; Aerothermal test of metallic TPS for X-33 reusable launch vehicle; in 'proceedings of the 3rd European workshop on Thermal Protection Systems'; ESA WPP-141, ESA, Noordwijk, 1998.

References

- [78] D.Sciulli; Finite element model of a large closed test model for enhanced radiation cooling; TU Delft / University of Pisa MSc thesis report, 2005.
- [79] S.J.Scotti, C.Clay, M.Rezin; Structures and materials technologies for extreme environments applied to reusable launch vehicles; AIAA paper 2003-2697, AIAA, Washington DC, 2003.
- [80] S.J.Scotti, C.C.Poteet, K.Daryabeigi, R.J.Nowak, S-Y Hsu, I.H.Schmidt, S-H.P.Ku; METAShield – hot metallic aeroshell concept for RLV/SOV; NASA TM-2003-212425; NASA, Washington DC, 2003.
- [81] C.N.Scully, J.Castelfranco; Air vehicle surface cooling means; US Patent 3,014,353, US Patent Office, Dec.1961.
- [82] S.Smith, J.Reuther, D.Kinney, D.Saunders; Low speed aerodynamics and landing characteristics of Sharp-class Crew Transfer Vehicle concepts; AIAA paper 2001-2888; AIAA, Washington DC, June 2001.
- [83] D.Stewart, S.Bouslog; Surface characterization of candidate metallic TPS for RLV; AIAA paper 1998-3458; AIAA, Washington DC, July 1998.
- [84] K.J.Sudmeijer, M.H.A.Ambaum, W.Thierfelder; Development of an ODS sandwich structure for the stiffened load carrying skin of the rudder of a reusable launcher; presented at 2nd International Conference on Atmospheric Reentry Vehicles And Systems; Arcachon, France, March 2001
- [85] K.J.Sudmeijer, E.Mooij; Shape optimization for a small experimental re-entry vehicle; AIAA paper 2002-5261; AIAA, Washington DC, October 2002.
- [86] K.J.Sudmeijer, J.Buursink; An enhanced radiation cooling system for re-entry vehicles, principle and mathematical modelling; 4th international Symposium on Atmospheric Re-entry Vehicles & Systems; AAAF, France, March 2005.
- [87] O.Sypkens; Enhanced radiation cooling system - Experimenteel onderzoek naar een thermal protection system; Final thesis report, HTS Haarlem / TU Delft, October 2004.
- [88] M.E.Tauber, L.Yang; Performance comparisons of manoeuvring vehicles returning from orbit; Journal of Spacecraft vol.25 #4, AIAA, Washington DC, July 1988
- [89] U.Trabandt, A.Gülhan, H.Weih; Gap and step tests on X-38 nose assembly; in ‘proceedings of the 4th European workshop on TPS for Space Vehicles, Palermo, nov 2002’; ESA SP-521, ESA, Noordwijk, April 2003.
- [90] U.Trabandt, G-F.Reinbold, G.Tumino, B.Esser, D.Koch, R.Knoche; RLV TPS and Hot structures operational cost evaluation after life cycle testing with rain, hail and low

- speed impacts; 4th international Symposium on Atmospheric Re-entry Vehicles & Systems; AAAF, France, March 2005.
- [91] G.Tumino; European development and qualification status and challenges in hot structures and TPS for space transportation concepts; in 'proceedings of the 4th European workshop on TPS for Space Vehicles, Palermo, nov 2002'; ESA SP-521, ESA, Noordwijk, April 2003.
- [92] J.Verpoorten; Materiaalstudie van de hoge temperatuurlegering PM1000 voor de DART terugkeerruimtecapsule (Material studies of the high temperature alloy PM1000 for the DART re-entry capsule); M.Sc.thesis report, TU Delft / KU Leuven, May 2003.
- [93] L.Walpot, H.Ottens; FESART/EXPERT aerodynamic and aerothermodynamic analysis of the REV and KHEOPS configurations; ESA document TOS-MPA/2718/LW, issue 2 rev 1; ESA, Noordwijk, May 2003
- [94] Ph.Watillon, Ph.Berthe, C.Chavagnac; Flight test demonstrators - experimental vehicles history; AIAA paper 2003-2913; AIAA, Washington DC, July 2003
- [95] H.Weihls, J.longo, A.Gülhan; The Sharp Edge Flight Experiment SHEFEX; in 'proceedings of the 4th European workshop on TPS for Space Vehicles, Palermo, nov 2002'; ESA SP-521, ESA, Noordwijk, April 2003.
- [96] K.Wildenrotter, R.Nika; Design aspects, essential design features and basic elements for hot structures / control surfaces; in 'proceedings of the 3rd European workshop on Thermal Protection Systems'; ESA WPP-141, ESA, Noordwijk, 1998.
- [97] K.E. Wurster; Lifting entry vehicle mass reduction through integrated thermostructural / trajectory design; Journal of Spacecraft vol.20 #6, AIAA, Washington DC, Nov 1983
- [98] M.Yamaguchi, H.Inui, K.Ito; High-temperature structural intermetallics; Acta Materiala, vol.48 (2000) page 307; Elsevier Science, 2000.
- [99] Zircar Ceramics Inc; online materials brochures for ZAL-15, ALC materials; online at www.zircarceramics.com/pages/rigidmaterials/aluminaproducts.htm (as of Dec.2003)

Websites

- [100] Brock University Physics Department; www.physics.brocku.ca/courses/1p23/Heat/ice.html
- [101] Encyclopaedia Astronautica; www.astronautix.com
- [102] Space Cowboy Saloon; <http://groups.msn.com/SpaceCowboySaloon/>
- [103] Stainless Steel World; <http://www.stainless-steel-world.net/glossary>
- [104] US Air Force Museum website; www.wpafb.af.mil/museum/space_flight/

References

A.1 PM1000

A.1.1 Basic properties

The composition of PM1000 is the following:

element	Nickel (Ni)	Chromium (Cr)	Iron (Fe)	Aluminium (Al)	Titanium (Ti)	Yttrium Oxide (Y ₂ O ₃)
percentage	75.6	20.0	3.0	0.3	0.5	0.6

TABLE A-1: composition of PM1000

Other basic properties given in the material brochure are:

- Melting point 1408°C
- Density 8.24 g/cm³

These properties were used where applicable in this study without further checks.

A.1.2 Strength properties

Strength properties of PM1000 were measured in a national Dutch technology development program, Aeolus. The data from those tests were used in the FE models in this study. Because this is proprietary information, it is not reproduced here.

A.1.3 Physical properties

Coefficient of thermal expansion

It must be noted that several definitions exist for this coefficient: the *true coefficient of thermal expansion* which gives the slope of the tangent to the length-temperature plot, i.e. the fractional increase in length per unit temperature increase at a specific temperature, and the *mean coefficient of thermal expansion* giving the rate of change in length over a certain temperature interval. The PM1000 brochure does not say which definition is used for the data given there.

The brochure gives a linear graph ranging from $13.5 \cdot 10^{-6}$ at 0°C to $33 \cdot 10^{-6}$ at 1300°C giving the following relationship:

$$\beta = (0.015 \cdot T + 13.5) \cdot 10^{-6} \quad \text{for } 0^\circ\text{C} < T < 1300^\circ\text{C}.$$

Thermal conductivity

The material brochure gives a graph for thermal conductivity increasing linearly in two parts:

from 11 W/mK at 0°C to 30 W/mK at 750°C

from 30 W/mK at 750°C to 42 W/mK at 1200°C .

This gives the following relationship (with T in $^\circ\text{C}$):

$$k = 0.25333 \cdot T + 11 \quad \text{for } 0^\circ\text{C} < T \leq 750^\circ\text{C}$$

$$k = 0.26667 \cdot (T-750) + 30 \quad \text{for } 750^\circ\text{C} < T < 1200^\circ\text{C}$$

Specific heat

Specific heat increases linearly from 410 J/kgK at 0°C to 900 J/kgK at 1200°C , giving the following relationship (T in $^\circ\text{C}$):

$$C_p = 0.408333 \cdot T + 410 \quad \text{for } 0^\circ\text{C} < T < 1200^\circ\text{C}$$

Temperature conductivity

This derived parameter is defined as $\delta = \sqrt{\frac{k}{C_p \cdot \rho}}$ with the unit of m²/s.

A.1.4 Emissivity

Emissivity of PM1000 has been measured in the Dutch Aeolus program. The function fit through the data points of those measurements is given by:

$$e = -1.49 \cdot 10^{-7} T^2 + 4.89 \cdot 10^{-4} T + 0.456 \quad \text{for } 950\text{K} < T < 1600\text{K}$$

The full measurements are available in the relevant (restricted) Aeolus reports.

A.2 ZAL-15

ZAL-15 is a trade name for Alumina board insulation material; the name is specifically linked to the board material. The supplier is Zircar Ceramics, in New York state, USA. The same material is available in other (mainly cylindrical) shapes under the name ALC.

The composition is 85% Alumina (Al₂O₃) and 15% Silica (SiO₂). The material is produced by chopping fibres of the oxides, mixing in the right composition in water, and then removing the water in a vacuum process followed by sintering at about 600°C.

Various density materials can in principle be made; standard materials are ZAL-15 and ZAL-45 at 15 and 45 lb/ft³ respectively (0.24 and 0.72 g/cm³). Intermediate densities should be no problem; whether lighter material than ZAL-15 can be made is not known, nor how much the strength properties of such a material would degrade. A test campaign with custom made lower density versions could be interesting in order to further optimise the cooled TPS, but due to the cost of the material this was not pursued thus far.

Brochure values for the material are [99]:

Density	240 kg/m ³
Maximum use temperature	1550°C continuous 1650°C intermittent
Melting point	1870°C
Open porosity	93 %
Specific heat	0.25 J/kgK
Shrinkage	1% after 1hr at 1550°C 2% after 1hr at 1650°C
Thermal conductivity	0.06 W/mK at 250°C 0.08 W/mK at 525°C 0.12 W/mK at 800°C 0.16 W/mK at 1075°C 0.22 W/mK at 1250°C 0.25 W/mK at 1350°C
Thermal expansion coeff.	$5.0 \cdot 10^{-6}$ from room temperature to 1000°C

Emissivity

Emissivity of ZAL-15 in dry condition and saturated with water was measured at Dutch Space at room temperature:

emissivity, dry	0.81
emissivity, wet	0.91

A.3 Water

All data for water has been taken from literature.

Density	1000 kg/m ³
---------	------------------------

As is well known, the density of water changes slightly with temperature and has a maximum at about 4°C (see Figure A-1). The density of 1000kg/m³ has been used in this thesis except in the detailed FE analysis of the large lab model.

Appendix A: Materials properties

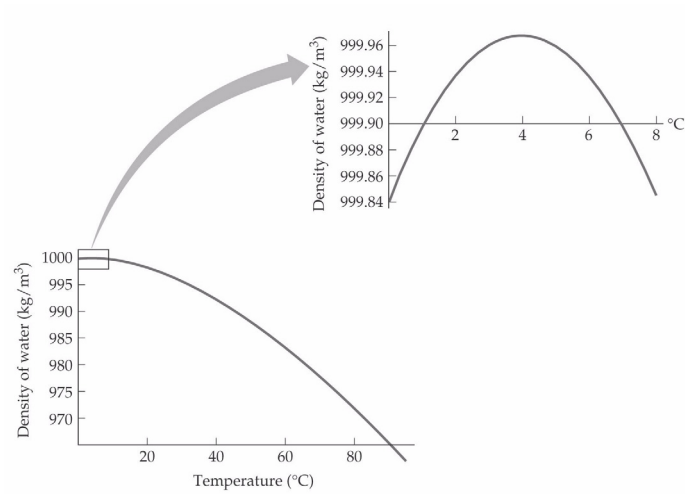


Figure A-1: density of water vs. temperature [100]

Heat of melting	334 kJ/kg
Heat of evaporation	2260 kJ/kg

Thermal conductivity for liquid water is given by:

$$k(T) = -0.7676 + 7.536 \cdot 10^{-3} T - 9.825 \cdot 10^{-6} T^2 \quad \frac{J}{m \cdot K} \quad (\text{A.1})$$

Heat capacity for liquid water is given by:

$$C_p(T) = 917.5 - 10.1016 T + 0.0454134 T^2 - 9.07517 \cdot 10^{-5} T^3 + 6.8070 \cdot 10^{-8} T^4 \quad \frac{J}{K \cdot mol} \quad (\text{A.2})$$

A.4 APA-2 Alumina paper

This material has been used for seals in the large lab model and the flight experiment lab model. The choice for this material was based on availability and temperature capability, without performing an exhaustive search for all potential candidates. Neither were material properties measured; brochure values are used everywhere.

APA-2 is a trade name for Alumina paper made by Zircar Ceramics in the USA, the same company that produces ZAL-15. Two thicknesses of flexible material are available; APA-1 of 1mm thickness and APA-2 of 1.27mm thickness, and a rigid material APA-3 of 0.31mm thickness.

APA-2 brochure values are reproduced here [99]:

Composition (weight %)	Al ₂ O ₃ : 95%, SiO ₂ : 5%
Weight	177.8 g/m ²
Thickness at 0 MPa pressure	1.27 mm
at 0.06 MPa pressure	0.97 mm
Density at 0.06 MPa pressure	0.14 g/cc
Maximum use temperature	1650 °C

The heat transfer coefficient is given in the brochure in a graph in Imperial units; translated to SI units it gives the following result:

Appendix A: Materials properties

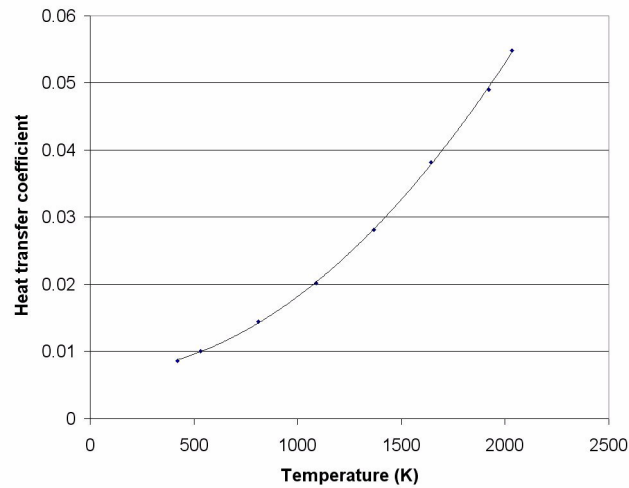


Figure A-2: Heat transfer coefficient in $\frac{W}{m^2 \cdot K \cdot m}$

The trend-line is given by the expression:

$$k = 1 \cdot 10^{-8} \cdot T^2 - 4 \cdot 10^{-7} \cdot T + 0.0069 \quad (\text{A.3})$$

This heat transfer coefficient is for uncompressed material; when used as a seal in our test samples, the material is compressed, which will lead to a higher heat transfer coefficient. This new coefficient should be determined in the lab, but this has not been done yet.

Appendix B *Colour plates*

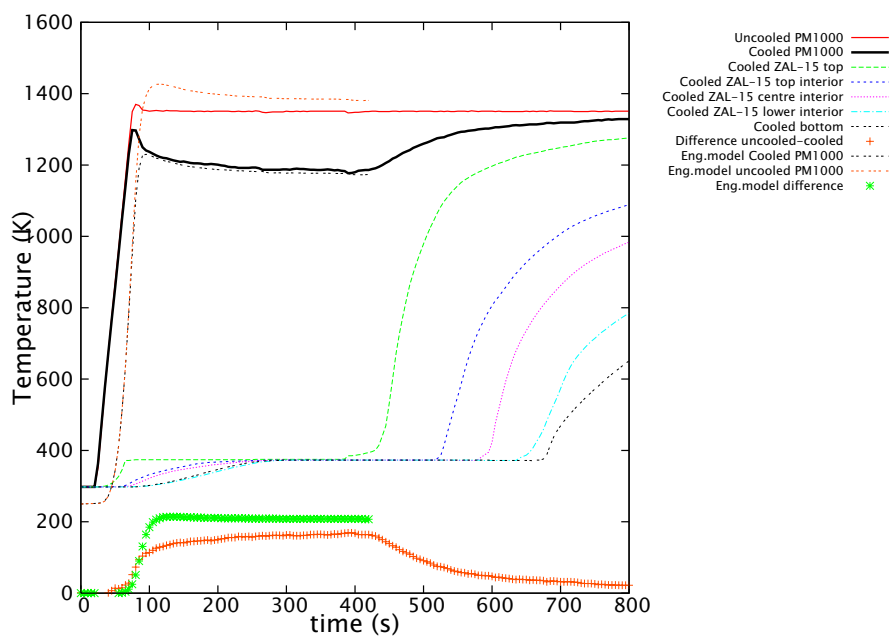
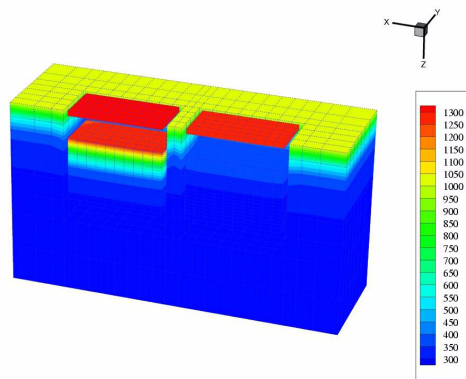
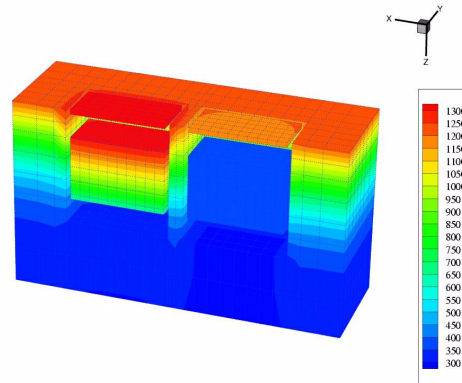


Figure B-1: Results and engineering model predictions for a drying-out test run. See also Figure 4-9.

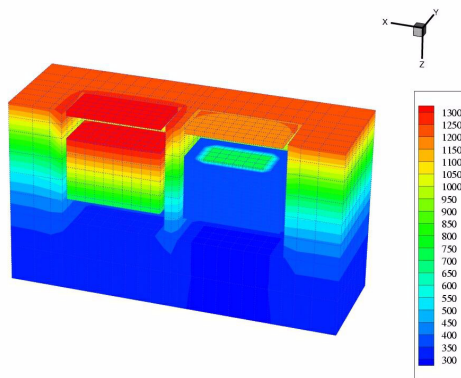
70 seconds



400 seconds



440 seconds



590 seconds

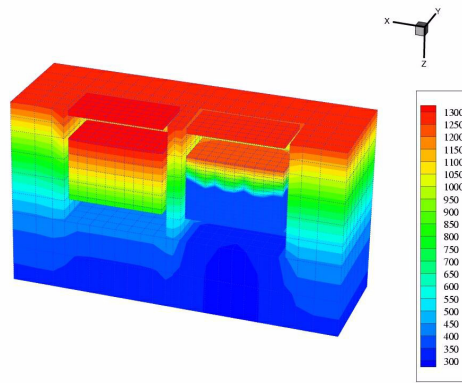


Figure B-2: Temperature distribution in the test model at various times during the heating test, continued in Figure B-3. See also Figure 4-13.

Appendix B: Colour plates

730 seconds

1000 seconds

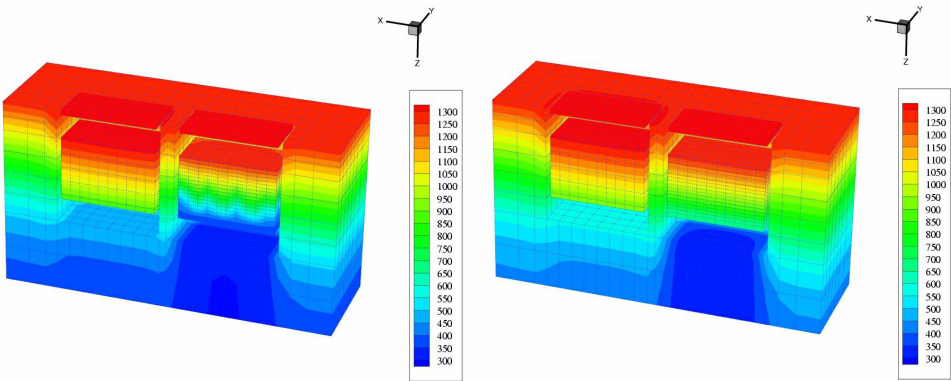


Figure B-3: Temperature distribution in the test model at various times during the heating test. Continued from Figure B-2. See also Figure 4-13.

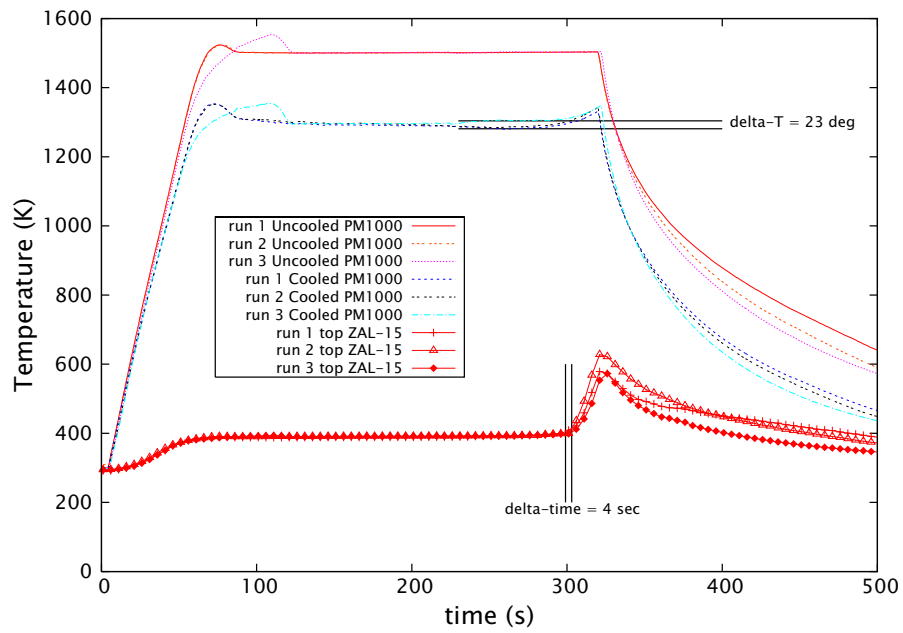


Figure B-4: Repeatability of tests; 3 runs with 0.75inch thick ZAL-15 to 1500K for the uncooled PM1000. See also Figure 4-17.

Appendix B: Colour plates

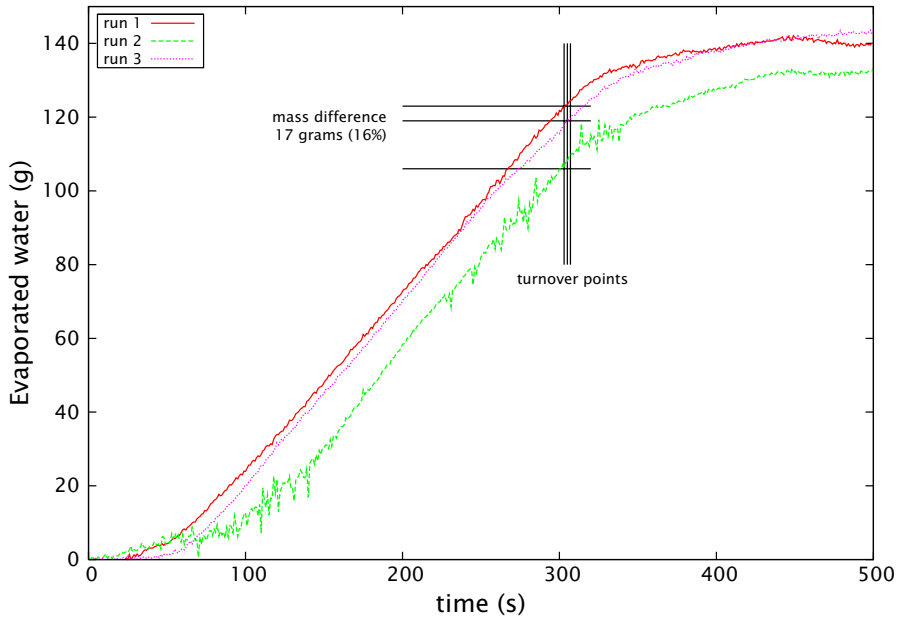


Figure B-5: Mass measurement of the test runs shown in Figure 4-17 / Figure B-4. See also Figure 4-18.

Appendix B: Colour plates

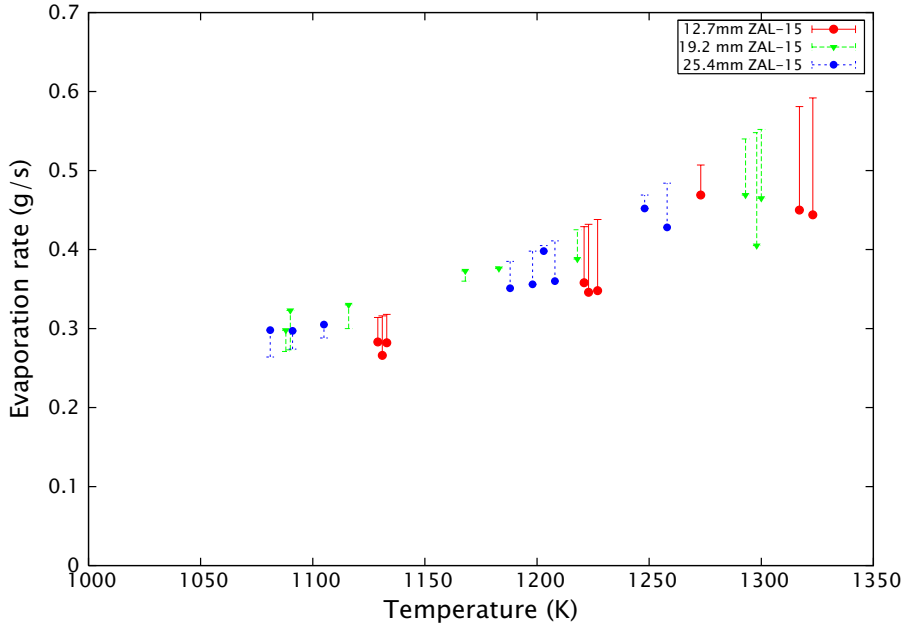


Figure B-7: Evaporation rate as a function of temperature, data collected from all runs. Error bars indicate expected evaporation rate based on 1-dimensional engineering model. See also Figure 4-20.

On the Development of a Cooled Metallic Thermal Protection System for Spacecraft

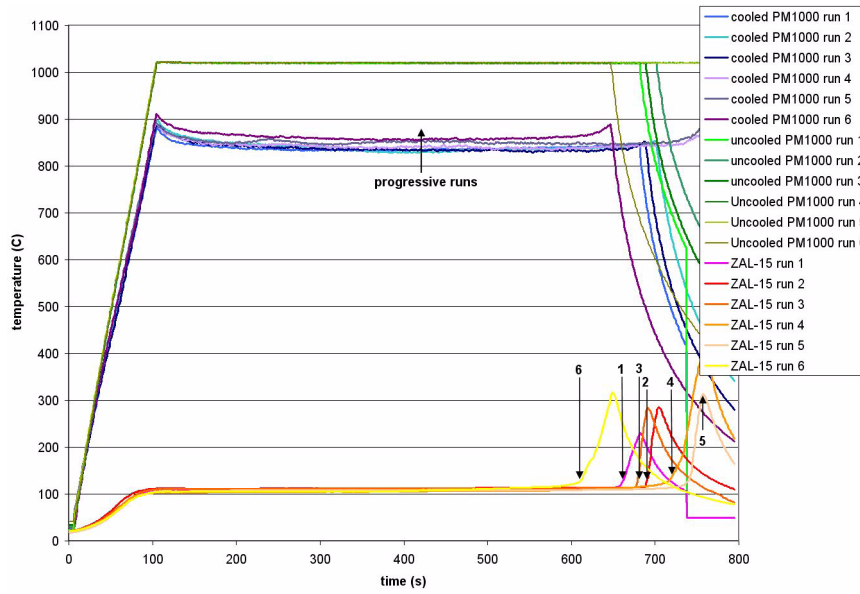


Figure B-8: Comparison of six runs with reduced surface tension. See also Figure 4-21.

Appendix B: Colour plates

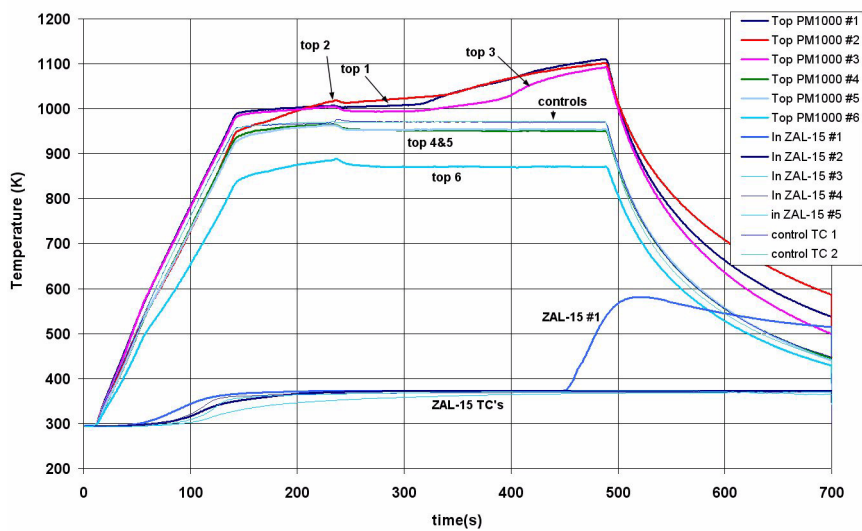


Figure B-9: temperature measurements of test run with large model. See also Figure 4-26.

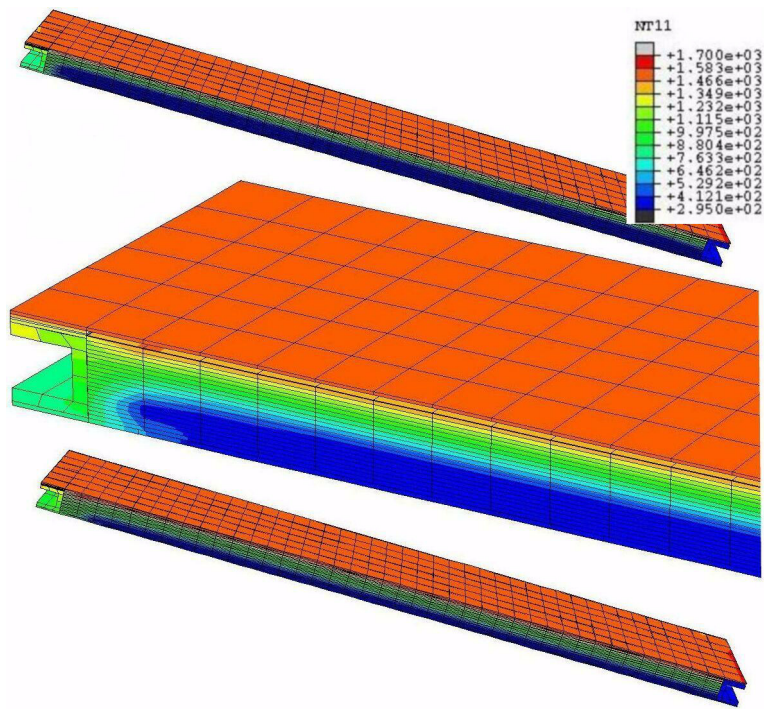


Figure B-10: the FE model of the large closed model, consisting of half the real model because of symmetry. Temperature fields at two points during the drying out phase of a test run. See also Figure 4-29.

Appendix B: Colour plates

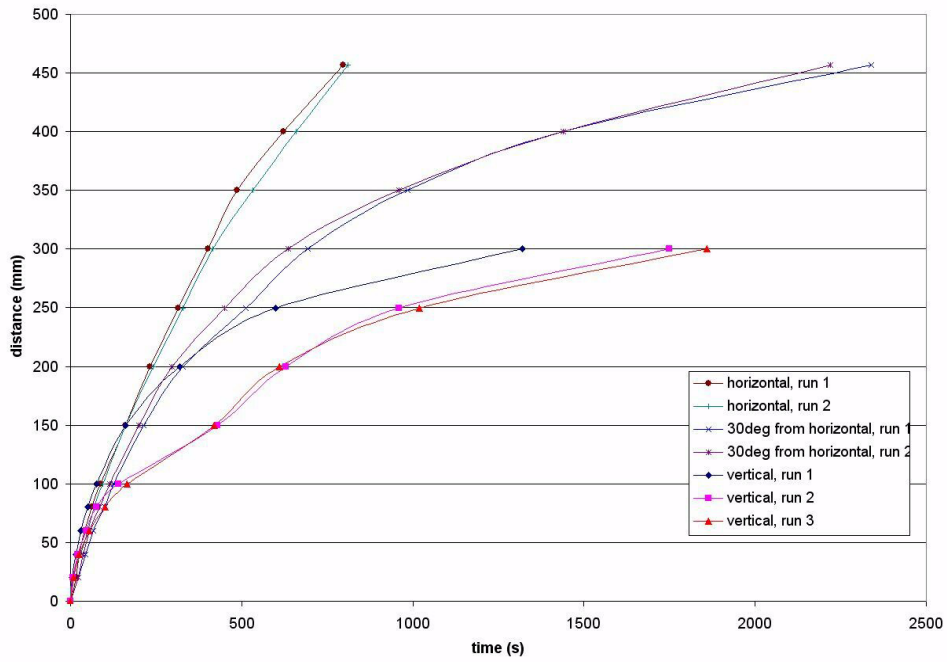


Figure B-11: water transport in a strip of ZAL-15 under three angles with the horizontal. See also Figure 4-34.

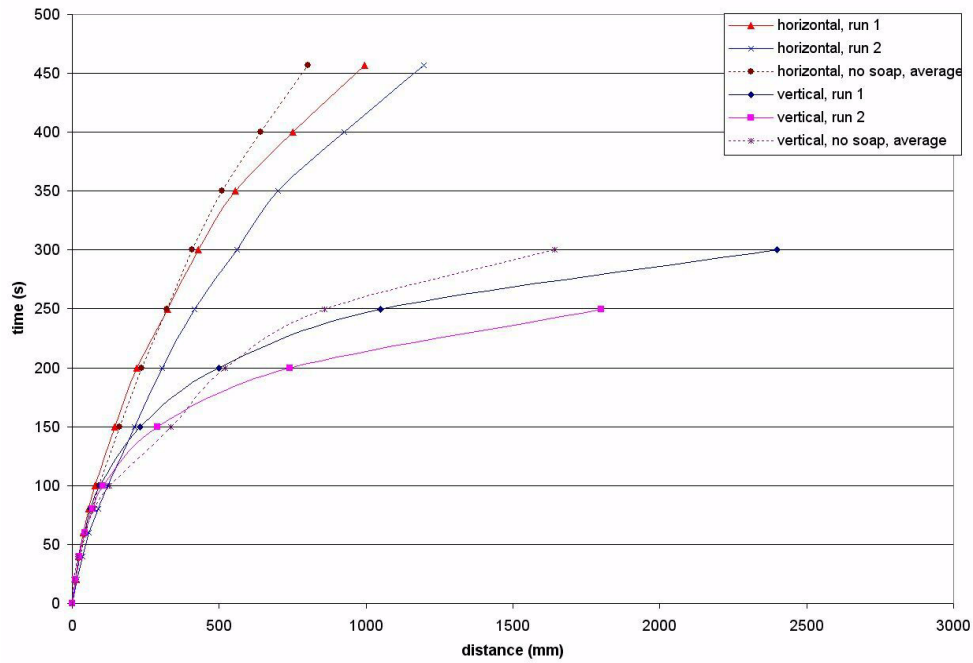


Figure B-12: water transport in a strip of ZAL-15 for water with reduced surface tension, horizontal and vertical, compared with the average of the transport velocity for pure water. See also Figure 4-35.

Appendix B: Colour plates

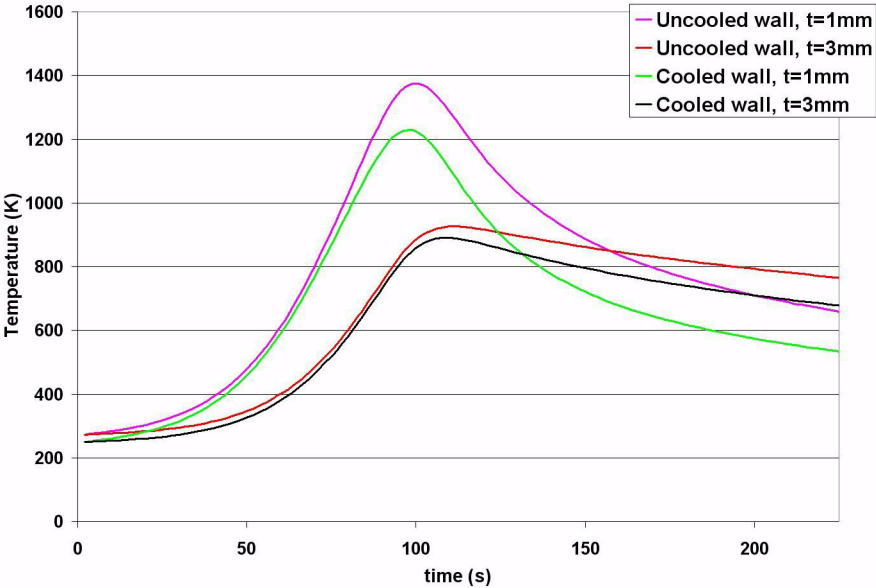


Figure B-13: temperature predictions from engineering model based of heating profile shown in Figure 5-11 for flight test model for different skin thickness. See also Figure 5-12.

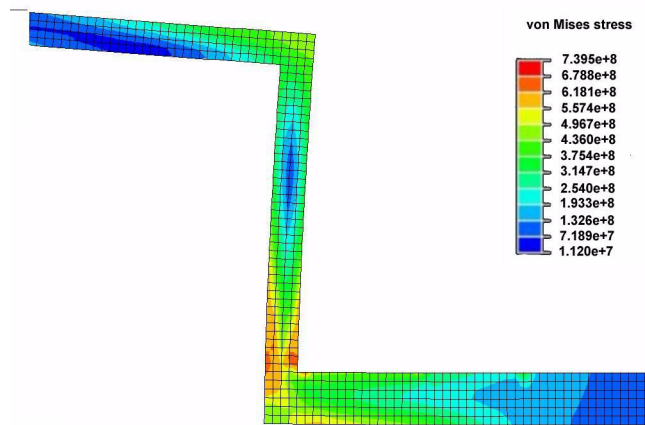


Figure B-14: Von Mises stresses in experiment outer cover due to thermal stresses at time of maximum stress level. See also Figure 5-14.

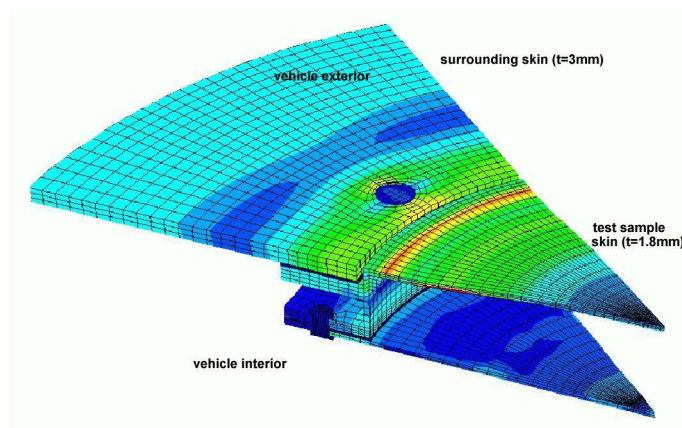


Figure B-15: 3D Finite element model of flight experiment; stress field. See also Figure 5-15

Appendix B: Colour plates

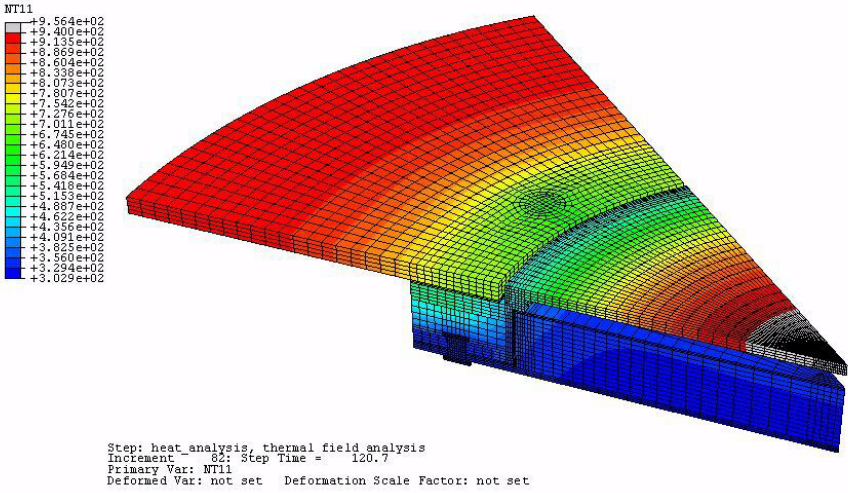


Figure B-16: temperature distribution in model according to FE simulation of lab test.
See also Figure 5-17.

Curriculum vitae

Jeroen Buursink was born in Borculo in the Netherlands in 1972. After graduating from the Rijks Scholen Gemeenschap Lochem secondary school he entered the Faculty of Aerospace Engineering of Delft University of Technology in 1990, resulting in a Masters degree in 1999 on the subject of ‘an assessment study into the recovery of the core stage of Ariane 5’. From 1999 he worked at the same Faculty on the design of a small re-entry test vehicle and the development of the water-cooled thermal protection system that is the subject of this thesis.